Geochemistry of supercritical fluids in active geothermal systems

Matylda Heřmanská

Faculty of Earth Sciences
University of Iceland
2020

Geochemistry of supercritical fluids in active geothermal systems

Matylda Heřmanská

Dissertation submitted in partial fulfillment of a
Philosophiae Doctor degree in Geology

Advisor
Dr. Andri Stefánsson
Faculty of Earth Sciences, University of Iceland

Ph.D. Committee
Dr. Barbara I. Kleine
Institute of Earth Sciences, University of Iceland

Dr. Thomas Driesner
Department of Earth Sciences, ETH Zürich, Switzerland

Dr. Sigurður R. Gíslason
Institute of Earth Sciences, University of Iceland

Opponents
Dr. Halldór Ármannsson
Iceland Geosurvey

Dr. Luigi Marini
Consultant in Applied Geochemistry, Italy

Faculty of Earth Sciences
School of Engineering and Natural Sciences
University of Iceland
Reykjavik, March 2020

Geochemistry of supercritical fluids in active geothermal systems
Dissertation submitted in partial fulfillment of a *Philosophiae Doctor* degree in Geology

Faculty of Earth Sciences
School of Engineering and Natural Sciences
University of Iceland
Askja, Sturlugata 7
101, Reykjavik
Iceland

Bibliographic information:
Matylda Heřmanská, 2020, *Geochemistry of supercritical fluids in active geothermal systems*
PhD dissertation, Faculty of Earth Sciences, University of Iceland, 91 pp.

Author ORCID: 0000-0002-4220-3434
ISBN 978-9935-9412-7-5

Printing: Háskólaprent
Reykjavik, Iceland, March 2020

Abstract

Supercritical fluids have been reported from both rift and subduction related geothermal systems. They typically form in the vicinity of magmatic intrusions at the roots of geothermal systems upon conductive heating and boiling of the subcritical geothermal reservoir fluids to supercritical conditions and/or from gases released from the magmatic body. However, the origin and chemistry of these supercritical fluids are not yet fully understood as their chemical composition can be easily overprinted by mixing with subcritical reservoir fluids at lower temperatures and shallower depths. This study aims to link the hydrology in active intrusion-related geothermal systems with fluid chemistry and associated secondary mineralogy. The origin and formation of supercritical fluid were investigated by combining geochemical modeling and flow-through experiments and comparing modeling and experimental results with natural data reported from supercritical environments.

Experimental and modeling work performed in this thesis revealed that supercritical fluids formed upon conductive heating and the boiling of subcritical geothermal reservoir fluids are characterized by low concentrations of non-volatile elements (Si, Na, K, Ca, Mg, Fe, Al, Cl) and similar concentrations of volatile elements as in the subcritical fluids (B, CO_2, H_2S). This process is predicted to be accompanied by mineral depositions dominated by silica, aluminum silicates and, in some cases, salts. Similar trends in fluid chemistry and mineralogy occur upon supercritical fluid formation in geothermal systems associated with rift and subduction zones.

The results of the modeling and experiments compared well with the chemical composition for supercritical fluid discharges from the IDDP-1 well at Krafla (Iceland). Other geothermal systems where supercritical fluid temperatures have been reported and display similar chemical characteristics include Menengai (Kenya), Los Humeros (Mexico), Larderello (Italy), and The Geysers (USA).

Útdráttur

Hitastig vökva í jarðhitageymum sumra innskotatengdra jarðhitakerfa um allan heim eru yfir krítískum gildum. Uppruni og efnafræði slíkra vökva er ekki að fullu þekkt þar sem efnafræðileg einkenni slíks vöka eru auðveldalega yfirprentuð af ýmsum öðrum ferlum sem eiga sér stað í jarðhitakerfum. Með samþáttun mismunandi aðferðir eins og forða- og efnafræðilegulíkön í bland við háhitatilraunir er hægt að auka skilning á myndun og efnasamsetningu slíks yfir krítísks jarðhitavökva. Markmið rannsóknarinnar var að tengja saman grunnvatnsfræði í virkum innskotatengdum jarðhitakerfum við jaðrefnafræði vövkvans, og þá sérstaklega í tenglsum við myndun yfir krítísks ökva í nágrenni kvikuhólfsins.

Tilraunir og líkanreikingar sem voru framkvæmdir sem hluti af þessari doktorsverkefni sýna fram á að suða á jarðhitavatni vegna varmaleiðni getur leitt til myndunar á yfirkrítískum jarðhitavökva. Efnasamsetning slíks yfirktítísks vökva einkennist af lágum styrk bergsækinna efna (Si, Na, K, Ca, Mg, Fe, Al, Cl) og svipuðum styrk rokgjarnra efna (B, CO_2, H_2S) og mælist í jarðhitavatninu. Samfara þessum efnabreytingum í jarðhitavökvanum myndast útfellingar sem eru ríkar af kvarsi, álsilikötum og salti. Sambærilegar niðurstöður fást fyrir myndun yfirkrítsísks vökva tengt jarðhitakerfum á rekbeltum og trogum.

Niðurstöður tilraunanna og líkanreikninganna á efnasamsetningu yfirkrítísks jarðhitavökva ber vel saman við mælingar á slíkum vökva úr IDDP-1 borholunni í Kröflu (Íslandi). Önnur jaðrhitakerfi þar sem mælst hefur hærri hiti en yfirkrítískur hiti vatns hafa einnig sambærilega efnasamsetningu vökvans, t.d. í Menegai (Kenýa), Los Humeros (Mexíkó), Lardarello (Ítalía) og The Geysers (Bandaríkin).

„Člověk mnoho vydrží, má-li cíl... “

-Tomáš Garrigue Masaryk

Dedicated to Olga.

Preface

This thesis is the outcome of research carried out between years 2014-2019 at the Faculty of Earth Sciences, University of Iceland. The thesis includes three research articles. Research articles I and II have been published in the international journals *Geothermics* and *Geofluids*, respectively and research article III has been accepted for publication to the *Journal of Volcanology and Geothermal Research*. The study was funded by the Swiss National Science Foundation (CRSII2_141843/1, Sinergia COTHERM) and The National Power Company of Iceland.

Research article I

Heřmanská, M., Stefánsson, A., Scott S. 2019. Supercritical fluids around magmatic intrusions: IDDP-1 at Krafla, Iceland. Geothermics, Volume 78, Pages 101-110, https://doi.org/10.1016/j.geothermics.2018.11.002. (reprinted with the permission of Elsevier Science Ltd.)

Research article II

Heřmanská, M., Kleine, B.I., Stefánsson, A. 2019. Supercritical Fluids in Geothermal systems – An Experimental study. Geofluids 2019, Article ID 6023534, 14 pages, https://doi.org/10.1155/2019/6023534. (reprinted with the permission of Wiley Hindawi)

Research article III

Heřmanská, M., Kleine, B.I., Stefánsson, A. Geochemical constraints on supercritical fluids in geothermal systems. J. Volcanol. Geotherm. Res. (reprinted with the permission of Elsevier Science Ltd.)

Parts of this work have been presented at various scientific conferences.

Heřmanská M., Stefánsson, A. 2014. Multicomponent fluid chemistry within multiphase system around cooling plutons with relation to the Krafla geothermal system, NE Iceland. The international Carbon Conference, Reykjavik, August 2014.

Heřmanská, M. Stefánsson, A. 2014. Geochemistry of Multicomponent Fluid Phases in the Krafla High-Enthalpy Geothermal System, NE Iceland. AGU fall meeting, San Francisco, December 2014.

Heřmanská, M., Stefánsson, A. 2015. Multicomponent Fluid Chemistry of the High-Enthalpy Geothermal System, Krafla Volcano, NE Iceland. Goldschmidt Abstracts, 2015, 1244.

Heřmanská, M., Kleine, B.I., Stefánsson, A. 2018. Supercritical fluids in Geothermal Systems: An Experimental Study. Goldschmidt Abstracts, 2018, 1004.

Table of Contents

Acknowledgments

This study was funded by the Swiss National Science Foundation (CRSII2_141843/1, Sinergia COTHERM) and the National Power company of Iceland.

First, I would like to thank to my supervisor Andri Stefánsson for giving me the opportunity to work on this project and for his supervision. Many thanks also go to Barbara and Sam, who always helped me to find a way whenever I got lost.

People previously working in Lab 252 know that to carry out experiments there can be quite stressful. I would like to thank Gylfi, Chiara, Andri Ísak, Maggi, Martin and Helgi for being around and for helping me overcome many technical issues, also to Sigurður Jónsson and Birgir Jóhannesson for their help with SEM and XRD analysis.

This project would never been completed without my partner Dave by my side. I will never be able to express how much I appreciate that you were patient with me and continuously supportive of me with your smile, good advice, or just a shot of Brennivín. You are probably the only person who truly knows how much energy I (we) put into this project. Thank you (and to our dog Kappi too)!

Many thanks to my colleagues from the Geysir research group Hanna, Jan, Prathap, Joi, Snorri, Rikey, and Jon Örn, and to members of the Askja crew: Rob, Deirdre, Hannah, Will, Becca, Eydís, Martin, Giulia, Vincent, Maren, Vaiva, Victor, Lea, Maja, Jed, Eduardo, and Anna. Special thanks belong to Nicole and Iwona for their words of encouragement (often so needed) and Iwona for that beer that she left in front of the lab when I was trying to stop the leak at my experiment.

Ph.D. life often changes people into isolated and introverted weirdos. I was not an exception. So many thanks to all my friends who did not give up on my existence and waited for me to leave that cold, dark cave again. Many thanks to Kate and Pavla for all the fun moments that we have experienced together; Linh for your 24/7 moral support; Dominika, Bianca and Kallia for their witty and sarcastic jokes and all the moments when you kept trying over and over again to explain to me that there is life after a PhD; Isa for showing me that there is light at the end of the tunnel, and many others.

I would like to express my gratitude to my family for their unconditional love and patience. You taught me that family should always be here for you, and you were.

Many thanks to all of you!

1 Introduction

Geothermal systems act as an increasingly vital source of global energy production and will continue to be a necessary option with the growing demand for a more diverse renewable energy mix. To date, energy produced from geothermal resources represents about 0.15% of the world's primary energy production (Conti et al., 2016; Lund and Boyd, 2016). Power production from geothermal resources mainly derives from high-temperature geothermal systems commonly associated with active or recent volcanism, but occasionally also in regions affected by extensive faulting (Fig. 1; Stimac et al., 2015; Rivera-Diaz et al., 2016). The reservoir temperatures of high-temperature geothermal systems are typically ~200-350°C. The average power production from a single high-temperature well is ~2-5MW_e (e.g., Ketilsson et al., 2015; Sanyal and Morrow, 2012). In some geothermal fields, such as The Geysers, Salton Sea, and Hawaii (USA); Kakkonda (Japan); Lardello (Italy); Los Humeros (Mexico); Menengai (Kenya); and Krafla and Nesjavellir (Iceland), measured fluid temperatures exceed the critical temperature of water (Reinsch et al., 2017). Utilization of such fluids could potentially increase power production per well of up to 30-50 MW_e (Friðleifsson and Elders 2005) due to increased specific enthalpy, lower viscosity, and density of supercritical fluids.

Even though utilization of such supercritical resources may multiply energy production from geothermal systems, their occurrence, formation mechanism, and especially chemical properties are not well constrained and understood. Deep drilling projects such as IDDP (Iceland Deep Drilling Project) aim to explore such supercritical resources. However, reservoir conditions, corrosive geothermal fluids, and mineral scaling limited the utilization of these fluids (e.g., Hauksson et al., 2014) and also represented a technical challenge for equipment and material used for the well-head or the valves (Þórhallsson et al., 2010, 2014; Kruszewski and Witig, 2018). This work investigates the supercritical fluid formation, geochemistry, and alteration mineralization in the roots of high-temperature geothermal systems with a magmatic heat source with a focus on Icelandic geothermal fields.

1.1 Active geothermal systems

High-temperature or volcanic geothermal systems form in the Earth's upper crust above a magmatic heat source, often at plate boundaries, where melt derived from the upper mantle can reach shallow depths within the crust (Henley and Ellis, 1983; Hedenquist and Lowenstern, 1994). After emplacement, magmatic intrusions start to cool and exchange heat with the surrounding rocks and groundwater system (Hanson, 1995, 1996). At hydrostatic pressures, heat released into the surrounding groundwater system results in the formation of density-driven convective fluid flow (Fig. 2). As the fluid temperatures and pressures within the geothermal reservoir are typically below the critical point of water, the convecting fluids form under so-called subcritical conditions (Hayba and Ingenbritsen, 1997). The geothermal system is supplied with an inflow of water (meteoric water, seawater or a mixture thereof) into a permeable reservoir around the intrusion. Magmatic gases (e.g., H_2O, CO_2, HCl, SO_2) may exsolve from the cooling and crystallizing magmatic intrusion into the geothermal reservoir. Upon geothermal fluid ascent to the surface, the overlying water column decreases resulting in depressurization boiling and the formation of liquid and vapor phase.

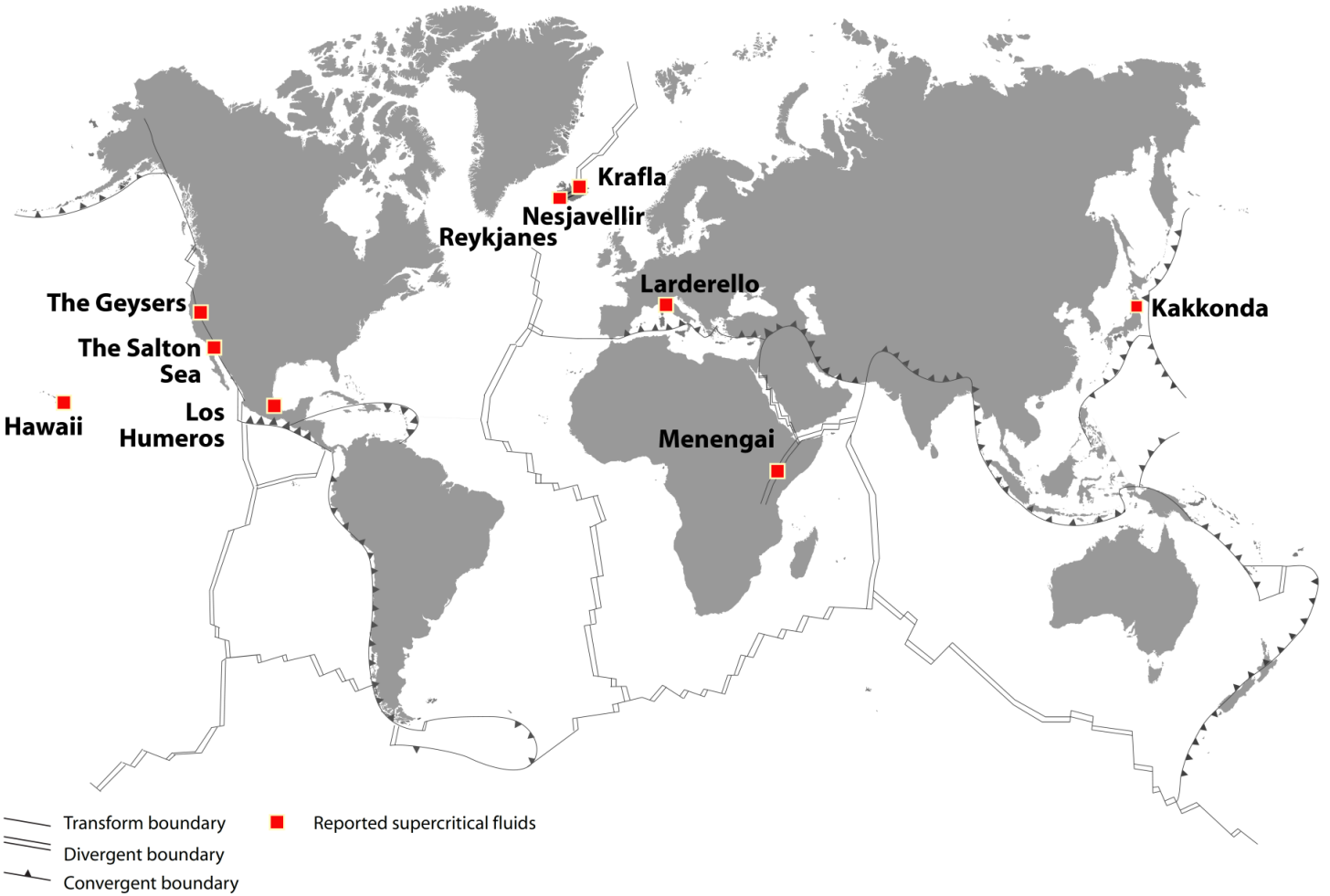

Figure 1 The distribution of geothermal fields that reported the occurrence of supercritical fluids (based on Reinsch et al., 2017).

It has been concluded that the composition of geothermal reservoir fluids is controlled by equilibrium between the fluids and thermodynamically stable secondary minerals for all major elements except for Cl and B that are considered mobile (e.g., Giggenbach, 1981; Arnórsson et al., 1983). As the fluid-mineral reactions are temperature dependent, it follows, that the concentration of major elements varies with reservoir fluid temperature. Such temperature effects are also reflected in depth-related distribution of secondary minerals with mixed-layered clays and chlorite being most common at shallow depths and low to moderate temperatures (<150°C), whereas epidote, chlorite, albite, sulfide, and quartz become predominant at greater depths and temperatures above ~200-250°C and eventually amphiboles such as actinolite or hornblende appearing at the highest temperatures or >300°C (Browne, 1978). At shallow depth, the ascending geothermal liquid and vapor may condense, mix and oxidize with non-thermal fluid, often resulting in fluid with acid to alkaline pH values, argillic alteration, and silica and carbonate travertines forming at the surface.

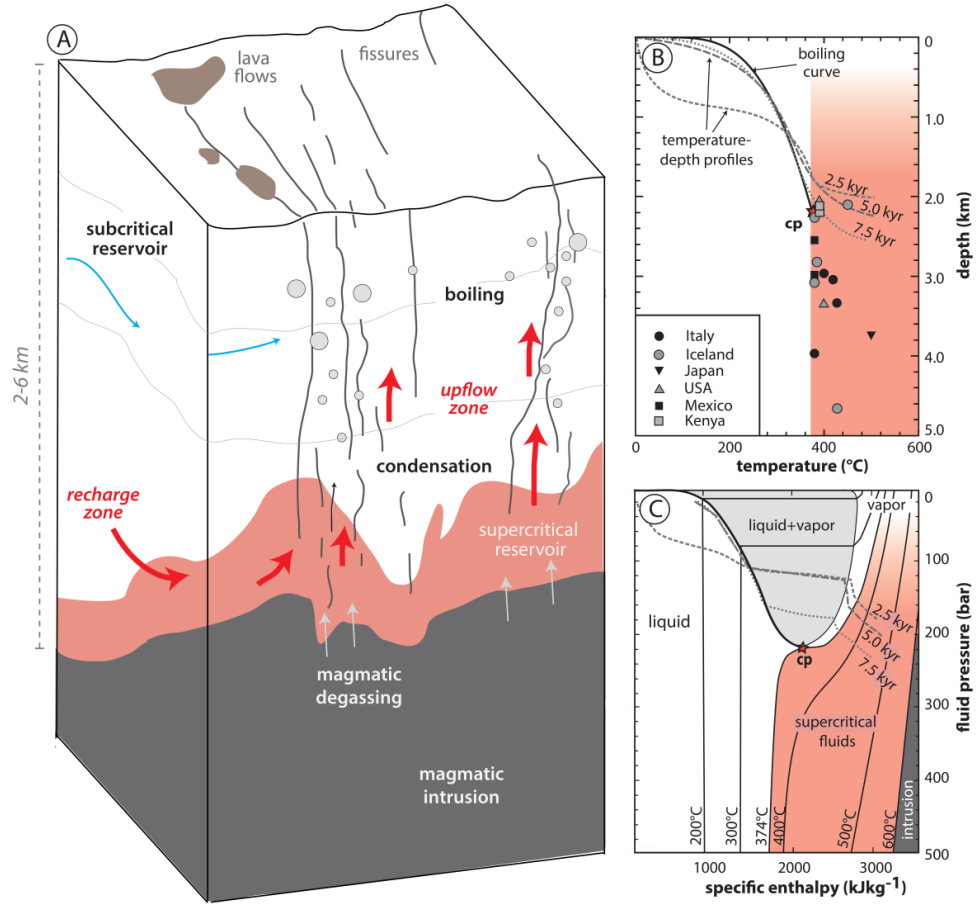

Figure 2 (A) Simplified crossection of active geothermal systems with focus on supercritical fluids (modified from Stefánsson, 1981 and Pope et al., 2015). (B) and (C) Corresponding pressure, temperature and enthalpy conditions of supercritical fluids and wells with observed supercritical conditions displayed on diagrams of pure water. Dashed lines indicate temperature-depth profiles above magmatic intrusions at selected times (after Hayba and Ingebritsen, 1997).

1.2 Supercritical fluids in geothermal systems

Supercritical geothermal fluids have commonly been defined based on the critical temperature (T_c = 373.976 °C) and pressure (P_c = 220.06 bar) of pure water (H_2O) (Haar et al., 1984). Such a definition can lead to an artificial and unphysical boundary in the phase diagram of water across which there is a continuous region of single-phase fluid. Here, and following Liebscher and Heinrich (2007), supercritical geothermal fluid is defined as fluid with temperatures above the critical temperature of water, irrespective of density in the case of pure water or phase state in the case of binary and higher salt-water systems (Fig. 2).

Based on heat and mass transfer modeling, geothermal fluids with temperatures exceeding the critical temperature of pure water have been suggested to exist in the roots of the geothermal systems in the vicinity of the magmatic intrusion. There, heat is transferred to the surrounding groundwater by conduction, resulting in the formation of supercitical fluids with temperatures >400°C and specific enthalpy >3000 kJ kg^{-1} (e.g., Hayba and Ingebritsen, 1997; Scott et al., 2016). Fluids with supercritical temperatures have been observed in several active geothermal systems worldwide such as The Geysers, Salton Sea, and Hawaii (USA); Kakkonda (Japan); Larderello (Italy); Los Humeros (Mexico); Menengai (Kenia); and Krafla, Nesjavellir and Reykjanes (Iceland) (Fig. 1; Reinsch et al., 2017).

Supercritical fluids may originate from magmatic degassing with such fluids being characterized by elevated CO_2, SO_2, HCl, and HF concentrations (e.g., Fischer and Chiodini, 2015). Supercritical fluids may also form as a result of conductive heat transfer from the magmatic intrusion to the surrounding subcritical geothermal fluid (e.g., Hayba and Ingebritsen, 1997). The chemical composition of such supercritical fluids remains somewhat unclear. The solubility of most minerals is poorly known in supercritical and low-density fluids with the exception of silica, for example (Fournier and Potter, 1982) and some common salts (Leusbrock et al., 2009, 2010a, 2010b). However, as a part of the present study, the combination of geochemical modeling and laboratory experiments have suggested such fluids to have similar volatile content as the subcritical geothermal reservoir fluids and low concentration of non-volatile elements (see research articles II and III)

Reported compositions of the fluid condensate discharged from the deep geothermal wells in various geothermal fields, for example at Los Humeros (Mexico) and Krafla (Iceland), showed low pH values of the condensed fluid at room temperature along with low concentrations of non-volatile elements such as Si, Na, K, Ca and Mg (see research articles I and III). This reinforced a discussion about the role of magma gas influx and condensation of supercritical fluids to form HCl rich liquid as a cause of the low pH and dilute fluids (Truesdell et al., 1989; D'Amore et al., 1990; Ármannsson et al., 1989, 2014; Heřmanská et al., 2019). In general, the character of the magmatic degassing is controlled by several factors, such as melt volatile content, reservoir changes during the melt emplacement, or redox conditions within the system (Giggenbach, 1987; Wallace, 2005; Shinohara, 2008). Once an intrusion is emplaced within the crust and starts to cool down, the most volatile elements are released first during depressurization degassing of the melt. Commonly, these are SO_2-rich magmatic fluids that reach the surface, often with minor interaction with the surrounding rocks. Eventually, the transition from hydrostatic to lithostatic pressure results in the formation of slower degassing of magmatic fluids that react with the surrounding rocks, governed by temperature and redox

conditions in the system, and eventually mix with shallower groundwater systems (e.g., Fournier, 1985; Giggenbach, 1987; Shinohara, 2008). Compositions of this type of magmatic fluids evolve with time, initially being CO_2-rich and evolving towards H_2O-rich fluids with less volatile elements, such as Cl.

1.3 The IDDP project

Iceland provides an ideal location for studying the heat and fluid transfer, fluid geochemistry and mineralogy associated with subcritical and supercritical fluids in active geothermal systems. High-temperature geothermal systems are abundant along the plate boundaries, and some of these systems are already utilized. The reported geothermal fluid discharge compositions are affected by the fluid source. At Krafla, Nesjavellir, and Hellisheiði, fluids are of meteoric or of mixed meteoric and seawater origin, whereas at Reykjanes, the geothermal reservoir fluids are sourced dominantly by seawater. Typical reservoir temperatures in these systems range from ~210 to ~325°C and specific enthalpy measured at wellhead ranges from <1000 to ~2750 kJ kg^{-1}, corresponding to liquid dominated to two-phase (vapor and liquid) reservoir fluids (Gudmundsson and Arnórsson, 2005; Scott et al., 2014; Óskarsson et al., 2015).

One of the most ambitious projects aimed at obtaining supercritical fluids for geothermal utilization is the Iceland Deep Drilling Project (IDDP, www.iddp.is). In 2009, the first well (IDDP-1) was drilled in Krafla (Fig. 3; NE Iceland) that came to a halt at ~2.1 km depth after drilling into rhyolite magma. After the initial heating up period, the well discharged supercritical fluids with temperatures of ~440°C, pressures of 140 bar, and enthalpy of ~3200 kJ kg^{-1} (Elders et al., 2014). However, due to operational difficulties, scaling and thermal damage to the well casings, utilization proved to be challenging, and the fluid discharge was eventually terminated (Hauksson et al., 2014). In 2017, the second well (IDDP-2) was drilled at Reykjanes (SW Iceland) that eventually reached a depth of ~4.5 km. The measured temperature at the bottom of the hole was 426°C, but no supercritical fluids have yet been discharged from the well head (Friðleifsson et al., 2017). The third IDDP borehole is already being planned for 2021-23 at Nesjavellir or Hellisheiði (SW Iceland). Previously, well number NJ-11 at Nesjavellir also reached a depth of 2.2 km and a temperature of >380°C (Steingrímsson et al., 1990). This implies that supercritical fluids may commonly form within different active geothermal systems in Iceland.

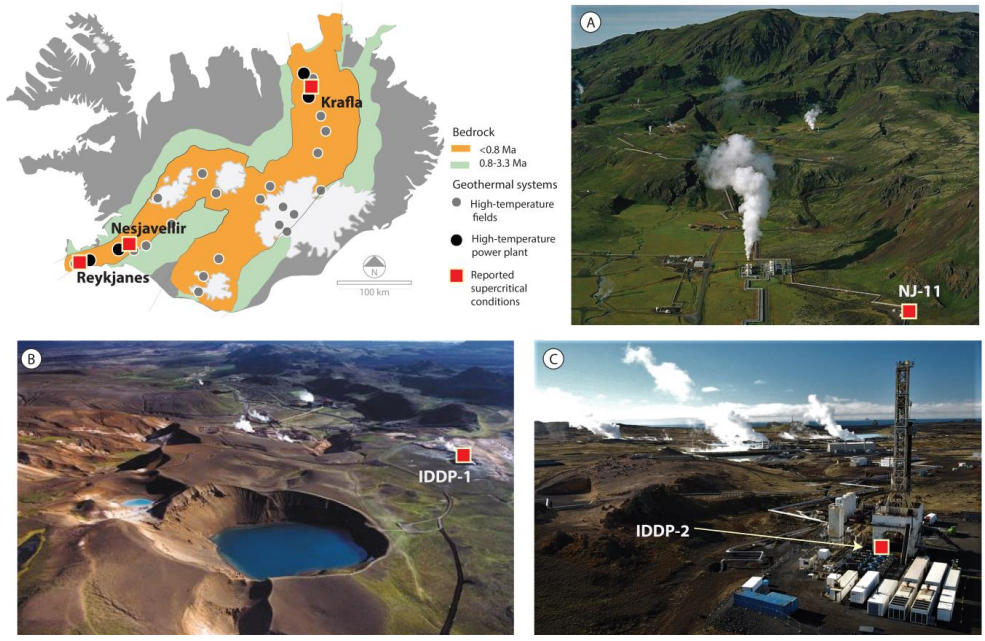

Figure 3 Icelandic high-temperature geothermal fields with reported supercritical conditions. (A) NJ-11 well at the Nesjavellir geothermal power plant (photo courtesy of Mats Wibe Lund), (B) IDDP-1 at the Krafla geothermal power plant (photo modified from Friðleifsson et al., 2014) and (C) the IDDP-2 well at the Reykjanes power plant (modified from Richter, 2019).

1.4 Aims of the study

The primary aims of this study were the following:

- To investigate the fluid chemical and mineralogical changes associated with supercritical fluid formation from conventional subcritical geothermal fluids near a shallow intrusion with emphasis on the IDDP-1 well at Krafla, Iceland, using geochemical modeling. Results have been summarized in the research article I.
- To investigate the chemical and mineralogical changes upon conductive heat addition and consequent boiling of subcritical geothermal fluids to form supercritical geothermal fluids using laboratory experiments. Results have been summarized in the research article II.
- To explore the effects of fluid source on the chemical composition of supercritical fluids using geochemical modeling and laboratory experiments. Results have been summarized in the research article III.

To achieve these aims, hydrological and geochemical modeling were combined to investigate the formation of supercritical fluids from subcritical fluids by conductive heat addition. Furthermore, laboratory experiments were conducted where the chemical and mineralogical changes accompanying supercritical fluid formation were investigated. Finally, the results obtained from modeling, experiments, and natural systems were compared.

2 Methodology

2.1 Field sampling and data collection

To investigate the different geochemical characteristics of subcritical and supercritical fluids, two-phase fluids (subcritical) and single-phase vapor condensates (supercritical) were collected from wells at the Krafla geothermal power plant, NE Iceland (Fig. 4). Fluid samples obtained by the field sampling were the subject of research articles I, II, and III.

Figure 4 Two-phase geothermal wells in the Krafla geothermal field (A) and (B); (C) the IDDP-1 well; D) close-up image of the sampling setup (images are courtesy of Nicole Keller).

Two-phase geothermal fluids were sampled using a Weber separator to separate liquid and vapor phases (Arnórsson et al., 2006). The liquid phase samples were cooled using an in-line cooling coil. Samples for the analysis of major cations (Na, K, Mg, Ca, Si, Al, Na, K, Mg, Fe, B) were filtered and acidified with concentrated HNO_3 on-site. The concentrations were determined using ICP-OES. Samples for the determination of F and Cl were filtered and otherwise left untreated. Samples for SO_4 analysis were filtered, and 2% Zn-acetate solution was added to precipitate the dissolved sulfide as zinc sulfide, leaving dissolved SO_4 in the

solution for analysis. All anions were analysed using ion chromatography. Samples for determination of carbonate plus sulfide alkalinity were collected into amber glass bottles and analyzed using the modified alkalinity titration method, consisting of an acidimetric titration, followed by degassing with N_2 gas and back titration (Arnórsson et al., 2006; Stefánsson et al., 2007). Total dissolved sulfide concentrations were analyzed on-site by titration with mercuric acetate using dithizone as an indicator (Arnórsson et al., 2006). The difference between the two titration results gives carbonate alkalinity. The pH was also determined on-site using a pH meter calibrated with commercial buffer solutions at pH 7 and pH 4, respectively. These analyses were carried out on-site to prevent degassing.

Vapor samples from the subcritical and supercritical discharge were treated similarly. The samples for non-volatile element determination were condensed to form a liquid. These samples were subsequently treated as described above. The volatile elements in the vapor samples were collected in pre-evacuated gas bottles containing 50% KOH, ~15 ml of a base in 100 ml flasks. The concentrations of CO_2 and H_2S in the vapor condensate were determined by a modified alkalinity titration (Stefánsson et al., 2007) and precipitation titration method using Hg acetate and a dithizone indicator (Arnórsson et al., 2006), respectively. The non-condensable gases, including H_2, N_2, Ar, and CH_4 were analyzed by gas chromatography.

2.2 Flow-through experiments

High-temperature flow-through experiments were carried out to reproduce a geothermal system with subcritical and supercritical temperatures (Fig. 5). With these experiments, the formation of both supercritical fluids and associated secondary minerals upon heat addition to subcritical fluids was investigated.

The subcritical conditions were represented by a flow-through reactor filled with basaltic glass and heated to 260°C. Supercritical conditions were simulated in a subsequent flow-through reactor that was heated to 400 or 420°C containing a stainless-steel threaded rod to collect precipitating solids. Absolute pressure was kept constant at 34 and 69 bar during the experiments to maintain subcritical and supercritical conditions in both reactors.

For this work, a total of seven flow-through experiments were carried out (Research articles II and III). The inlet solution used in the experiments was natural geothermal water from Krafla and Spóastaðir. Using a High-Performance Liquid Chromatography (HPLC) pump, the inlet solution was pumped through both the subcritical and supercritical reactor. After passing through the reactors, the fluids were cooled down by an in-line cooling jacket, followed by depressurization using a back-pressure regulator (BPR). The fluids were collected at the low-pressure end of the BPR and subsequently prepared for the analysis of major elements, CO_2, and H_2S following the same routines as described above. At the end of each experiment, the solid deposits from both the subcritical and supercritical reactors were collected, dried at 50°C and mounted on a sample holder. The rod itself was imbedded into epoxy, cut parallel and perpendicular to the flow direction in the reactor, and then polished. The chemical composition of the solids was determined using a scanning microscope (SEM).

In research article II, the flow-through experiments were used to study the formation mechanism and fluid chemistry of supercritical fluids that form upon boiling of subcritical fluids. This was conducted by using geothermal (subcritical) fluids from Krafla as inlet solutions. Here, two interconnected reactors representing subcritical and supercritical conditions, respectively, were used to reproduce the geothermal system. However, the fluids collected from the subcritical reactor were comparable with the concentrations measured in the

inlet solution. Therefore, the sampled geothermal water was directly pumped through the supercritical reactor in subsequent experiments (Fig. 5).

In research article III, the flow-through experiments were carried out to test the effects of the subcritical fluid composition on the supercritical fluid composition. For this purpose, the chemistry of the inlet solutions was varied to represent supercritical fluid formation in (1) young geothermal systems at rift zones with low chloride and low volatile immature water, (2) mature and reacted geothermal systems with fluids containing a low chloride but reacted fluid, and (3) subduction-related geothermal systems with Cl-rich fluids with high volatile gas input, either HCl or CO_2. Results from high-temperature experiments were further compared with reported reservoir fluid compositions from high-temperature geothermal systems in various plate tectonics settings.

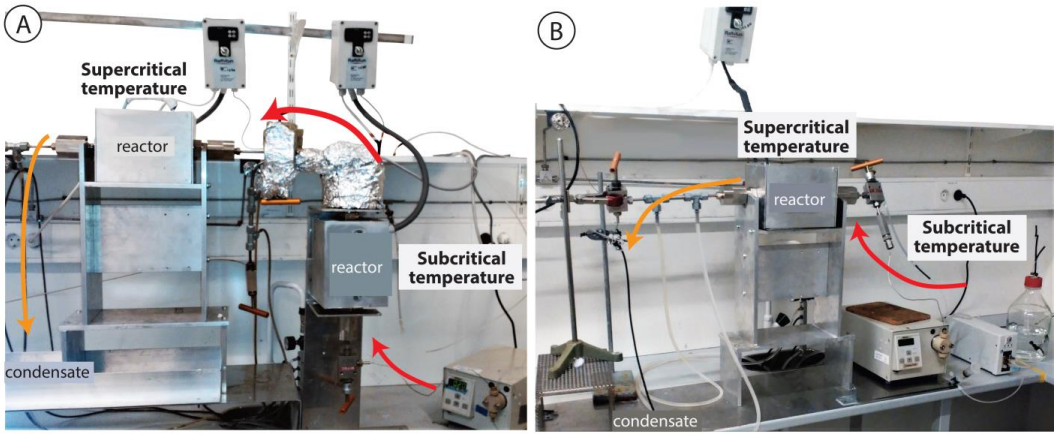

Figure 5 Design of the experimental set-up: (A) two connected flow-through reactors used in research article II; (B) one flow-through reactor used in research article III.

2.3 Hydrological model

The pressure-temperature conditions and fluid flow paths in high-temperature geothermal systems were obtained from hydrological modeling. The modeling was conducted using HYDROTHERM software (Hayba and Ingebritsen, 1994) and the results were presented in the research article I.

The heat transfer and fluid flow above a 2 km deep intrusion of basaltic composition were simulated for a pure H_2O system to reproduce the geothermal system at Krafla. Even though assuming a pure H_2O system is a simplification, since geothermal fluids contain dissolved salts and gases, this is justified as Krafla exhibits fluids with low concentrations of NaCl, and such low NaCl concentrations do not affect the fluid phase distribution and thermodynamic properties of water significantly. The magmatic heat source was treated in a similar simplifying manner. The physical properties of the intrusion used in the HYDROTHERM simulations include an initial temperature (1100°C), density (2900 kg m^{-3}), and temperature-dependent heat capacity, decreasing linearly from 2000 J kg^{-1} K^{-1} at 1100°C to 1000 J kg^{-1} K^{-1} at <850°C to simulate the effect of latent heat of crystallization (Hanson and Barton, 1989; Hayba and Ingebritsen, 1997).

The initial intrusion radius (0.5 km) of the modeled intrusion is large enough to support the development of a boiling geothermal system in an initially 'cold' crust. The initial permeability of basaltic host rock was set to be 10^{-15} m^2, which is close to the permeability estimated for the Krafla geothermal system (Bödvarsson et al., 1984). Simulated permeabilities were temperature-dependent, decreasing from 10^{-15} m^2 to 10^{-22} m^2 at 550°C (Scott et al., 2015). The intrusion was assumed to be emplaced instantaneously, and subsequent heat and mass transfer were simulated as a function of time for 10000 years.

2.4 Geochemical model

Geochemical (multicomponent-multiphase) modeling was carried out to assess supercritical fluid formation and evolution upon ascent to the surface. The geochemical modeling was conducted using PHREEQC (Parkhurst and Appelo, 2013) and WATCH (Bjarnason, 2010) geochemical software.

The model considered two main fluid flow regimes: (1) supercritical fluid formation by conductive heat addition to circulating subcritical geothermal fluids near a subsurface intrusion (research articles I, II and III) and (2) supercritical fluid ascent, condensation and mixing with shallow geothermal fluids (research article I). In scenario 1, the specific enthalpy of a single-phase liquid (i.e., subcritical fluid) was increased at a close to constant pressure. This enthalpy increase would result in boiling of the liquid to complete dryness (supercritical fluid formation). In scenario 2, depressurization of a supercritical fluid at decreasing pressure-enthalpy conditions was simulated, causing condensation of the liquid from the initially single-phase vapor. Subsequently, the condensate was mixed with shallow subcritical geothermal fluids. For the detailed explanation and diagram with the flow paths see section 3.2 and Figure 2 in the research article I.

The model involved the reaction of major components within a given fluid phase and amongst vapor, liquid, and solid phases (i.e., secondary minerals) along specified pressure-temperature-enthalpy paths. Conservation of mass (closed-system behavior) was assumed for isobaric (constant pressure) boiling, whereas an open-system behavior was considered in the case of phase segregation and fluid mixing.

The chemical elements and compounds included in the model were Si, B, Na, K, Ca, Mg, Al, Fe, Cl, F, SO_4 H_2, H_2S, CO_2, and respective aqueous and vapor species. The secondary minerals considered in the calculations were those commonly observed in high-temperature geothermal systems in Iceland and included quartz, chlorites, garnets, amphiboles, clay minerals, epidote, clinozoisite, prehnite, wollastonite, feldspars, zeolites, carbonates, anhydrite and pyrite (Kristmannsdóttir, 1979) and salts (NaCl, KCl, $CaCl_2$, $MgCl_2$, $NaSO_4$, KSO_4). Fluorine content was not considered in fluid-rock interactions. The thermodynamic database used for the calculations was adopted from WATEQ4f (Ball and Nordstrom, 2001) and llnl.dat database (Johnson et al., 2000). The databases included updates of the solubility constants of secondary minerals (Holland and Powell, 1998, 2011; Stefánsson et al., 2011; Leusbrock et al., 2009, 2010a, 2010b) and H_2S and CO_2 gas (Fernández-Prini et al., 2003). The initial fluid compositions, pressure and temperature conditions used in the geochemical model calculations were the same as the corresponding concentrations and conditions used in the experiments.

3 Summary of scientific contribution

The research presented in this dissertation consists of three research articles, one published in *Geothermics* (research article I, reprinted with permission from Elsevier Ltd.), the second published in *Geofluids* (research article II, reprinted with permission from Wiley Hindawi) and the third accepted for publication in *Journal of Volcanology and Geothermal Research* (research article III, reprinted with the permission of Elsevier Science Ltd.).

3.1 Research Article I (Appendix A)

Heřmanská, M., Stefánsson, A., Scott S. 2019. Supercritical fluids around magmatic intrusions: IDDP-1 at Krafla, Iceland, Geothermics 78, 101-110, https://doi.org/10.1016/j.geothermics.2018.11.002.

The first research article focuses on the formation mechanism and chemical composition of supercritical fluids in high-temperature geothermal systems by combining heat transfer and fluid flow modeling using HYDROTHERM software and geochemical modeling using WATCH and PHREEQC software. The modeling results were compared with the chemical composition of subcritical and supercritical (IDDP-1) fluids from Krafla (NE Iceland).

In the article, it is proposed that an important mechanism of such supercritical fluid formation is the conductive heating of surrounding subcritical geothermal fluids near a shallow intrusion. According to the modeling calculations, supercritical fluids formed by isobaric heating of initially liquid geothermal groundwater display similar volatile concentrations (C, S, B, Cl, F) as the initial fluid. In contrast, the low concentrations of non-volatile elements (Si, Na, K, Ca, Mg, Al, Fe) in the supercritical fluid result from intensive, quartz-dominated mineral deposition near the magmatic intrusion during boiling of liquid to dryness. Liquid condensed out of ascending supercritical fluid in the upflow zone has a low pH (~2) due to the dissociation of volatile components like HCl. However, the chemical signatures of supercritical fluid ascent are likely to be overprinted by mixing of the condensing (acid) fluids with cooler subcritical fluids, fluid-rock interaction, depressurization boiling, and phase segregation.

Geothermal reservoir fluids at Krafla had temperatures between ~200 and 440°C, specific enthalpies of 852-3200 kJ kg^{-1}, low Cl concentrations of 0.42-6.61 mmol $kg^{-1,}$ and neutral to alkaline pH of 6.49-9.75. The chemical composition of supercritical fluids discharged by IDDP-1 was characterized by similar concentration of volatile elements (C, S, Cl, F, B) but much lower concentrations of non-volatile elements (Si, Na, K, Ca, Mg) compared to subcritical geothermal reservoir fluids. These similarities between modeled fluid compositions and the measured composition of the IDDP-1 suggest that ~440°C discharged supercritical fluids were formed by heating of circulating geothermal groundwater without significant magmatic fluid input. This is further supported by the volatile element stable isotope composition (i.e., δD, $\delta^{18}O$, $\delta^{13}C$, $\delta^{34}S$, $\delta^{37}Cl$) of the fluids.

3.2 Research Article II (Appendix B)

Heřmanská, M., Kleine, B.I., Stefánsson, A. 2019. Supercritical Fluid Geochemistry in Geothermal Systems. Geofluids 2019, Article ID 6023534, 14 pages; https://doi.org/10.1155/2019/6023534.

The second research article investigated supercritical fluid formation and associated secondary mineral precipitation using laboratory experiments. The experimental results were compared to natural fluid discharge from Krafla including the IDDP-1 fluids and modeling results previously reported in research article I.

Flow-through experiments at 260°C and 400-420°C were performed to study the chemical and mineralogical changes associated with supercritical fluid formation near shallow magmatic intrusions by conductive heating and boiling of conventional subcritical geothermal fluids. Supercritical fluids formed by isobaric heating of liquid geothermal water had similar volatile element concentrations (B, C, and S) as the subcritical water. In contrast, mineral-forming element concentrations (Si, Na, K, Ca, Mg, and Cl) in the supercritical fluid were much lower. The results are consistent with the observed mineral deposition of quartz, aluminum silicates, and the minor amount of salts during boiling. Silica deposits formed upon supercritical fluid formation may result in decreased rock permeability close to the magmatic intrusion. In this respect, the boiling of 1 kg of fluid may lead to the closure of a crack in as soon as a few hours (crack width around 0.01 mm and fluid mass flux 10^{-4} kg m^{-2} s^{-1}) or as long as tens of years (crack width around 0.05 mm and fluid mass flux 10^{-5} kg m^{-2} s^{-1} and slower).

The comparison of the experimental data with measured subcritical and supercritical fluid compositions from Krafla implied that supercritical fluids discharged by the IDDP-1 may have formed by conductive heat addition and boiling of subcritical geothermal fluid. Lower concentrations of Cl and volatile elements of experimental supercritical fluids suggest that fluids discharged from the IDDP-1 well were additionally subjected to minor magmatic degassing.

3.3 Research Article III (Appendix C)

Heřmanská, M., Kleine, B.I., Stefánsson, A. (accepted for publication to Journal of Volcanology and Geothermal Research): Chemical constraints on supercritical fluids in geothermal systems

The third research article describes the effect of fluid source on the chemical composition of supercritical fluids using laboratory experiments and geochemical modeling. This article builds on the results published in the first and second research article. Four scenarios were considered to test the effects of the subcritical geothermal source composition on the supercritical fluids: (1) heating of low chloride and low volatile immature water of meteoric origin typical for young geothermal systems at rift zones, (2) heating of reacted and low chloride water of meteoric origin typical for many reservoir fluids at divergent plate boundaries, and (3 and 4) formation of supercritical fluids from subcritical NaCl fluids containing elevated CO_2 or HCl concentration typical for geothermal reservoir fluids at subduction zones. In summary, similar mineral deposition occurred in all NaCl-dominated experiments with cation (Na-Ca-K)-rich silicates and quartz being the dominant alteration products, accompanied by halite at elevated NaCl fluid concentrations. In contrast, fluids containing high concentrations of acids (HCl)

may result in insignificant mineral deposition upon boiling of subcritical geothermal waters to form supercritical fluids.

Upon supercritical fluid formation by conductive heating of subcritical fluids, the elemental mobility was experimentally observed and predicted by geochemical modeling to be significantly reduced with respect to rock-forming elements like Si, Na, K, Ca, Mg and Al but remained unchanged for volatile element compositions like B, C and S. This suggests that mineral-fluid reactions also control the chemical composition of many major elements in supercritical fluids, which is similar to previous findings for subcritical geothermal fluids. However, such predictions are limited to our knowledge of mineral solubilities in low-density and high-temperature fluids. In fact, available data are restricted to solubility of quartz, common salts such as NaCl, KCl, and $CaCl_2$, and some volcanic gases at these conditions (e.g., Fournier and Potter 1982; Symonds et al., 1992; Leusbrock et al., 2009, 2010a and 2010b).

4 Conclusive remarks and future directions

Volcanic geothermal systems are commonly associated with a magmatic heat source at ~2-6 km depth (Hayba and Ingebritsen, 1997; Stimac et al., 2015). Utilization of such systems typically involves 2-3 km deep boreholes sunk into the geothermal reservoir, discharging liquid and vapor at the surface with subcritical temperatures to produce ~2-5 MW electric power per well (Sanyal and Morrow, 2012; Ketilsson et al., 2015). The conductive heat transfer from the magmatic body to the circulating geothermal water above commonly occurs below the depth of the production wells within the roots of the geothermal systems. Recent studies have suggested that the geothermal fluids occurring at these depths may have temperatures exceeding the critical temperature of water (Hayba and Ingebritsen, 1997; Scott et al., 2015, 2016, 2017). Indeed, such fluid temperatures have been observed in several active geothermal systems worldwide (Reinsch et al., 2017).

Here, the chemical characteristics of such supercritical fluids formed by close to isobaric boiling of subcritical geothermal reservoir fluids were studied. Based on geochemical modeling and laboratory experiments, the following has been concluded:

- Similarities of chemical composition were observed for the IDDP-1 fluids at Krafla (NE Iceland) and those predicted by geochemical modeling and laboratory experiments suggesting the origin of the supercritical IDDP-1 fluid discharges to be the subcritical geothermal reservoir fluids at Krafla.
- Supercritical fluids formed by conductive heating of conventional geothermal groundwater by a magmatic body will be characterized by low concentrations of non-volatile elements (Si, Na, K, Ca, Mg, Fe, Al, Cl) and similar volatile element concentration as the subcritical fluids (B, C, S).
- The concentration of non-volatile elements is controlled by mineral (salts, oxides, silicates, etc.) solubility in supercritical fluids.
- The formation of supercritical fluids from subcritical geothermal fluids results in mineral deposits dominated by silica, aluminum silicates, and, in some cases, salts.
- Similar trends in fluid chemistry and mineralogy occur in the case of supercritical fluid formation in geothermal systems located at rift zones and subduction zones: cation (Na-Ca-K)-rich silicates and quartz dominates alteration products along with halite at elevated NaCl fluid concentrations, whereas fluids that contain high concentrations of acids (HCl) may result in insignificant mineral deposition upon boiling of subcritical geothermal waters to form supercritical fluids.

This work provides insights into the formation of supercritical fluids and associated secondary mineral formation. Nonetheless, many questions remain unanswered, which allow for possible future research directions and initiatives:

- Assuming supercritical fluids are a common phenomenon associated with many active volcanic geothermal systems, what geochemical methods can we apply in order to target such resources for possible drilling?

- The general focus in this study has been on supercritical fluids formed by conductive heating of subcritical geothermal fluids. But what is the role and effect of magmatic gas input knowing that in many volcanic geothermal systems, especially related to subduction zone environments, such gases can be a large part of the fluids? The effect of mixing geothermal fluids with volcanic gas on supercritical fluid composition and associated mineralogical properties remains uncertain.
- Many subcritical geothermal reservoir fluids have elevated salt and gas contents, and the geochemistry of supercritical fluids formed from such complex fluids was not systematically studied here and thus remains unclear.
- The concentrations of many elements in supercritical fluids are likely to be controlled by the respective solubility of minerals in such high-temperature and low-density fluids. However, these remain poorly constrained for most minerals (oxides, many salts, silicates, aluminum silicates, carbonates, sulfides, and sulfates) that limit predictions of supercritical fluid composition using conventional geochemical approaches.

References

Ármannsson, H., Benjamínsson, J., Jeffrey, A.W.A. 1989. Gas changes in the Krafla geothermal system, Iceland. Chemical Geology 76, 175–96.

Ármannsson, H., Fridriksson, Th., Gudfinnsson, G.H., Ólafsson, M., Óskarsson, F., Thorbjörnsson, D. 2014. IDDP – The chemistry of the IDDP-01 well fluids in relation to the geochemistry of the Krafla geothermal system. Geothermics 49, 66–75.

Arnórsson, S., Gunnlaugsson, E., Svavarsson, H. 1983. The Chemistry of Geothermal Waters in Iceland. II. Mineral Equilibria and Independent Variables Controlling Water Compositions. Geochimica et Cosmochimica Acta 47 (3), 547–66, https://doi.org/10.1016/0016-7037(83)90277-6.

Arnórsson, S., Bjarnason, J.Ö., Giroud, N., Gunnarsson, I., Stefánsson, A. 2006. Sampling and Analysis of Geothermal Fluids. Geofluids 6 (3), 203–16, https://doi.org/10.1111/j.1468-8123.2006.00147.x.

Ball, J.W., Nordstrom, D. 2001. User's manual for WATEQ4F with revised thermodynamic database and test cases for calculation speciation of major, trace and redox elements in natural waters. U.S. Geological Survey, Water-Resources Investigation Report, Menlo Park, California.

Bjarnason, J.Ö. 2010. The Chemical Speciation Program WATCH, Version 2.4. Iceland GeoSurvey, Reykjavík, Iceland.

Bödvarsson, G.S., Benson, S.M., Sigurdsson, O., Stefansson, V., Eliasson, E.T. 1984. The Krafla Geothermal Field, Iceland: 1. Analysis of Well Test Data. Water Resources Research 20 (11), 1515–30, https://doi.org/10.1029/WR020i011p01515.

Browne, P.R.L. 1978. Hydrothermal alteration in active geothermal fields. Annual Review of Earth and Planetary Sciences 6, 229–250.

Conti, J., Holtberg, P., Diefenderfer, J., LaRose, A., Turnure, J.T., Westfall, L. 2016. International Energy Outlook 2016 With Projections to 2040. DOE/EIA-0484. Washington, DC, USA: USDOE Energy Information Administration, https://doi.org/10.2172/1296780.

D'Amore, F., Truesdell, A.H., Haizlip, J.R. 1990. Production of HCl by Mineral Reactions in High-Temperature Geothermal Systems. Proceedings, 15th Workshop on Geothermal Reservoir Engineering, 23–25.

Elders, W.A., G.Ó. Friðleifsson, and A. Albertsson. 2014. Drilling into Magma and the Implications of the Iceland Deep Drilling Project (IDDP) for High-Temperature Geothermal Systems Worldwide. Geothermics 49, 111–18, https://doi.org/10.1016/j.geothermics.2013.05.001.

Fernández-Prini, R., Alvarez, J.L., Harvey, A.H. 2003. Henry's Constants and Vapor–Liquid Distribution Constants for Gaseous Solutes in H_2O and D_2O at High Temperatures. Journal of Physical and Chemical Reference Data 32 (2), 903–16, https://doi.org/10.1063/1.1564818.

Fischer, T.P., Chiodini, G. 2015. Volcanic, Magmatic and Hydrothermal Gases. In The Encyclopedia of Volcanoes, edited by Sigurdsson, H., 779–797, Amsterdam, Academic Press, Second Edition, https://doi.org/10.1016/B978-0-12-385938-9.00045-6.

Fournier, R.O., Potter, R.W. 1982. Revised and Expanded Silica (Quartz) Geothermometer. The Geothermal Resources Bulletin 11 (10), Davis, California, United States.

Fournier, R.O. 1985. The Behavior of Silica in Hydrothermal Solutions. Reviews in Economy Geology 2: Geology and Geochemistry of Epithermal Systems, edited by Berger, B.R.,

Bethke, P.M., 1-34, The Economic Geology Publishing, Co., El Paso, https://doi.org/10.5382/Rev.02.03.
Friðleifsson, G.O., Elders, W.A. 2005. The Iceland Deep Drilling Project: A Search for Deep Unconventional Geothermal Resources. Geothermics 34 (3), 269–85, https://doi.org/10.1016/j.geothermics.2004.11.004.
Friðleifsson, G.Ó., Ármannsson, H., Guðmundsson, Á., Árnason, K., Mortensen, A.K., Pálsson, B., Einarsson, G.M. 2014. Site Selection for the Well IDDP-1 at Krafla. Geothermics 49, 9–15. https://doi.org/10.1016/j.geothermics.2013.06.001.
Friðleifsson, G.Ó., Elders, W.A., Zierenberg, R.A., Stefánsson, A., Fowler, A.P.G., Weisenberger, T.B., Harðarson, B.S., Mesfin, K.G. 2017. The Iceland Deep Drilling Project 4.5 Km Deep Well, IDDP-2, in the Seawater-Recharged Reykjanes Geothermal Field in SW Iceland Has Successfully Reached Its Supercritical Target. Scientific Drilling 23, 1–12, https://doi.org/10.5194/sd-23-1-2017.
Giggenbach, W.F. 1981. Geothermal Mineral Equilibria. Geochimica et Cosmochimica Acta 45 (3), 393–410, https://doi.org/10.1016/0016-7037(81)90248-9.
Giggenbach, W.F. 1987. Redox Processes Governing the Chemistry of Fumarolic Gas Discharges from White Island, New Zealand. Applied Geochemistry 2 (2), 143–61, https://doi.org/10.1016/0883-2927(87)90030-8.
Gudmundsson, B.T., Arnórsson, S. 2005. Secondary Mineral–Fluid Equilibria in the Krafla and Námafjall Geothermal Systems, Iceland. Applied Geochemistry 20 (9), 1607–25, https://doi.org/10.1016/j.apgeochem.2005.04.020.
Haar, L., Gallagher, J.S., Kell, G.S. 1984. NBS/NRC Steam Tables Thermodynamic and Transport Properties and Computer Programs for Vapor and Liquid States of Water in SI Units. Hemisphere Publishing, Washington, DC, USA.
Hanson, R.B. 1995. The Hydrodynamics of Contact Metamorphism. GSA Bulletin 107 (5), 595–611.
Hanson, R.B. 1996. Hydrodynamics of Magmatic and Meteoric Fluids in the Vicinity of Granitic Intrusions. In Special Paper 315: The Third Hutton Symposium on the Origin of Granites and Related Rocks, Geological Society of America, 251–59, https://doi.org/10.1130/0-8137-2315-9.251.
Hanson, R.B., Barton, M.D. 1989. Thermal Development of Low-Pressure Metamorphic Belts: Results from Two-Dimensional Numerical Models. Journal of Geophysical Research: Solid Earth 94 (B8), 10363–77, https://doi.org/10.1029/JB094iB08p10363.
Hauksson, T., Markusson S., Einarsson, K., Karlsdóttir, S.N., Einarsson, T., Möller, A., Sigmarsson, T. 2014. Pilot Testing of Handling the Fluids from the IDDP-1 Exploratory Geothermal Well, Krafla, NE Iceland. Geothermics 49, 76–82, https://doi.org/10.1016/j.geothermics.2013.07.003.
Hayba, D.O., Ingebritsen, S.E. 1994. The Computer Model Hydrotherm, a Three-Dimensional Finite-Difference Model to Simulate Ground-Water Flow and Heat Transport in the Temperature Range of 0 to 1,200 Degrees C. USGS Numbered Series 94–4045. Water-Resources Investigations Report. U.S. Geological Survey, 94-4045, Reston, VA, http://pubs.er.usgs.gov/publication/wri944045.
Hayba, D.O., Ingebritsen, S.E. 1997. Multiphase Groundwater Flow near Cooling Plutons. Journal of Geophysical Research: Solid Earth 102 (B6), 12235–52, https://doi.org/10.1029/97JB00552.
Hedenquist, J.W., Lowenstern, J.B. 1994. The Role of Magmas in the Formation of Hydrothermal Ore Deposits. Nature 370 (6490), 519–27, https://doi.org/10.1038/370519a0.

Henley, R.W., Ellis, A.J. 1983. Geothermal Systems Ancient and Modern: A Geochemical Review. Earth-Science Reviews 19 (1), 1–50, https://doi.org/10.1016/0012-8252(83)90075-2.

Heřmanská, M., Stefánsson, A., Scott, S. 2019. Supercritical Fluids around Magmatic Intrusions: IDDP-1 at Krafla, Iceland. Geothermics 78, 101–10, https://doi.org/10.1016/j.geothermics.2018.11.002.

Heřmanská, M., Kleine, B.I., Stefánsson, A. 2019. Supercritical Fluid Geochemistry in Geothermal Systems. Geofluids, 2019, Article ID 6023534, https://doi.org/10.1155/2019/6023534.

Heřmanská, M., Kleine, B.I., Stefánsson, A. Chemical constraints on supercritical fluids in geothermal systems. Accepted for publication to Journal of Volcanology and Geothermal Research in February 2020.

Holland, T.J.B., Powell, R. 1998. An Internally Consistent Thermodynamic Data Set for Phases of Petrological Interest. Journal of Metamorphic Geology 16 (3), 309–43.

Holland, T.J.B., Powell, R. 2011. An Improved and Extended Internally Consistent Thermodynamic Dataset for Phases of Petrological Interest, Involving a New Equation of State for Solids. Journal of Metamorphic Geology 29 (3), 333–83, https://doi.org/10.1111/j.1525-1314.2010.00923.x.

Johnson, J., Anderson, F., Parkhurst, D.L. 2000. Database thermo.com. V8. R6. 230, Lawrence Livermore National Laboratory, Livermore, California.

Ketilsson, J., Pursdóttir, H.þ., Thoroddssen, S., Oddsdóttir, A.L., Bragadóttir, E.R., Gudmunsdóttir, M., Johannesson, G.A. 2015. Legal Framework and National Policy for Geothermal Development in Iceland. Proceedings, World Geothermal Congress 2015, Melbourne, Australia, 19-25 April 2015.

Kristmannsdóttir, H. 1979. Alteration of Basaltic Rocks by Hydrothermal-Activity at 100-300°C. In Developments in Sedimentology, edited by Mortland, M.M., Farmer, V. C., 27, 359–67, International Clay Conference 1978, Elsevier, https://doi.org/10.1016/S0070-4571(08)70732-5.

Kruszewski, M., Wittig, V. 2018. Review of failure modes in supercritical geothermal drilling projects. Geothermal Energy 6, 28. https://doi.org/10.1186/s40517-018-0113-4

Leusbrock, I., Metz, S.J., Rexwinkel, G., Versteeg, G.F. 2009. Solubility of 1:1 Alkali Nitrates and Chlorides in Near-Critical and Supercritical Water. Journal of Chemical and Engineering Data 54 (12), 3215–23, https://doi.org/10.1021/je900175b.

Leusbrock, I., Metz, S.J., Rexwinkel, G., Versteeg, G.F. 2010a. The Solubilities of Phosphate and Sulfate Salts in Supercritical Water. The Journal of Supercritical Fluids 54 (1), 1–8, https://doi.org/10.1016/j.supflu.2010.03.003.

Leusbrock, I., Metz, S.J., Rexwinkel, G., Versteeg, G.F. 2010b. The Solubility of Magnesium Chloride and Calcium Chloride in Near-Critical and Supercritical Water. The Journal of Supercritical Fluids, Selected papers from the 9th International Symposium on Supercritical Fluids (ISSF 2009) - New Trends in Supercritical Fluids: Energy, Materials, Processing, Arcachon, France, May 18-20, 2009, 53 (1), 17–24, https://doi.org/10.1016/j.supflu.2009.12.015.

Liebscher, A., Heinrich, C.A. 2007. Fluid–Fluid Interactions in the Earth's Lithosphere. Reviews in Mineralogy and Geochemistry 65 (1), edited by Liebscher, A., Heinrich, C.A., 1–13, The Mineralogical Society of America, Virginia, USA, https://doi.org/10.2138/rmg.2007.65.1.

Lund, J.W., Boyd, T.L. 2016. Direct Utilization of Geothermal Energy 2015 Worldwide Review. Geothermics 60, 66–93, https://doi.org/10.1016/j.geothermics.2015.11.004.

Óskarsson, F., Fridriksson, þ., Thorbjörnsson, D. 2015. Geochemical Monitoring of the Reykjanes Geothermal Reservoir 2003 to 2013. Proceedings, World Geothermal Congress 2015, Melbourne, Australia, 19-25 April 2015.

Parkhurst, D., Appelo, T. 2013. Description of Input and Examples for PHREEQC Version 3—a Computer Program for Speciation, Batch-Reaction, One-Dimensional Transport, and Inverse Geochemical Calculations. U.S. Geological Survey, Techniques and Methods, book 6, chap. A43.

Pope, E.C., Bird, D.K., Arnórsson, S., Giroud, N. 2015. Hydrology of the Krafla geothermal system, northeast Iceland. Geofluids 16, 175-197.

Reinsch, T., Dobson, P., Asanuma, H., Huenges, E., Poletto, F., Sanjuan, B. 2017. Utilizing Supercritical Geothermal Systems: A Review of Past Ventures and Ongoing Research Activities. Geothermal Energy 5 (16), https://doi.org/10.1186/s40517-017-0075-y.

Reyes A.G., Giggenbach W.F., Saleras J.R.M., Salonga N.D., Vergara M.C. 1993. Petrology and geochemistry of Alto Peak, a vapor-cored hydrothermal system, Leyte Province, Philippines. Geothermics 22, 479-519.

Richter, A. 2019. IDDP – The economics of a plant utilising ultra-high temperature geothermal resources, January 2019. Think GeoEnergy - Geothermal Energy News. Retrieved 2019-10-10, 2019.

Rivera-Diaz, A., Kaya, E., Zarrouk, S.J. 2016. Reinjection in Geothermal Fields − A Worldwide Review Update. Renewable and Sustainable Energy Reviews 53, 105–62, https://doi.org/10.1016/j.rser.2015.07.151.

Sanyal, S.K, Morrow, J.W. 2012. Success and the Learning Curve Effect in Geothermal Well Drilling. Proceedings, 37th Workshop on Geothermal Reservoir Engineering, SGP-TR-194, Stanford, California, Stanford University.

Scott, Samuel, Gunnarsson, I., Arnórsson, S., Stefánsson, A. 2014. Gas Chemistry, Boiling and Phase Segregation in a Geothermal System, Hellisheiði, Iceland. Geochimica et Cosmochimica Acta 124, 170–89, https://doi.org/10.1016/j.gca.2013.09.027.

Scott, S., Driesner, T., Weis, P. 2015. Geologic Controls on Supercritical Geothermal Resources Above Magmatic Intrusions. Nature Communications 6 (1), https://doi.org/10.1038/ncomms8837.

Scott, S., Driesner, T., Weis, P. 2016. The Thermal Structure and Temporal Evolution of High-Enthalpy Geothermal Systems. Geothermics 62, 33–47, https://doi.org/10.1016/j.geothermics.2016.02.004.

Scott, S., Driesner, T., Weis, P. 2017. Boiling and Condensation of Saline Geothermal Fluids Above Magmatic Intrusions: Hydrology of Saline Hydrothermal Systems. Geophysical Research Letters, 44 (4), https://doi.org/10.1002/2016GL071891.

Shinohara, H. 2008. Excess Degassing from Volcanoes and Its Role on Eruptive and Intrusive Activity. Reviews of Geophysics 46 (4). https://doi.org/10.1029/2007RG000244.

Stefánsson, V. 1981. The Krafla geothermal field, Northeast Iceland. In: Geothermal systems: principles and case histories. edited by L. Rybach, L., Muffler, L., 273–294, Wiley and Sons, New York.

Stefánsson, A., Gunnarsson, I., Giroud, N. 2007. New Methods for the Direct Determination of Dissolved Inorganic, Organic and Total Carbon in Natural Waters by Reagent-Free™ Ion Chromatography and Inductively Coupled Plasma Atomic Emission Spectrometry. Analytica Chimica Acta 582 (1), 69–74, https://doi.org/10.1016/j.aca.2006.09.001.

Stefánsson, A., Arnórsson, S., Gunnarsson, I., Kaasalainen, H., Gunnlaugsson, E. 2011. The Geochemistry and Sequestration of H_2S into the Geothermal System at Hellisheiði, Iceland. Journal of Volcanology and Geothermal Research 202 (3), 179–88, https://doi.org/10.1016/j.jvolgeores.2010.12.014.

Steingrímsson, B., Gudmundsson, Á., Franzson, H., Gunnlaugsson, E. 1990. Evidence of a supercritical fluid at depth in the Nesjavellir field. Proceedings, 15th Workshop on Geothermal Reservoir Engineering, 1990, 81–88.

Stimac, J., Goff, F., Goff, C.J. 2015. Intrusion-Related Geothermal Systems. In The Encyclopedia of Volcanoes, edited by Sigurdsson, H., 799–822, Amsterdam, Academic Press, Second Edition, https://doi.org/10.1016/B978-0-12-385938-9.00046-8.

Symonds, R.B., Reed, M.H., Rose, W.I., 1992. Origin, speciation, and fluxes of trace-element gases at Augustine volcano, Alaska: Insights into magma degassing and fumarolic processes. Geochim. Cosmochim. Acta 56 (2), 633-657.

Truesdell, A.H., Haizlip, J.R., Ármannsson, H., D'Amore, F. 1989. Origin and Transport of Chloride in Superheated Geothermal Steam. Geothermics 18 (1–2), 295–304. https://doi.org/10.1016/0375-6505(89)90039-4.

Wallace, P.J. 2005. Volatiles in Subduction Zone Magmas: Concentrations and Fluxes Based on Melt Inclusion and Volcanic Gas Data. Journal of Volcanology and Geothermal Research 140 (1–3), 217–40, https://doi.org/10.1016/j.jvolgeores.2004.07.023.

Þórhallsson S., Bjarni Palsson B, Hólmgeirsson S, Ingason K, Matthíasson M, Bóasson HA, Sverrisson H. Well design and drilling plans of the Iceland Deep Drilling Project (IDDP). In: Proceedings world geothermal congress 2010 Bali, Indonesia, 25–29 April 2010.

Þórhallsson S, Palsson B, Holmgeirsson S, Ingason K, Matthiasson M, Boasson HA, Sverrisson H. Well design for the Iceland Deep Drilling Project (IDDP). Geothermics. 2014;49:16–22.

Appendix A: Research article I

Heřmanská, M., Stefánsson, A., Scott S. 2019. Supercritical fluids around magmatic intrusions: IDDP-1 at Krafla, Iceland, Geothermics 78, 101-110, https://doi.org/10.1016/j.geothermics.2018.11.002.

Reprinted with the permission of Elsevier Science Ltd.

Geothermics 78 (2019) 101–110

Contents lists available at ScienceDirect

Geothermics

journal homepage: www.elsevier.com/locate/geothermics

Supercritical fluids around magmatic intrusions: IDDP-1 at Krafla, Iceland

Matylda Heřmanská[a,*], Andri Stefánsson[a], Samuel Scott[b]

[a] Institute of Earth Sciences, University of Iceland, Sturlugata 7, 101, Reykjavík, Iceland
[b] Department of Science and Engineering, Reykjavík University, Menntavegur 1, 101, Reykjavik, Iceland

ARTICLE INFO

Keywords:
Magma intrusion
Supercritical fluids
Geothermal
Krafla
IDDP-1

ABSTRACT

High-enthalpy supercritical geothermal fluids were obtained from the IDDP-1 well at Krafla, Iceland, which had a discharge temperature of ~440 °C and specific enthalpy of ~3200 kJ kg^{-1}. Utilization of such fluids may multiply power production from geothermal well fields. However, the origin of supercritical fluids in the roots of volcanic geothermal systems is poorly understood. Here, we propose that an important mechanism of such supercritical fluid formation is conductive heating of surrounding subcritical geothermal fluids near a shallow intrusion. Predictions from hydrologic and chemical models of supercritical fluid formation and ascent are compared with measured fluid compositions from the Krafla geothermal system. Supercritical fluids formed by close to isobaric heating of liquid geothermal groundwater display similar volatile concentrations (C, S, B, Cl, F) as the initial fluid. In contrast, the low concentrations of non-volatile elements (Si, Na, K, Ca, Mg, Al, Fe) in the supercritical fluid result from intensive, quartz-dominated mineral deposition near the magmatic intrusion during boiling of liquid to dryness. Liquid condensed out of ascending supercritical fluid has a low pH (~2) due to the dissociation of volatile components like HCl. Such 'acid' geothermal fluids have been encountered in wells in the Krafla system. However, the chemical signatures of supercritical fluid ascent are likely to be overprinted by mixing of the acid fluids with cooler subcritical fluids, fluid-rock interaction, depressurization boiling and phase segregation.

1. Introduction

Many high-enthalpy geothermal systems are associated with shallow subsurface intrusions (e.g., Kato et al., 1993; Elders et al., 2014; Stimac et al., 2015; Reinsch et al., 2017). Supercritical[1] fluids in the close vicinity of the intrusion may form by a combination of groundwater circulation near the intrusion (e.g., Hayba and Ingebritsen, 1997; Scott et al., 2015) and magma degassing (e.g., Kennedy and Truesdell, 1996; Lowenstern et al., 2015; Stefánsson, 2017). The Iceland Deep Drilling Project (IDDP-1) encountered fluids with a temperature of ~440 °C at ~2 km depth during drilling into the Krafla volcanic geothermal system in northeast Iceland (Elders et al., 2014). However, the high gas and silica concentrations in the discharge fluids proved challenging to handle (Hauksson et al., 2014). To enable utilization of such fluids for power production, further research is required into the chemical changes that accompany the formation of supercritical geothermal resources, and particularly the source of acid gases in the produced vapor.

High-enthalpy geothermal fluids may result from phase segregation, conductive heating of groundwater near an intrusion, magma degassing or condensation of liquid out of ascending supercritical fluid. The relatively common 'excess-enthalpy' wells, which feature a much higher discharge specific enthalpy than the initial aquifer fluid, result from phase segregation and retention of liquid in the reservoir rock upon depressurization of the boiling aquifer and two-phase flow towards the wellbore (e.g., Arnórsson et al., 2007; Scott et al., 2014). Although the specific enthalpy of the typical subcritical geothermal fluids corresponds to that of vapor-saturated liquid at temperatures below 300 °C

* Corresponding author.
E-mail address: mattylda@hi.is (M. Heřmanská).

[1] There is considerable disagreement in the geothermal literature about whether the term 'supercritical' applies solely to water with both temperature and pressure above the critical values (T_c = 373.976 °C, P_c = 220.1 bar; Haar et al., 1984), or also includes fluids at temperatures above the critical temperature but pressures below the critical pressure (which are often referred to as 'superheated'). We believe the supercritical/superheated distinction introduces an artificial boundary in the phase diagram of pure water across which there is a continuous change in fluid properties. In this study, we treat the fluid phase relations in the dilute geothermal fluids at Krafla (0.42-6.61 mmol kg^{-1} Cl) as equivalent to those of pure water, and use the term 'supercritical' to describe single-phase vapor with a temperature above the critical temperature. However, in saline fluids, use of the term 'supercritical' is meaningless, as critical behavior occurs along critical curves and raising $T > T_c$ at a given pressure implies fluid phase separation rather than homogenization. See discussion in Liebscher and Heinrich (2007).

https://doi.org/10.1016/j.geothermics.2018.11.002
Received 12 November 2017; Received in revised form 1 November 2018; Accepted 8 November 2018

(< 1500 kJ kg^{-1}), phase segregation may cause such wells to have discharge enthalpies as high as ~2700 kJ kg^{-1}. Supercritical geothermal resources with temperature greater than the critical temperature of pure water (T_c = 373.976 °C; Haar et al., 1984) may form from groundwater circulation near an intrusion and heat conduction across an impermeable rind surrounding the intrusion (Hayba and Ingebritsen, 1997; Scott et al., 2015). Liquid will condense out of ascending supercritical fluids as it depressurizes, and the liquid condensate may correspond to the fluid encountered in so-called 'acid' wells, which generally have reservoir temperatures of ~300-350 °C and discharge specific enthalpies of ~2600–2800 kJ kg^{-1} (Einarsson et al., 2010).

The different processes of high-enthalpy fluid formation display different chemical signatures, as evidenced by fluids obtained from the Krafla geothermal system. Phase segregation reduces the bulk fluid concentration of non-volatile elements in the discharge fluid but increases the bulk fluid concentration of volatile components, compared to the initial subcritical geothermal fluids. While most subcritical fluids at Krafla have near-neutral pH values and Cl concentrations of < 5 mmol kg^{-1}, 'acid' well discharges have up to 5 times higher Cl content and low pH values (~2-3 at 25 °C) because of low alkalinity and dissociation of HCl and/or hydrolysis of SO_2 (Ármannsson et al., 1989; Einarsson et al., 2010). In comparison, the IDDP-1 fluid contained elevated concentrations of some volatile components like CO_2 and H_2S, chloride concentrations of ~3 mmol kg^{-1} and low or non-measurable concentrations of other non-volatile components (Ármannsson et al., 2014). The similarity between the chloride content and isotopic composition of the IDDP-1 fluid to that of normal aquifer fluids (Darling and Ármannsson, 1989, 2014; Pope et al., 2015; Stefánsson et al., 2017a) suggests that the supercritical fluids may originate from meteoric groundwater. While it has long been known that quartz will precipitate during fluid flow near intrusions (e.g., Taylor, 1974; Fournier, 1999; Scott and Driesner, 2018), the precipitation of minerals other than quartz and the geochemical behavior of major components during supercritical fluid formation are not well understood.

In this study, we investigated how phase segregation, conductive heating of subcritical geothermal fluids near a shallow intrusion, and liquid condensation out of ascending supercritical fluids affect the chemical characteristics of the groundwater system. Thermal conditions derived from fluid flow and heat transfer near shallow intrusions were used as inputs for chemical models of fluid chemical composition and mineral precipitation during supercritical fluid formation, ascent and mixing. The results of the model calculations were compared with the physical, chemical and mineralogical observations at Krafla and the IDDP-1 well to determine how these processes interact to control resource characteristics. By combining the physical and chemical properties of the geothermal fluids, one can distinguish between the different processes leading to the formation of various fluid discharges at Krafla and how they affect the fluid chemical composition and the associated alteration mineralogy.

2. Methods

2.1. Geothermal fluid sampling and analysis

Samples of geothermal fluids considered in this study included two-phase well and vapor discharges from the Krafla geothermal system, NE Iceland (Fig. 1). For the two-phase well discharges, liquid and vapor phases were separated using a Webre separator (Arnórsson et al., 2006). For the vapor-only discharges, no such separation was needed. The liquid phase samples were cooled using an in-line cooling coil and then filtered through a 0.2 µm cellulose acetate filter into polypropylene bottles. Samples for major cation analysis were acidified with 0.5 ml concentrated HNO_3 (Suprapur®, Merck) per 100 ml sample and concentrations were determined using ICP-OES (Spectro Ceros Vision). Two samples for major anion analysis were collected: one that was untreated and used for F and Cl concentration determination, and another to which 2% Zn-acetate solution was added to precipitate dissolved sulfide as zinc sulfide leaving dissolved SO_4 in solution for analysis. All anion analyses were carried out using ion chromatography (Dionex ICS-2000). Samples for determination of CO_2 concentrations were collected into amber glass bottles and analyzed using the modified alkalinity titration method (Stefánsson et al., 2007). Dissolved sulfide concentrations and pH were analyzed on-site using H_2S titration (Arnórsson et al., 2006) and a pH electrode calibrated with commercial buffer solutions, respectively. In the case of vapor samples from the IDDP-1 well, samples for non-volatile elements determination were condensed to form a liquid and the various samples subsequently treated and analyzed as for the liquid samples previously described.

For determination of the volatile element concentration in vapor samples, samples were collected into pre-evacuated gas-bottles containing 50% KOH (~10 ml in 100 ml). The concentrations of CO_2 and H_2S in the vapor condensate were determined by modified alkalinity titration (Stefánsson et al., 2007) and a precipitation titration method using Hg-acetate and dithizone indicator (Arnórsson et al., 2006), respectively. The non-condensable gases, including H_2, N_2, Ar and CH_4, were analyzed by gas chromatography (GC-2010 Plus, Schimadzu).

The analytical precision for all major elements based on duplicate determination was found to be < 3% at the 95% confidence level and for pH < ± 0.05.

2.2. HYDROTHERM modeling

Heat transfer and fluid flow above a 2 km deep intrusion were simulated using the HYDROTHERM program (Hayba and Ingebritsen, 1994) for a pure H_2O system. This is a simplification, since the fluid contains dissolved salts and gases; however, the system considered here is predominantly dilute (< 0.42–6.61 mmol kg^{-1} Cl) and we assume that the low concentrations of NaCl do not affect the fluid phase relationships or thermodynamic properties (notably, specific enthalpy and density). The magmatic heat source was also treated in a simplified way. Although the IDDP-1 well intersected a rhyolitic intrusion (Elders et al., 2011; Zierenberg et al., 2013), values that are appropriate for basaltic rock were used in the HYDROTHERM simulations. We base this assumption on the model that rhyolite forms by remelting of hydrothermally altered granophyre or altered crust of basaltic origin near the roof of a larger basaltic intrusion (Jónasson, 1994). Additionally, basaltic melt is also observed in most geothermal systems linked to divergent boundaries. The physical properties of the intrusion used in the HYDROTHERM simulations are listed in Table 1 and include initial temperature (1100 °C), density (2900 kg m^{-3}), and temperature-dependent heat capacity (decreasing linearly from 2000 J kg^{-1} K^{-1} at 1100 °C to 1000 J kg^{-1} K^{-1} at < 850 °C to simulate the effect of latent heat of crystallization; Hanson and Barton, 1989; Hayba and Ingebritsen, 1997) The initial intrusion radius (0.5 km) of the modeled intrusion is large enough to support the development of a boiling geothermal system in initially 'cold' crust. The intrusion was assumed to be emplaced instantaneously, and subsequent heat and mass transfer were simulated as a function of time for 10000 years.

Fluid pressure and temperature were fixed at the ground surface at 1.02 bar and 20 °C, respectively. The lateral boundaries located 8.5 km from the intrusion assumed a Dirichlet fluid pressure boundary condition (no-flow). The bottom boundary was also set to be a no-flow boundary, with a constant heat flux of 60 mW m^{-2} into the basement and 120 mW m^{-2} into the intrusion. The initial permeability of the geothermal system was set to be 10^{-15} m^2, which is close to the permeability estimated for the Krafla geothermal system (Bodvarsson et al., 1984). Permeability in our simulation was temperature-dependent, decreasing from 10^{-15} m^2 to 10^{-22} m^2 at 550 °C (Scott et al., 2015).

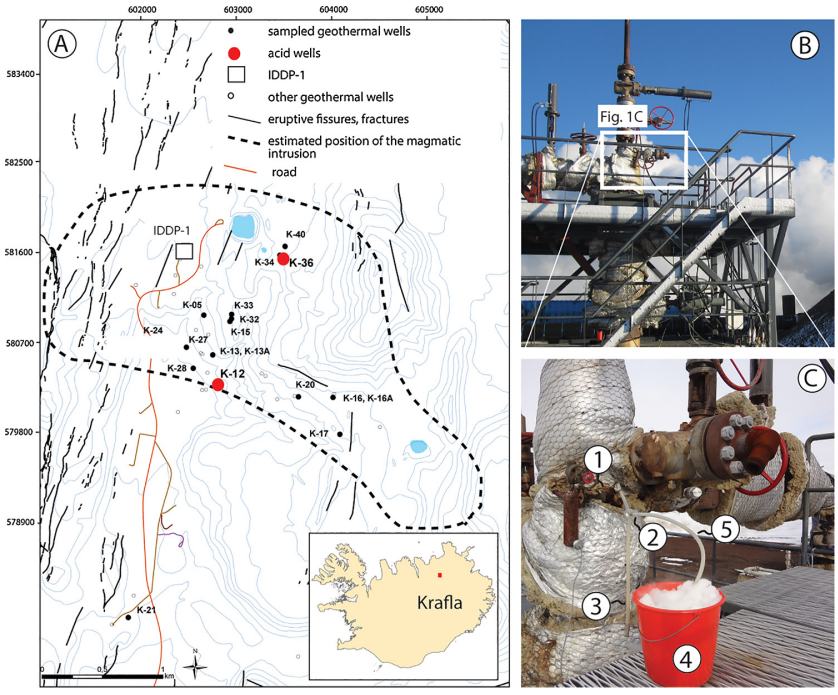

Fig. 1. The Krafla geothermal field and the IDDP-1 well. a) Map of the Krafla geothermal field showing sampled wells (IDDP-1 shown as white box and the acid wells shown as red circles), eruptive fissures and fractures based on Hjartardóttir et al. (2012), with suggested location of the magmatic intrusion, topography (10 m contour) and road. The area of the magmatic intrusion/chamber is defined based on the interpretation of S-wave velocities at depths between 3–7 km, as described in Einarsson (1978). Circles show the locations of wellheads. Most of the wells are vertical, except for KJ-36. However, the location of the bottom of this well is still within the expected upflow zone of the geothermal system. b) Picture of IDDP-1 well-head at Krafla. The white box shows the area depicted in sub-figure c. c) Sampling apparatus for collecting single-phase vapor discharges from IDDP-1 well head (1-sample valve, 2-tee, 3-check valve, 4-bucket with cooling water, 5-silicon tube). (For interpretation of the references to colour in this figure legend, the reader is referred to the web version of this article).

Table 1
Thermal rock properties used in HYDROTHERM simulations [a].

Properties	Units	Intrusion basalt	Host rock
Initial temperature	°C	1100	*f* (depth)
Rock density	kg m^{-3}	2900	2500
Thermal conductivity	W m^{-1} K^{-1}	1	2
Specific heat	J kg^{-1} K^{-1}	*f*(*t*)	1000
Porosity	%	0.05	0.1

[a] Based on Hayba and Ingebritsen (1997) with modifications by Hanson and Barton (1989).

2.3. Multicomponent-multiphase geochemical modeling

Based on the heat and mass transfer modeling, schematic pressure-temperature-enthalpy (*P-T-h*) paths along selected flow vectors within the geothermal system were assessed and used as input conditions for multicomponent-multiphase geochemical modeling. Two main flow regimes were considered: (1) supercritical fluid formation by conductive heat addition to circulating geothermal groundwater near a subsurface intrusion and (2) supercritical fluid ascent, condensation and mixing with shallower geothermal fluids. The former scenario increases the specific enthalpy of single-phase liquid at a constant temperature and pressure, eventually resulting in boiling of the liquid to dryness (supercritical fluid formation). The latter scenario involves depressurization of supercritical fluid at a constant temperature, causing liquid to condense out of the initially single-phase vapor, followed by variable mixing with shallower subcritical geothermal fluids.

For the multicomponent-multiphase geochemical modeling, major components react within a given fluid phase and between the vapor, liquid, and solid phases along the specified *P-T-h* path, assuming conservation of mass (closed-system behavior) for isobaric boiling and open system behavior in case of phase segregation and fluid mixing. The elements and compounds included in the calculations were Si, B, Na, K, Ca, Mg, Al, Fe, Cl, F, H_2, H_2S, and CO_2 and respective aqueous and vapor species and minerals included in the updated WATEQ4f database (Ball and Nordstrom, 1991). The secondary minerals considered here were those typically associated with high-temperature geothermal systems in Iceland (e.g., Kristmannsdóttir, 1979), including quartz, clinochlore, daphnite, epidote, clinozoesite, prehnite, grossular, wollastonite, low-albite, microcline, wairakite, calcite, actinolite, magnetite, and pyrite.

Table 2
Chemical composition of IDDP-1 fluid discharge obtained in the present study. Units are in mmol. kg^{-1}.

Sample	12-KRA-01	12-KRA-02	12-KRA-03
Location	Wellhead	Wellhead	Wellhead
h (kJ kg^{-1})	3200 [b]	3200 [b]	3200 [b]
p (bars)	140 [b]	140 [b]	140 [b]
T (°C)	440	440	440
pH/°C [a]	2.65/17	2.58/19	2.25/21
SiO_2	0.137	0.063	0.095
B	0.099	0.149	0.140
Na	0.019	0.010	0.035
K	5.24E-03	2.89E03	1.43E-03
Ca	8.48E-03	2.50E-03	2.25E-03
Mg	2.06E-03	8.23E-04	4.11E-04
Fe	0.041	0.194	0.046
Al	3.71E-03	2.22E-03	1.11E-03
Cl	2.25	3.32	3.34
F	0.590	0.774	0.700
CO_2	47.9	29.8	34.1
SO_4	0.44	0.28	0.29
H_2S	19.6	18.1	17.9
SO_2	< 0.008	< 0.008	< 0.008
S_{TOT}	20.0	18.4	18.2
H_2	9.69	7.57	7.57
N_2	7.00	30.9	27.8
Ar	0.120	0.448	0.416
CH_4	0.036	0.055	0.040

[a] pH of condensed vapor.
[b] Ingason et al. (2014).

Table 3
Chemical composition of the two-phase well discharges collected in the Krafla geothermal system. Concentration units are in mmol kg^{-1}.

sample #	Well #	date	source[a]	T^s [b]	T^{res} [c]	p^{sample}	h	Liquid phase																Vapor phase	
				°C		bar	kJ/kg	pH	/	°C	SiO_2	B	Na	K	Ca	Mg	Fe	Al	Cl	F	CO_2	SO_4	H_2S	H_2	CO_2	H_2S
97-3098	K-21	25.10.97	[1]	208	251	18.5	1739	8.71	/	21	9.07	0.063	6.21	0.510	0.030	3.00E-04	4.00E-04	0.054	1.61	0.051	0.80	0.720	1.95	14.3	110	19.4
97-3099	K-14	25.10.97	[1]	173	245	8.5	2267	8.78	/	20	9.32	0.238	6.84	0.530	0.030	2.00E-04	2.70E-04	0.042	1.00	0.091	3.01	0.470	1.26	31.1	317	32.0
97-3102	K-13	26.10.97	[1]	192	233	13.2	1551	8.60	/	21	7.38	0.097	12.16	0.800	0.150	2.00E-04	3.70E-04	0.043	0.43	0.045	1.16	4.67	1.83	20.5	228	27.2
97-3103	K-28	26.10.97	[1]	162	235	6.5	1015	9.75	/	21	7.98	0.046	9.66	0.660	0.100	1.00E-04	1.50E-04	0.039	0.49	0.048	0.70	2.99	1.08	1.00	64.0	2.50
97-3104	K-15	26.10.97	[1]	187	283	11.7	1790	8.99	/	19	13.3	0.180	8.97	0.980	0.040	2.00E-04	2.10E-04	0.075	0.69	0.083	0.99	2.07	2.43	21.2	250	37.5
98-3201	K-21	23.06.98	[1]	198	250	14.9	1698	8.88	/	25	9.03	0.057	6.22	0.490	0.010	2.00E-04	6.70E-04	0.051	2.11	0.051	0.57	1.40	0.740	15.9	178	29.0
98-3205	K-5	24.06.98	[1]	123	207	2.2	1038	9.67	/	23	6.12	0.050	8.49	0.460	0.110	4.00E-04	1.00E-04	0.032	0.80	0.052	0.68	2.72	0.970	4.40	66.0	6.20
98-3207	K-13	24.06.98	[1]	186	226	11.5	1658	8.16	/	24	6.85	0.098	11.91	0.770	0.130	1.00E-04	1.00E-04	0.038	0.62	0.039	1.57	5.46	1.90	29.4	204	25.0
98-3208	K-24	25.06.98	[1]	125	209	2.3	938	9.73	/	24	6.04	0.045	9.48	0.440	0.090		6.00E-05	0.031	0.86	0.040	0.41	3.29	0.850	0.200	59.0	7.40
04-3009	K-21	20.10.04	[2]	198	243	15	1167	8.58	/	18	8.35	0.056	6.52	0.506	0.030	3.29E-05	6.27E-05	0.056	2.04	0.054	1.13	0.697	1.82	5.26	97	7.20
04-3010	K-13	20.10.04	[2]	200	230	15.5	1941	8.34	/	18	7.19	0.083	10.61	0.680	0.112	6.99E-05	7.16E-05	0.043	0.90	0.049	1.54	3.16	2.13	47.0	158	11.90
04-3012	K-34	20.10.04	[2]	206	251	17.5	2636	7.24	/	19	9.22	0.064	7.05	0.785	0.029	1.52E-04	2.45E-04	0.046	2.81	0.071	2.06	0.463	2.61	110	413	27.60
04-3014	K-32	20.10.04	[2]	197	295	14.5	1910	8.40	/	19	14.4	0.150	10.22	1.379	0.039	3.70E-05	3.94E-05	0.062	4.17	0.073	0.41	1.74	2.63	24.4	80	24.20
04-3015	K-15	20.10.04	[2]	197	275	14.5	1499	8.68	/	18	12.1	0.104	9.66	1.000	0.051	2.06E-05	2.15E-05	0.070	1.03	0.067	0.36	2.58	2.73	11.7	58.0	12.60
04-3019	K-20	21.10.04	[2]	184		11	2543	7.80	/	18	14.3	0.201	11.27	1.340	0.049	6.58E-05	3.94E-05	0.040	6.40	0.067	3.59	0.060	2.21	41.5	437	25.80
04-3021	K-17	21.10.04	[2]	231	278	28.5	2547	7.88	/	19	10.9	0.126	5.13	0.506	0.005	1.23E-05	3.04E-05	0.071	0.42	0.097	1.58	0.049	3.18	32.2	166	18.90
04-3022	K-16	21.10.04	[2]	184	262	11	2451	7.36	/	19	11.0	0.160	8.44	0.839	0.022	8.23E-05	6.80E-05	0.038	3.76	0.11	3.62	0.129	1.82	78.3	600	32.20
04-3023	K-24	21.10.04	[2]	132	216	2.9	887	9.29	/	17	6.34	0.051	9.61	0.448	0.089	2.88E-05	4.83E-05	0.032	1.29	0.043	0.46	2.51	0.930	0.350	24	3.40
11-KRA-01	K-17	15.10.11	[2]	207	263	18.0	2399	8.80	/	23	10.7	0.127	5.61	0.523	0.007	3.66E-04	4.79E-04	0.055	0.51	0.096	1.91	0.056	2.99	22.9	102	24.1
11-KRA-02	K-16A	15.10.11	[2]	182	251	10.5	2660	7.35	/	24	10.9	0.185	8.45	0.811	0.021	1.48E-04	5.10E-04	0.039	3.88	0.093	5.23	0.113	2.11	35.1	482	39.0
11-KRA-04	K-32	16.10.11	[2]	178	241	9.5	1468	9.12	/	18	8.81	0.059	11.30	1.035	0.076	2.59E-04	1.23E-04	0.054	1.18	0.061	1.36	2.91	3.03	12.6	57.0	23.5
11-KRA-05	K-33	16.10.11	[2]	173		8.5	2769	8.42	/	19	12.9	0.271	7.01	0.734	0.019	1.56E-04	4.49E-04	0.016	2.75	0.099	3.69	0.076	3.53	27.0	75.8	45.6
11-KRA-06	K-20	17.10.11	[2]	182		10.5	2776	8.25	/	17	15.0	0.305	12.09	1.277	0.038	3.38E-04	2.73E-04	0.008	6.61	0.090	4.48	0.053	2.84	34.7	389	40.4
11-KRA-08	K-24	18.10.11	[2]	138	213	3.4	852	9.59	/	18	6.11	0.056	8.85	0.422	0.068	1.60E-03	2.09E-04	0.028	1.25	0.041	1.04	2.32	0.832	0.242	43.9	1.28
11-KRA-09	K-13A	18.10.11	[2]	170	228	8.0	1553	9.08	/	15	7.55	0.092	9.85	0.644	0.086	2.53E-04	2.82E-04	0.043	1.09	0.058	1.31	2.73	2.01	17.6	67.6	18.4
11-KRA-10	K-21	18.10.11	[2]	180	244	10.0	1058	8.90	/	21	8.54	0.068	7.52	0.589	0.033	7.41E-05	1.79E-04	0.049	3.80	0.049	1.23	0.569	1.23	6.54	67.7	11.7
11-KRA-11	K-5	19.10.11	[2]	138	205	3.4	998	9.22	/	16	5.84	0.055	8.82	0.456	0.076	1.00E-03	2.17E-04	0.032	1.17	0.051	1.16	2.27	0.810	1.07	20.3	5.16
11-KRA-12	K-27	19.10.11	[2]	186	229	11.5	1370	9.25	/	15	7.58	0.055	8.96	0.696	0.065	7.17E-04	3.23E-03	0.054	1.07	0.052	1.30	2.62	1.26	3.24	43.2	6.86
11-KRA-16	K-40	20.10.11	[2]	184	199	11.0	2774	6.49	/	9	8.65	0.262	3.72	0.387	0.053	2.01E-03	4.30E-04	0.054	0.58	0.085	21.0	0.208	0.963	8.70	473	30.4
11-KRA-17	K-34	20.10.11	[2]	206	247	17.5	2763	7.27	/	9	9.85	0.463	7.64	0.778	0.043	3.40E-04	5.37E-04	0.035	4.43	0.079	1.59	0.543	1.85	25.1	246	53.9
KJ-36	KJ-36	19.01.08	[3]	147		4.35	2803	3.96	/	22	5.98	0.294	9.57	2.26	1.11	9.1E-02	5.23	0.009	25.0	0.174	191	0.302	39.8	13.8		
KG-12 1979	KG-12	1979	[4]	170		7.9	2776	3.48	/	19	0.47	0.043	0.01		0.011	1.6E-03	0.47		3.16	0.013				22.1	0.39	33.1
KJ-36-2007	KJ-36	2007	[4]	175		9	2676	3.30	/	21									11.3	0.421		0.068		16.3	147	97.4

[a] Source of data: [1] Gudmundsson and Arnórsson (2005); [2] This study; [3] Einarsson et al. (2010); [4] Ármannsson et al. (2014).
[b] T^s = sampling temperature.
[c] T^{res} = reservoir temperature calculated assuming quartz equilibrium and with the aid of the WATCH program (Bjarnason, 2010).

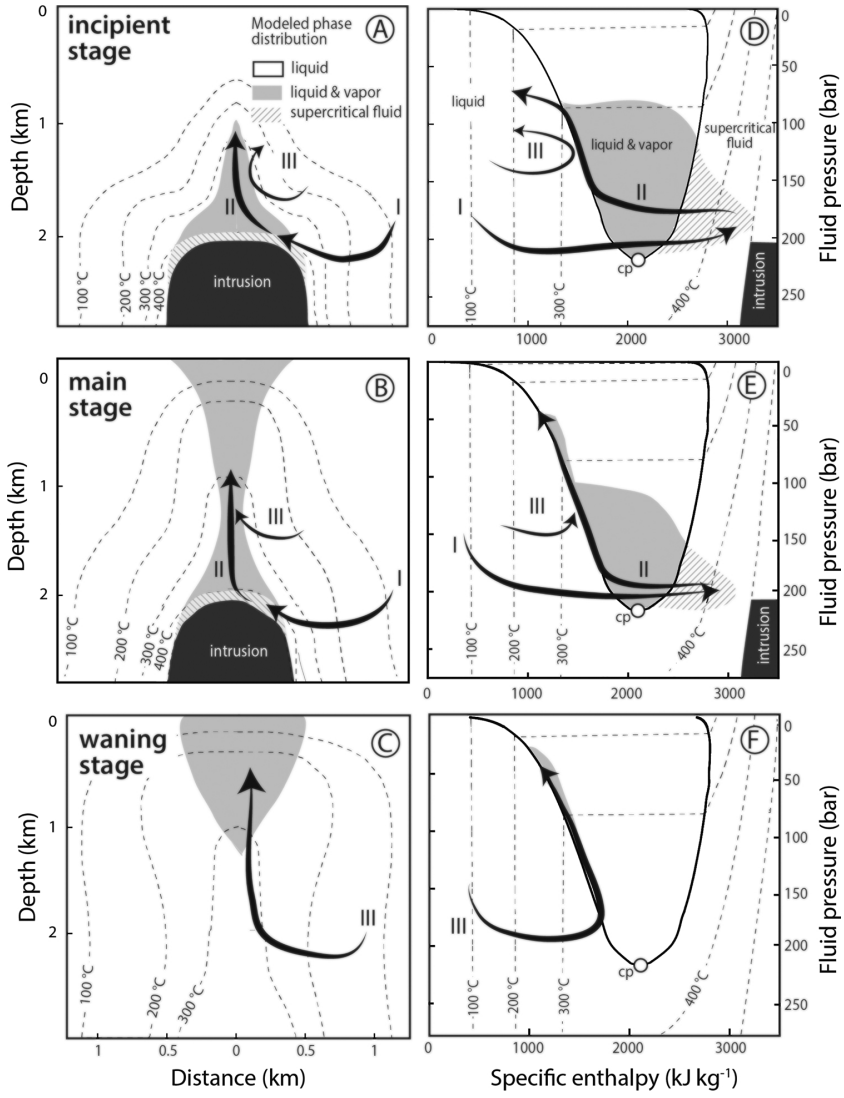

Fig. 2. (a–c) The evolution of high-enthalpy geothermal system with time, divided into incipient, main and waning stage (Scott et al., 2016). Fluid dynamics in the system are indicated with thick black arrows and further divided into 3 possible fluid paths: (Path **I**) supercritical fluid formation, **(II)** shallow convection and (**III**) mixing. For further description of the simulations and interpretation, see text. (d–f) The corresponding pressure-enthalpy trajectory along these main flow vectors is presented with thick black lines. Coexisting phases for a given time highlighted with white, grey and dashed lines.

The calculations were conducted using the WATCH and PHREEQC geochemical programs (Bjarnason, 2010; Parkhurst and Appelo, 1999). The thermodynamic database used for the calculations was adopted from WATEQ4f (Ball and Nordstrom, 1991) with updates of the solubilities of secondary minerals (Stefánsson et al., 2011). Moreover, the solubilities of H_2, H_2S and CO_2 were calculated based on Fernández-Prini et al. (2003), whereas HCl and HF were assumed to enter the vapor phase upon complete boiling via ion association.

3. Results

3.1. Chemical composition of thermal fluids

The chemical composition of two-phase well discharges and IDDP-1 at Krafla are listed in Tables 2 and 3, respectively. The data include those obtained in this study and previously reported (Gudmundsson and Arnórsson, 2005; Einarsson et al., 2010; Ármannsson et al., 2014).

Reservoir temperatures calculated using the quartz geothermometer (Gunnarsson and Arnórsson, 2000) and measured downhole were 198.8–440 °C (Ingason et al., 2014), and the measured discharge enthalpies 852–3200 kJ kg^{-1}. The average discharged liquid at Krafla was generally dilute with Cl concentrations of 0.42-6.61 mmol kg^{-1} and neutral to alkaline pH of 6.49-9.75. However, some well discharges (KJ-36, KG-12) had higher Cl concentrations of 4.26-25.0 mmol kg^{-1} and acid pH values of 3.30-3.96. A considerable range was also observed for other major elements including SiO_2, CO_2 and H_2S between wells at Krafla.

The chemical composition of supercritical fluids discharged by IDDP-1 was characterized by elevated concentrations of volatile elements including CO_2, H_2S, Cl, F and B (Table 2). In contrast, the

Table 4
Comparison of measured and modeled geothermal fluids at Krafla. Concentration is in mmol. kg^{-1}.

	Average measured subcritical fluid Krafla	Average measured IDDP-1*	Modeled Supercritical fluid*	Measured acid fluid (KJ-36)	Modeled condesing supercritical fluid		Mixing of the subcritical fluid (99 wt. %) with 1 wt % of	
					1 wt % cond.	10 wt % cond.	condensed supercritical fluids (liquid)	supercritical fluids (total composition)
t°C	295	440	295	147	340	340	295	295
pH	7.10	–	–	3.96	0.823	1.64	7.04	7.05
SiO_2	10.0	9.84.E-02	5.29.E-02	5.98	0.803	9.75.E-02	9.89	9.89
B	0.129	0.129	0.129	0.294	12.5	1.52	0.253	0.129
Na	7.48	2.16.E-02	7.31	9.57	2.10	0.255	7.43	7.41
K	0.870	3.19.E-03	0.814	2.26	0.445	5.40.E-02	0.865	0.861
Ca	2.74.E-02	4.41.E-03	4.96.E-06	1.11	0.434	5.26.E-02	3.15.E-02	2.72.E-02
Mg	8.23.E-05	1.10.E-03	5.92.E-08	9.09.E-02	0.119	1.44.E-02	1.27.E-03	9.24.E-05
Fe	1.79.E-04	9.36.E-02	7.28.E-05	5.23	4.15	0.503	4.17.E-02	1.11.E-03
Al	4.08.E-02	2.35.E-03	1.62.E-05	8.93.E-03	2.50.E-02	3.04.E-03	4.06.E-02	4.04.E-02
Cl	3.10	2.97	3.09	25.0	286	34.7	5.93	3.10
F	7.90.E-02	0.688	7.85.E-02	0.174	66.6	8.08	0.744	8.50.E-02
CO_2	37.0	37.2	37.0	191	2.35	2.53	36.7	37.0
SO_4	4.37E-02	0.337	4.34.E-02	0.302	16.1	1.95	0.204	4.67.E-02
H_2S	11.6	18.5	11.6	39.9	2.41	2.57	11.5	11.7
H_2	5.95	8.28	–	13.8	0	0	5.89	5.98

* pH was not calculated in the case of supercritical fluids.

concentration of non-volatile elements like Na, K, Ca, Mg, Al and Fe was low, < 0.05 mmol kg^{-1} in all cases. Silica differs as it was found in considerable concentrations of 0.08-0.3 mmol kg^{-1} relative to the other non-volatile elements, but still in much lower concentrations than for liquid phase samples of two-phase well discharges.

3.2. Principal flow paths in geothermal systems

Fluid flow patterns near subsurface intrusions change over time (Fig. 2). Scott et al. (2016) proposed that magma-driven geothermal systems pass through a three-stage temporal evolution, consisting of the incipient, main and waning stages. During the incipient stage of a geothermal system, supercritical fluids around the intrusion are overlain by deep boiling zones restricted to depths > 1 km and relatively cool liquid at shallower depths (Fig. 2a). The boiling zones may extend to the surface during the main stage (Fig. 2b). During the waning stage, supercritical fluid is not present anymore around the cooled heat source, and the geothermal reservoir consists of convecting liquid at depth with depressurization boiling restricted to shallow levels (Fig. 2c).

The simulations reveal three principal flow paths, which can be described in terms of *P-T-h* changes (Fig. 2d-f):

(1) Path **I**: Supercritical fluid formation: liquid circulating near the intrusion is heated to supercritical temperatures as a result of conductive heat transfer across the boundary of the impermeable intrusion (shown in black)

(2) Path **II**: Liquid condensation out of ascending, depressurizing supercritical fluid and mixing with shallower geothermal fluids

(3) Path **III**: Convection of shallow geothermal fluids not heated to supercritical conditions, followed by depressurization boiling at shallow depths.

While paths **I** and **II** are only present in incipient and main stages of the development of geothermal systems (Fig. 2d, e), path **III** is observed in all three stages.

3.3. Fluid composition and secondary mineralization during supercritical fluid formation

The initial fluid compositions for the geochemical modeling corresponds to that of typical liquid reservoir fluids (used for the modeling of supercritical fluid formation) and supercritical fluids (modeling of supercritical fluid condensation) at Krafla. The former was based on the average composition of fluid discharges with liquid-dominated specific enthalpy < 1500 kJ kg^{-1} (Table 3) and the latter type was similar to IDDP-1 well discharge fluid. The compositions are shown in Table 4.

The calculated concentrations of non-volatile (SiO_2) and volatile (CO_2) components during supercritical fluid formation (Path **I**) are shown in Fig. 3 and compared with Krafla well discharges and expected trends resulting from phase segregation (Path **I**). During isobaric conductive heating, the vapor fraction grows linearly as bulk fluid specific enthalpy increases from that of a typical subcritical geothermal fluid at 300 °C (black star, Fig. 3a) to that of the IDDP-1 discharge fluid (black square). The concentration of silica in the bulk fluid is nearly constant up to a bulk fluid specific enthalpy of 2000 kJ kg^{-1}, but is strongly reduced by precipitation of quartz and other silicate minerals at higher fluid specific enthalpies (solid line, Fig. 3a). Boiling and phase segregation (loss of liquid) generate a linear decrease in bulk fluid SiO_2 concentrations with increasing bulk fluid specific enthalpy (dashed line). Krafla discharge fluids show nearly constant SiO_2 concentrations up to a specific enthalpy of ~2000 kJ kg^{-1}, as predicted for the early stages of conductive heating. However, in fluids with a specific enthalpy above ~2000 kJ kg^{-1}, bulk fluid SiO_2 concentration decreases with increasing specific enthalpy, corresponding to the expected trend from phase segregation.

The bulk fluid concentrations of volatile components such as CO_2 remain constant during isobaric conductive heating (Fig. 3b, solid line) due to partitioning of volatile components into the vapor phase and undersaturation of carbonate minerals in the liquid in this particular case. However, phase segregation increases the bulk fluid volatile concentrations with increasing fluid specific enthalpy by increasing the vapor fraction of the discharge fluid (Fig. 3b, dashed line). While the low and nearly-constant concentrations of CO_2 in the Krafla discharge fluids with specific enthalpies < 2000 kJ kg^{-1} resemble the models of conductive heating, the measured fluid compositions for higher specific enthalpy wells more closely match the phase segregation trend.

Fig. 4 shows the secondary mineralogy formed during conductive heating and supercritical fluid formation. Initially, liquid is at equilibrium with a typical propylitic alteration mineral assemblage, including quartz, calcite, pyrite, epidote, chlorite, albite and prehnite. As vapor fraction increases with increasing bulk fluid specific enthalpy, non-volatile elements including Si, Ca, and Al concentrate in the liquid phase, and are eventually lost to secondary minerals (Fig. 4a). Secondary minerals are not formed from volatile components including CO_2 and H_2, which partition into the vapor phase during heating, and

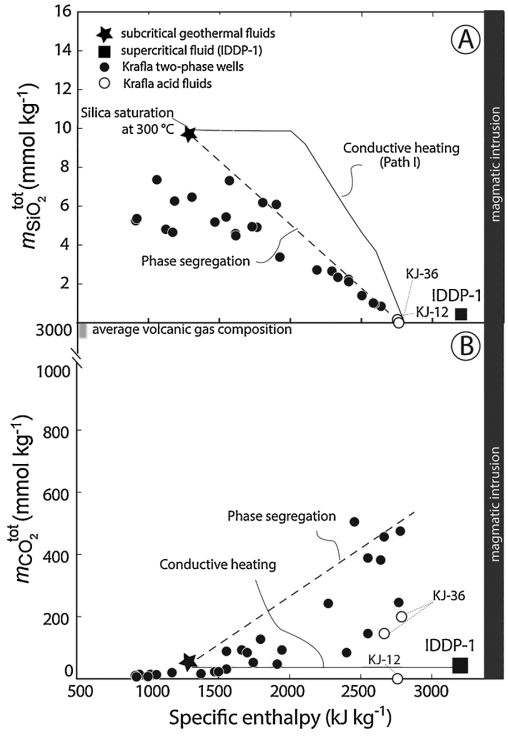

Fig. 3. The effect of heat addition on concentrations of a) non-volatile components (SiO_2) and b) volatile components (CO_2) during supercritical fluid formation compared to bulk fluid concentrations in samples obtained from the Krafla geothermal field (black circles) and acid fluids (white circles), recalculated from samples listed in Table 3 using conservation equations for mass and enthalpy (Arnórsson et al., 2007). Model calculations for a typical liquid reservoir at 300 °C (star) are shown with black lines. Expected trends given phase segregation are shown with dashed lines. The calculated vapor mass fraction (X^{vap}) increases linearly from 0 to 1 with increasing enthalpy in the two-phase region. The SiO_2 and CO_2 concentrations in the IDDP-1 discharge fluid (Table 4) are shown with a large black squares. The concentration of CO_2 in volcanic gases presented here is an average value from data published in Sigvaldason and Elíasson (1968), Shinohara (2008) and references therein. Note that the specific enthalpy of volcanic gases is not specified.

conservative (non-reactive) elements such as B, F and Cl, which only enter the vapor phase once the fluid has been boiled to dryness. The secondary mineralogy shows a zonation with progressive heating and increasing vapor fraction, with early precipitation of small quantities of pyrite and Al-Si minerals like albite and chlorite, followed by precipitation of wollastonite and quartz (Fig. 4b). By mass, quartz is the dominant secondary mineral precipitated during supercritical fluid formation. At the modeled temperatures and pressures of the supercritical fluids, hornblende, plagioclase, and pyrrhotite are important, often dominant, alteration minerals (Ferry et al., 1987), however, these minerals were not observed to precipitate according to our geochemical models.

3.4. Fluid composition and secondary mineralization upon supercritical fluid ascent

As the supercritical fluid ascends above the magmatic heat source, depressurization results in the condensation of a liquid phase. The changes in fluid composition upon supercritical fluid condensation and variable mixing with reservoir subcritical geothermal fluids are shown in Fig. 5. Upon depressurization, soluble volatile components like HCl

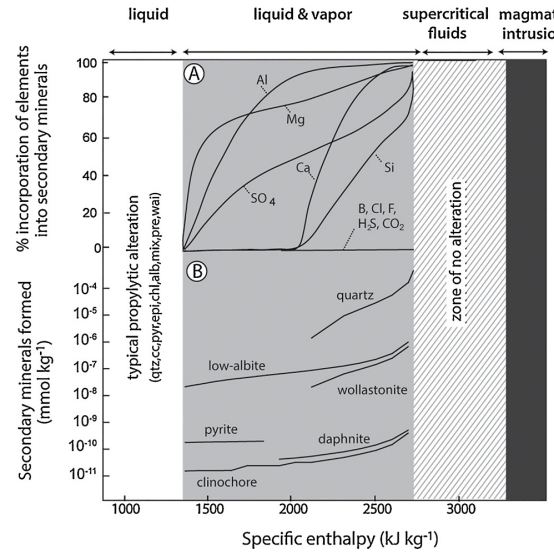

Fig. 4. Patterns of rock alteration during heat addition and supercritical fluid formation. a) Element mobility expressed in terms of percentage incorporation of select elements into secondary minerals. b) Moles of secondary minerals formed as a function of heat addition.

strongly partition into the small fraction of liquid condensate. The liquid condensate displays a low pH (~2) due to the low alkalinity of the water, the dissociation of HCl (Fig. 5a) and a high concentration of Cl due to partitioning into the liquid phase (Fig. 5c). The concentration of mineral-forming elements like SiO_2 in the condensed liquid decreases as the vapor fraction decreases (Fig. 5b). However, the concentration of volatile elements in the vapor increases as the vapor fraction decreases (Fig. 5d).

The condensed liquid may react immediately with the surrounding basaltic rock (Fig. 5 – number 2). This causes the pH of the mixture to approach that of the subcritical geothermal fluids (~7–8), with concentrations of mineral-forming elements in the liquid controlled by temperature dependent fluid-rock equilibria. Further mixing with subcritical geothermal fluids dominates the composition of the condensing fluids (Fig. 5b – number 3 and 4). However, the volatile element concentrations of the two end-members is similar (Fig. 5c).

4. Discussion

4.1. Comparison between modeled and measured enthalpy conditions

Modeled *P-T-h* conditions are compared with the measured enthalpies of Krafla well discharges in Fig. 6. The pressures of the well discharges are the calculated saturation pressure at the recalculated reservoir temperature (not the measured feedzone temperature), and therefore provide a lower-bound estimate. Phase segregation causes many of the two-phase wells to have higher specific enthalpies than predicted by the fluid flow model. At < 300 °C, the models predict enthalpies in the upflow zone to be close to the liquid limb of the two-phase field, consistent with previous studies of Krafla fluids that have shown that aquifer fluids are mostly liquid with a small fraction of vapor (< 2% by mass; Gudmundsson and Arnórsson, 2005). Since most of the producing wells are located within the upflow zone of the geothermal system (Ármannsson et al., 2014; Pope et al., 2015) where fluid ascends and depressurizes above the intrusion (path **II**), the elevated discharge enthalpies of such 'excess enthalpy' wells are not directly caused by heating near an intrusion (path **I**). However, this study identifies the latter process as the mechanism by which supercritical

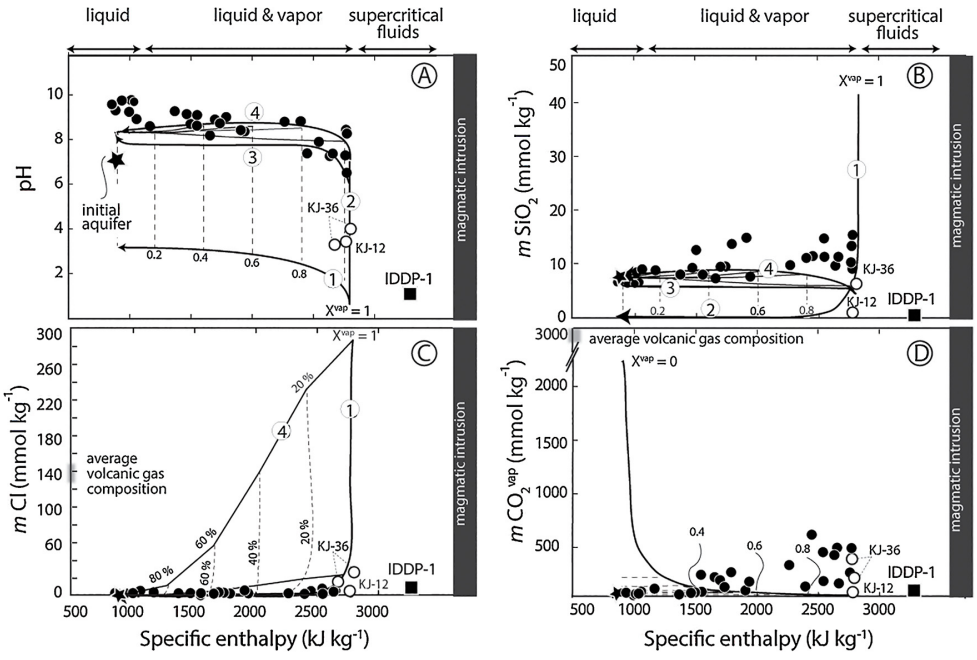

Fig. 5. Condensation (Path **II**) and mixing (Path **III**) with subcritical fluids: Evolution of a) pH, b) SiO_2, c) Cl and d) CO_2 in the liquid and vapor phase associated with condensation due to conductive heat loss in supercritical fluids (black line) calculated assuming closed-system (numbers 1 and 2 on the figure), open-system mixing (number 3, thin, dashed line) and re-equilibration with the host rocks (number 4). Symbols have the same notation as in Fig. 3. Concentrations of volcanic gases were obtained in the same way as in case of Fig. 3.

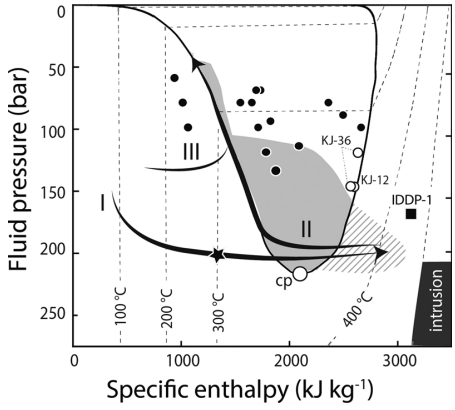

Fig. 6. Comparison of the model for the main stage (see Fig. 2) with the Krafla geothermal reservoir fluids. Symbols have the same notation as in Fig. 3.

fluids similar to the IDDP-1 fluid are generated (Fig. 3). Intuitively, it makes sense for such well discharges to be relatively rare, as the conductive heating process only occurs in the direct vicinity of the intrusion (Fig. 2). As the supercritical fluid ascends, an acidic liquid condenses out. Thus, the observation that enthalpies and pressures of the 'acid' wells lie close to the vapor limb of the two-phase field is consistent with the notion they are generated by supercritical fluid ascent.

4.2. Composition of supercritical fluids formed by conductive heating

In this study, we propose that an important mechanism of supercritical fluid formation in the roots of volcanic geothermal systems is conductive heating of the surrounding geothermal groundwater of meteoric origin by circulation near a magmatic intrusion, without significant degassing from the magmatic intrusion. This is supported by the similarity between the chemical composition of modeled supercritical fluids formed by this mechanism and the measured IDDP-1 fluid composition (Fig. 3, Table 4). The modeled concentrations of non-reactive elements like Cl and B and volatile components are similar to the IDDP-1 reservoir fluids. The main discrepancy between the measured and modeled fluids is the high concentration of sodium and potassium in modeled fluids, which is caused by the inability of PHREEQC to model high ionic strength fluids close to the two-phase and supercritical phase transition. However, it is reasonable to assume that at this point liquid becomes increasingly saline as the vapor fraction increases, which may potentially result in precipitation of Cl-minerals like halite (Scott et al., 2017) or Na-K silicates.

That supercritical fluids originate by conductive heating of groundwater near an intrusion is further supported by the similarity between the isotopic composition of IDDP-1 fluid and subcritical reservoir fluids. While the δD and $\delta^{18}O$ ratios of subcritical geothermal groundwater are -94 to -87‰ and -11.5 to -9.1‰, respectively (Pope et al., 2015), the IDDP-1 fluids have similar ratios of δD of -85‰ and $\delta^{18}O$ of -10‰ (Ármannsson et al., 2014). These values are consistent with modern day precipitation in the area (Árnason, 1976) and progressive fluid-rock interaction (Stefánsson et al., 2017a), suggesting that meteoric water is the fluid source for the supercritical IDDP-1 fluids, with insignificant input of magmatic fluids.

Based on analyses of stable isotopes it has been concluded that the main source of Cl, S and CO_2 in the subcritical geothermal fluids at Krafla is rock leaching, with possible magmatic degassing in the case of Cl and CO_2 (Ármannsson et al., 1989; Stefánsson and Barnes, 2016; Stefánsson et al., 2017a). The $\delta^{37}Cl$ values in the IDDP-1 fluids were 0 to +0.4‰, similar to subcritical geothermal fluids, which had ratios of +0.2 to +2.1‰ (Stefánsson and Barnes, 2016). The $\delta^{34}S$ ratios in H_2S in the IDDP-1 discharge fluid were +0.5 to +1.1‰, similar to the

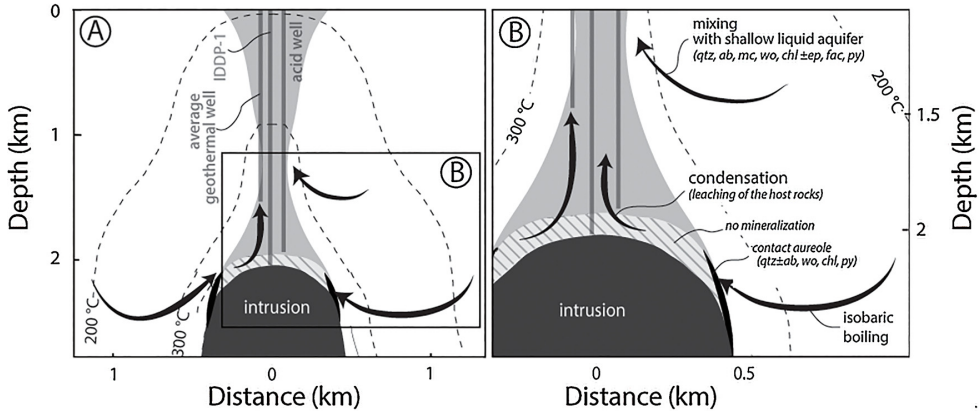

Fig. 7. a) Conceptual model of fluid dynamics in magma driven geothermal systems, showing the schematic location of normal geothermal wells and acid wells relative to the IDDP-1, with b) focus on fluid flow and mineralization linked to supercritical fluid formation (qtz – quartz, ab-albite, mc-microcline, chl-chlorite, wo – wollastonite, ep – epidote, fac-ferroactinolite, py-pyrite).

vapor in the two-phase well discharges with $\delta^{34}S$ of +0.05 to +1.28‰ (Stefánsson et al., 2015). In the case of CO_2, the $\delta^{13}C$ values for Krafla fluids are -5.3 to -1.4‰ (Arnórsson and Barnes, 1983; Sano et al., 1985; Barry et al., 2014), with the CO_2 and $\delta^{13}C$ relationship suggesting magmatic source (Stefánsson et al., 2017a). However, a low contribution of magmatic gas to the IDDP-1 fluid is supported by comparison of measured volatile concentrations from current Krafla fluids to measured concentrations after the Krafla fires in 1984–1987 (Ármannsson et al., 1989; Fig. 5c,d), during which the concentrations of both CO_2 and Cl were approximately of one order of magnitude higher than currently observed in the Krafla geothermal reservoir.

4.3. The formation of 'acid' fluids from ascending supercritical fluid

Liquid that condenses out of ascending supercritical fluid is characterized by elevated concentrations of volatile components and an acidic pH due to the dissociation of HCl transported in the supercritical vapor. Thus, acid reservoir fluids may represent the liquid condensate formed during supercritical fluid ascent, without additional input of HCl and SO_2 from magma degassing. Such acid fluids have been observed at Krafla with pH values of 3.3–4.9, Cl of 3.2–25 mmol kg^{-1} and SiO_2 concentrations of 0.5-6.0 mmol kg^{-1} in wells K-12 and K-36 (e.g., Einarsson et al., 2010; Ármannsson et al., 2014). Moreover, the ratios of some common volatile components like CO_2, H_2S and H_2, are similar in the acid, supercritical and the subcritical geothermal fluids, but differ from the ratios commonly observed in magmatic gas in Iceland (Stefánsson et al., 2017b). These observations suggest that acid reservoir geothermal fluids at Krafla represent liquid condensed out of ascending supercritical fluids.

The acidic liquid condensate is undersaturated with respect to most secondary minerals (Fig. 6), which promotes dissolution of primary minerals while limiting precipitation of secondary minerals. However, these fluids are mixed with shallower geothermal fluids to various degrees within the upflow zone. Based on our chemical models (Fig. 6), we estimate that the mixing ratio between the liquid condensate and shallower geothermal fluids is approximately < 0.1. In this case, the reservoir fluid dominates chemical signatures, making recognition of the added condensate difficult at the surface.

5. Summary and conclusions

This study describes patterns of heat and mass transfer in the roots of volcanic geothermal systems with a focus on the generation of supercritical fluids. We compare hydrological and geochemical models with data from the Krafla geothermal system in Iceland, including the IDDP-1 well. A conceptual model of the key fluid flow and geochemical processes in high-enthalpy geothermal systems like Krafla is presented in Fig. 7.

We propose that an important mechanism of supercritical fluid formation in the roots of volcanic and high-enthalpy geothermal systems is conductive heating of the surrounding subcritical geothermal fluids by a magmatic intrusion. High-enthalpy well discharges may also be formed by depressurization boiling and phase segregation in the upflow zone of the geothermal system, above the intrusion. The two processes can be distinguished from each other by the chemical and physical properties of resulting geothermal fluids.

The composition of supercritical fluids formed by conductive heating near a subsurface intrusion is characterized by negligible concentrations of non-volatile elements (i.e., Si, Na, K, Ca, Mg, Al, Fe), but similar volatile element concentrations (i.e., C, S, B, Cl, F) as the surrounding subcritical geothermal fluids. Boiling of the liquid groundwater to dryness results in intensive mineral formation dominated by quartz within the boiling zone around the magmatic intrusion, whereas insignificant rock alteration by the supercritical fluids is predicted to occur. The similarity between modeled fluid compositions and the measured composition of the IDDP-1 suggests that the ~440 °C supercritical fluids discharged were formed by heating of circulating groundwater without significant magmatic fluid input. This is further supported by the volatile element stable isotope composition (i.e., δD, $\delta^{18}O$, $\delta^{13}C$, $\delta^{34}S$, $\delta^{37}Cl$) of the fluids.

The low-density supercritical fluid ascends towards the surface within permeable pathways above the magmatic intrusion. Depressurization of the fluid results in condensation of an acidic liquid (pH < 4) characterized by elevated Cl concentrations and similar volatile element ratios as in subcritical geothermal fluids. Such acid fluids are encountered in a few wells at Krafla, suggesting the presence of underlying supercritical fluids. However, at shallower depths the signatures are masked by mixing with subcritical geothermal fluids and secondary processes like fluid-rock interaction, depressurization boiling and phase segregation.

Acknowledgements

The reviewers and associate editor are acknowledged for their stimulating remarks and suggestions, which led to a substantial improvement in the manuscript. Nicole S. Keller and Jóhann Gunnarsson-Robin are thanked for helping with sampling and analysis, and David Ostman for his help with the map. This work has been funded by the

Swiss National Science Foundation (CRSII2_1418431/1, Sinergia COTHERM), Georg (11-04-003) and Landsvirkjun Energy Research Fund.

References

Ármannsson, H., Benjamínsson, J., Jeffrey, A.W.A., 1989. Gas changes in the Krafla geothermal system, Iceland. Chem. Geol. 76, 175–196.

Ármannsson, H., Fridriksson, T., Gudfinnsson, G.H., Ólafsson, M., Óskarsson, F., Thorbjörnsson, D., 2014. IDDP—The chemistry of the IDDP-01 well fluids in relation to the geochemistry of the Krafla geothermal system. Geothermics 49, 66–75.

Árnason, B., 1976. Groundwater systems in Iceland traced by deuterium. Societas Scientiarum Islandica 42.

Arnórsson, S., Barnes, I., 1983. The nature of carbon dioxide waters in Snaefellsnes, Western Iceland. Geothermics 12, 171–176.

Arnórsson, S., Bjarnason, J.O., Giroud, N., Gunnarsson, I., Stefánsson, A., 2006. Sampling and analysis of geothermal fluids. Geofluids 6, 203–216.

Arnórsson, S., Stefánsson, A., Bjarnason, J.Ö., 2007. Fluid-fluid interactions in geothermal systems. Rev. Min. Geochem. 65, 259–312.

Ball, J.W., Nordstrom, D.K., 1991. User's manual for WATEQ4F, with revised thermodynamic data base and test cases for calculating speciation of major, trace and redox elements in natural waters. US Geol. Surv. Open-File Rep. 91–183.

Barry, P.H., Hilton, D.R., Füri, E., Halldórsson, S.A., Grönvold, K., 2014. Carbon isotope abundance systematics of Icelandic geothermal gases, fluids and subglacial basalts with implications for mantle plume- related CO_2fluxes. Geochim. Cosmochim. Acta 134, 74–99.

Bjarnason, J.Ö., 2010. The Speciation Program WATCH, Version 2.4, User's Guide. Iceland water chemistry group, Reykjavik.

Bodvarsson, G.S., Benson, S.M., Sigurdsson, O., Stefánsson, V., Eliasson, E.T., 1984. The Krafla geothermal field, Iceland. 1. Analysis of well test data. Water Res. Res. 20, 1515–1530.

Darling, W.G., Ármannsson, H., 1989. Stable isotopic aspects of fluid flow in the Krafla, Námafjall and Theistareykir geothermal systems of Northeast Iceland. Chem. Geol. 76, 175–196.

Einarsson, P., 1978. S-wave shadows in the Krafla Caldera in NE-Iceland, evidence for a magma chamber in the crust. Bull. Volcanol. 41, 1–9.

Einarsson, K., Pálsson, B., Gudmundsson, Á., Hólmgeirsson, S., Ingason, K., Matthíasson, J., Hauksson, T., Ármannsson, H., 2010. Acid Wells in the Krafla geothermal Field. Proceedings World Geothermal Congress.

Elders, W., Friðleifsson, G.O., Zierenberg, R.A., Pope, E., Mortensen, A., Gudmundsson, A., Lowenstern, J., Marks, N., Owens, L., Bird, D.K., Reed, M.H., Olsen, N.J., Schiffman, P., 2011. Origin of a rhyolite that intruded a geothermal well while drilling at the Krafla volcano, Iceland. Geol. 39, 231–234.

Elders, W.A., Fridleifsson, G.Ó., Pálsson, B., 2014. Iceland Deep Drilling Project: The first well, IDDP-1, drilled into magma. Geothermics 49, 1.

Fernández-Prini, R., Alvarez, J.L., Harvey, A.H., 2003. Henry's constants and vapor-liquid distribution constants for gaseous solutes in H_2O and D_2O at high temperatures. J. Phys. Chem. Ref. Data 32, 903–916.

Fournier, R.O., 1999. Hydrothermal processes related to movement of fluid from plastic into brittle rock in the magmatic-epithermal environment. Econ. Geol. 94, 1193–1212.

Ferry, J.M., Mutti, L.J., Zuccala, G.J., 1987. Contact metamorphism/hydrothermal alteration of Tertiary basalts from the Isle of Skye, northwest Scotland. Contr. Mineral. Petrol. 166, 95–166.

Gudmundsson, B.T., Arnórsson, S., 2005. Secondary mineral-fluid equilibria in the Krafla and Namafjall geothermal systems, Iceland. Appl. Geochem. 20, 1607–1625.

Gunnarsson, I., Arnórsson, S., 2000. Amorphous silica solubility and the thermodynamic properties of H_4SiO_4 in the range of 0° to 350°C at P_{sat}. Geochim. Cosmochim. Acta 64 (13), 2295–2307.

Hanson, R.B., Barton, M.D., 1989. Thermal development of low-pressure metamorphic belts: results from two-dimensional numerical models. J. Geophys. Res. 94 (10), 377 363-10.

Haar, L., Gallagher, J.S., Kell, G., 1984. NBS/NRC steam tables. Hemisphere.

Hauksson, T., Markússon, S., Einarsson, K., Karlsdóttir, S.N., Einarsson, A., Möller, A., Sigmarsson, Th., 2014. Pilot testing of handling the fluids from the IDDP-1 exploratory geothermal well, Krafla, N.E. Iceland. Geothermics 49, 76–82.

Hayba, D.O., Ingebritsen, S.E., 1994. The computer model HYDROTHERM, a three-dimensional finite-difference model to simulate ground-water flow and heat transport in the temperature range of 0 to 1200 °C. USGS Rep. 94–4045.

Hayba, D.O., Ingebritsen, S.E., 1997. Multiphase groundwater flow near cooling plutons. J. Geophys. Res. Solid Earth 102, 12235–12252.

Hjartardóttir, Á.R., Einarsson, P., Bramham, E., Wright, T.J., 2012. The Krafla fissure swarm, Iceland and its formation by rifting events. Bull. Volcanol. 74, 2139–2153.

Ingason, K., Kristjánsson, V., Einarsson, K., 2014. Design and development of the discharge system of IDDP-1. Geothermics 49, 58–65.

Jónasson, K., 1994. Rhyolite volcanism in the Krafla central volcano, north-east Iceland. Bull. Volcanol. 56, 516–528.

Kato, O., Doi, N., Muramatsu, Y., 1993. Neo-granitic pluton and geothermal reservoir at the Kakkonda geothermal field, Iwata prefecture, Japan. J. Geotherm. Res. Soc. Jpn. 15, 41–57.

Kennedy, B.M., Truesdell, A.H., 1996. The Northwest Geysers high-temperature reservoir: evidence for active magmatic degassing and implications for the origin of the Geysers geothermal field. Geothermics 25, 365–387.

Kristmannsdóttir, H., 1979. Alteration of basaltic rocks by hydrothermal-activity at 100–300 C. Dev. Sedimentol. 27, 359–367.

Liebscher, A., Heinrich, C.A., 2007. Fluid–fluid interactions in the Earth's lithosphere. Rev. Min. Geochem. 65, 1–14.

Lowenstern, J.B., Bergfeld, D., Evans, W.C., Hunt, A.G., 2015. Origins of geothermal gases at Yellowstone. J. Volcanol. Geotherm. Res. 302, 87–101.

Parkhurst, D.L., Appelo, C.A.J., 1999. User's Guide to PHREEQC (Version 2) - A Computer Program for Speciation, Batch-Reaction, One-Dimensional Transport, and Inverse Geochemical Calculations. Report 99–4259. U.S. Geological Survey, Water-Resources Investigations.

Pope, E.C., Bird, D.K., Arnórsson, S., Giroud, N., 2015. Hydrology of the Krafla geothermal system, northeast Iceland. Geofluids 16, 175–197.

Reinsch, T., Dobson, P., Asanuma, H., Huenges, E., Poletto, F., Sanjuan, B., 2017. Utilizing supercritical geothermal systems: a review of past ventures and ongoing research activities. Geotherm. Energy 5, 1–25.

Sano, Y., Urabe, A., Wakita, H., Chiba, H., Sakai, H., 1985. Chemical and isotopic compositions of gases in geothermal fluids in Iceland. Geochem. J. 19, 135–148.

Scott, S., Driesner, T., 2018. Permeability changes resulting from quartz precipitation and dissolution around upper crustal intrusions. Geofluids 2018.

Scott, S., Gunnarsson, I., Arnórsson, S., Stefánsson, A., 2014. Gas chemistry, boiling and phase segregation in a geothermal system, Hellisheidi Iceland. Geochim. Cosmochim. Acta 124, 170–189.

Scott, S., Driesner, T., Weis, P., 2015. Geologic controls on supercritical geothermal resources above magmatic intrusions. Nat. Commun. 6, 7837.

Scott, S., Driesner, T., Weis, P., 2016. The thermal structure and temporal evolution of high-enthalpy geothermal systems. Geothermics 62, 33–47.

Scott, S., Driesner, T., Weis, P., 2017. Boiling and condensation of saline geothermal fluids above magmatic intrusions. Geophys. Res. Lett. 44.

Shinohara, H., 2008. Excess degassing from volcanoes and its role on eruptive and intrusive activity. Rev. Geophys. 46.

Sigvaldason, G.E., Elíasson, G., 1968. Collection and analysis of volcanic gases at Surtsey, Iceland. Geochim. Cosmochim. Acta 32, 797–805.

Stefánsson, A., 2017. Gas chemistry of Icelandic thermal fluids. J. Volcanol. Geotherm. Res. 346, 81–94.

Stefánsson, A., Barnes, J.D., 2016. Chlorine isotope geochemistry of Icelandic thermal fluids: implications for geothermal system behavior at divergent plate boundaries. Earth Planet. Sci. Lett. 449, 69–78.

Stefánsson, A., Gunnarsson, I., Giroud, N., 2007. New methods for the direct determination of dissolved inorganic, organic and total carbon in natural waters by reagent-free™ ion chromatography and inductively coupled plasma atomic emission spectrometry. Anal. Chim. Acta 582, 69–74.

Stefánsson, A., Arnórsson, S., Gunnarsson, I., Kaasalainen, H., Gunnlaugsson, E., 2011. The geochemistry and sequestration of H_2S into the hydrothermal system at Hellisheidi, Iceland. J. Volcanol. Geotherm. Res. 202, 179–188.

Stefánsson, A., Keller, N.K., Robin, J.G., Ono, S., 2015. Multiple sulfur isotope systematics of Icelandic geothermal fluids and the source and reactions of sulfur in volcanic geothermal systems at divergent plate boundaries. Geochim. Cosmochim. Acta 165, 307–323.

Stefánsson, A., Hilton, D.R., Sveinbjörnsdóttir, Á.E., Torssander, P., Heinemeier, J., Barnes, J.D., Ono, S., Halldórsson, S.A., Fiebig, J., Arnórsson, S., 2017a. Isotope systematics of Icelandic thermal fluids. J. Volcanol. Geotherm. Res. 337, 146–164.

Stefánsson, A., Stefánsdóttir, G., Keller, N.S., Barsotti, S., Sigurdsson, Á., Thorláksdóttir, S.B., Pfeffer, M.A., Eiríksdóttir, E.S., Jónasdóttir, E.B., Löwis, S., Gíslason, S.R., 2017b. Major impact of volcanic gases on the chemical composition of precipitation in Iceland during the 2014–2015 Holuhraun eruption. J. Geophys. Res. Atmos. 122, 1971–1982.

Stimac, J., Goff, F., Goff, C.J., 2015. Intrusion-related geothermal systems. In: Sigurdsson, H. (Ed.), The Encyclopedia of Volcanoes, 2nd ed. Academic Press, Amsterdam, pp. 799–822.

Taylor, H.P., 1974. Application of oxygen and hydrogen isotope studies to problems of hydrothermal alteration and ore deposition. Econ. Geol. 69, 845–883.

Zierenberg, R., Schiffman, P., Barfod, G., Lesher, Ch, Marks, N., Lowenstern, J., Mortensen, A., Pope, E., Bird, D.K., Reed, M.H., Friðleifsson, G.Ó., Elders, W., 2013. Composition and origin of rhyolite melt intersected by drilling in the Krafla geothermal field, Iceland. Cont. Min. Petrol. 165, 327–347.

Appendix B: Research article II

Heřmanská, M., Kleine, B.I., Stefánsson, A. 2019. Supercritical Fluid Geochemistry in Geothermal Systems. Geofluids 2019, Article ID 6023534, 14 pages, https://doi.org/10.1155/2019/6023534.

Reprinted with the permission of Wiley Hindawi

Hindawi
Geofluids
Volume 2019, Article ID 6023534, 14 pages
https://doi.org/10.1155/2019/6023534

Research Article

Supercritical Fluid Geochemistry in Geothermal Systems

Matylda Heřmanská, Barbara I. Kleine, and Andri Stefánsson

Institute of Earth Sciences, University of Iceland, Sturlugata 7, Reykjavík 101, Iceland

Correspondence should be addressed to Matylda Heřmanská; mattylda@hi.is

Received 2 May 2019; Accepted 1 July 2019; Published 5 August 2019

Academic Editor: John A. Mavrogenes

Supercritical fluids exist in the roots of many active high-temperature geothermal systems. Utilization of such supercritical resources may multiply energy production from geothermal systems; yet, their occurrence, formation mechanism, and chemical properties are poorly constrained. Flow-through experiments at 260°C and 400-420°C were performed to study the chemical and mineralogical changes associated with supercritical fluid formation near shallow magmatic intrusions by conductive heating and boiling of conventional subcritical geothermal fluids. Supercritical fluids formed by isobaric heating of liquid geothermal water had similar volatile element concentrations (B, C, and S) as the subcritical water. In contrast, mineral-forming element concentrations (Si, Na, K, Ca, Mg, and Cl) in the supercritical fluid were much lower. The results are consistent with the observed mineral deposition of quartz, aluminum silicates, and minor amount of salts during boiling. Similar concentration patterns have been predicted from geochemical modeling and were observed at Krafla, Iceland, for the IDDP-1 supercritical fluid discharge. The experimental results confirm previous findings that supercritical fluids may originate from conductive heating of subcritical geothermal reservoir fluids characterized by similar or lower elemental concentrations with minor input of volcanic gas.

1. Introduction

Volcanic geothermal systems are associated with magmatic intrusions in the upper part of the Earth's crust characterized by increased temperature, specific fluid enthalpy, and convection of groundwater [1]. Conventional exploitation of geothermal fluids from such systems typically produces an average of ~3–5 MW electric power per well [2] with a world total exploitation of geothermal energy in 2018 corresponding to ~14.4 GW [3]. Conductive heat transfer from a magmatic intrusion to the surrounding groundwater occurs in the roots of the geothermal system below the depth of typical conventional geothermal wells. Recent modeling suggests that supercritical fluids with temperatures and enthalpies exceeding ~400°C and ~3000 kJ kg^{-1}, respectively, exist at the boundary between geothermal systems and the magmatic heat source, with such fluids possibly capable of generating up to ~30-50 MW of electricity from a single well or ten times more than conventional geothermal wells [4].

Supercritical geothermal fluids have commonly been classified based on the critical temperature (T_c = 373.976°C) and pressure (P_c = 22.01 MPa) of pure water (H_2O) [5]. Such a definition can lead to an artificial boundary in the phase diagram of water, across which there is actually a continuous change in fluid properties. Moreover, for binary salt-water fluids, the term "supercritical" may not fully describe the fluid phase properties, as critical behavior occurs along critical temperature and pressure, implying fluid phase separation rather than homogenization. Here and following Liebscher and Heinrich [6], the term supercritical is defined as a single-phase vapor with a temperature above the critical temperature. Supercritical fluids have been suggested to form by groundwater circulation near the intrusion [1, 7, 8] with or without input from magmatic gas [9–11]. More than 25 deep wells sunk into the geothermal fields at The Geysers, Salton Sea, and Hawaii (USA); Kakkonda (Japan); Larderello (Italy); Krafla, Nesjavellir, and Reykjanes (Iceland); Los Humeros (Mexico); and Menengai (Kenya) have reached

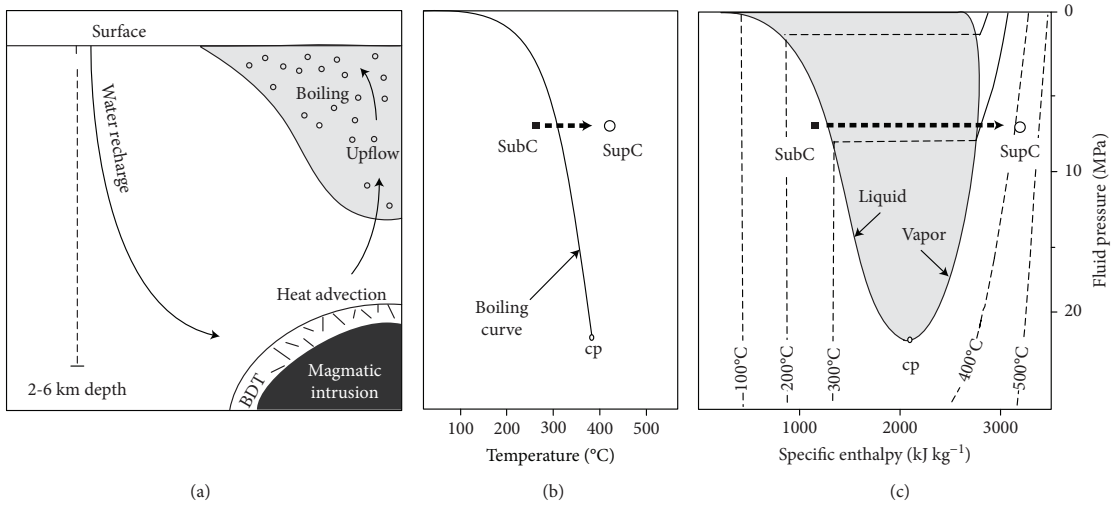

Figure 1: Main characteristics of a volcanic geothermal system. (a) Conceptual model showing fluid flow paths, the brittle-ductile transition (BDT) between the magmatic heat source and the circulating geothermal fluid, and depressurization boiling near the surface. Constructed based on Arnórsson et al. [60] and Scott et al. [8]. (b) The boiling curve of water. (c) The phase diagram of water showing pressure, specific enthalpy, and temperature relations. Also shown are the subcritical (SubC) to supercritical (SupC) conditions of the experiments carried out in this study.

temperatures in excess of the critical temperature of water and, in some cases, have even encountered magma [12]. The most extensive project aiming at obtaining supercritical fluids for geothermal utilization is the Iceland Deep Drilling Project (http://www.iddp.is). In 2009, the IDDP-1 well at Krafla (NE Iceland) came to a halt after drilling into molten magma at ~2.1 km depth [13]. After an initial heating period, the well discharged supercritical fluids with temperatures of ~440°C and eventually reached a maximum temperature of 459°C and specific enthalpy of ~3200 kJ kg^{-1} [14, 15]. From March 2010 until September 2011, series of flow tests were conducted; however, due to the corrosive nature of the fluids, silica scaling, and thermal damage to the well casings, utilization proved to be challenging and the fluid discharge was eventually terminated [16]. In 2017, the second IDDP-2 well at Reykjanes (SW Iceland) reached its target depth of 4.6 km with a measured bottom hole temperature of 426°C [17]. At present, fluid discharges from IDDP-2 at surface are not characterized by supercritical temperatures. Thus, deep reservoir fluid composition has been estimated from fluid inclusion analysis of felsic veins consisting of a vapor phase dominated by water (97.5 mol% H_2O, ~1.5 mol% CO_2, 0.7 mol% H_2S, and traces of H_2), Cl-rich brine (Fe-K chlorides, sylvite-halide solid solutions), and sulfides [18].

Magmatic intrusions emplaced into the upper parts of the Earth's crust may exsolve magmatic fluids at near lithostatic pressure, resulting in fracturing of the surrounding rocks and magmatic fluid migration [19, 20]. Near magmatic intrusions, conductive heat addition to the surrounding groundwater system may also potentially form high-temperature supercritical fluids [1, 7]. However, permeability may rapidly decrease at the brittle-ductile transition (BDT), possibly limiting the formation of such supercritical fluids to lithologies with basaltic glass transition temperatures above ~400-450°C [1, 7, 21–23]. While the relations between rock permeability and brittle-ductile behavior, as well as reservoir simulations around magmatic intrusions, have received considerable interest, less attention has been drawn to the geochemical properties of such supercritical fluids. Fluids originating from degassing magma are rich in CO_2, SO_2, HCl, and HF [24]. In contrast, supercritical fluids formed by boiling of subcritical geothermal water of meteoric or seawater origin are considered to display similar concentrations of many volatile elements (CO_2, H_2S, H_2, and B) as the original water, much lower than corresponding magmatic-gas concentrations, but negligible nonvolatile element concentrations (Si, Na, K, Ca, and Mg) [25–31]. The formation of supercritical fluids may also produce a silica deposit around the magmatic intrusion [25, 31, 32] (Figure 1).

In this study, flow-through experiments at 260°C and 400-420°C were performed to study how conductive heating of subcritical water form geothermal fluids at supercritical temperatures and how this affects fluid chemistry and associated secondary mineral formation. The results of the experiments were further compared with the recent model simulations of the chemical nature of supercritical fluids near magmatic intrusions and with the observed composition of the supercritical fluid discharged by the IDDP-1 [31].

2. Methods

2.1. Experimental Set-Up. Flow-through experiments at 260°C and 400-420°C and 6.9 MPa reproduce geothermal reservoir conditions at subcritical and supercritical

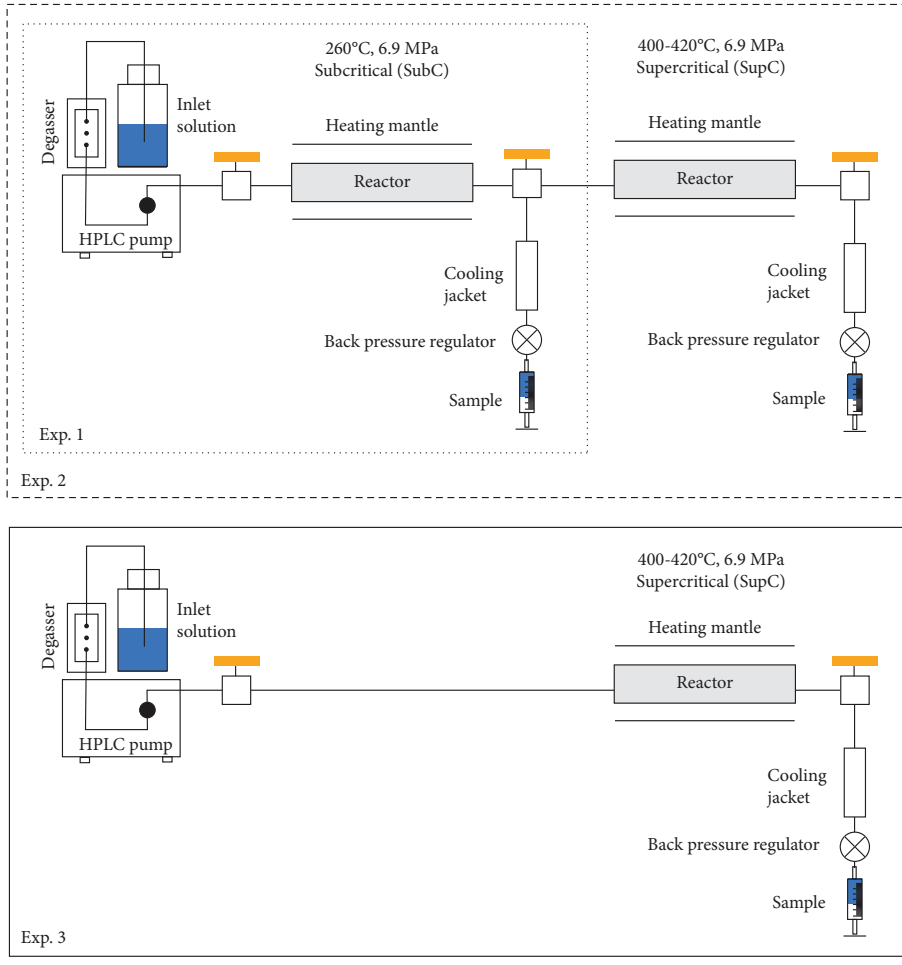

Figure 2: Schematic set-up of the experiments described in this study.

Table 1: Initial conditions of the experiments.

#	t (°C)	P (MPa)	Q (g min^{-1})	Material	Grain size (μm)
SubC-1	260	6.9	0.09-0.26	BAS	45-125
SupC-1	420	6.9	0.19-0.21	SS316-rod	
SupC-2	400	6.9	0.10-0.19	SS316-rod	

temperatures, respectively. A schematic illustration of the experimental set-up is shown in Figure 2, and a summary of experimental conditions is given in Table 1. All wetted parts of the experimental apparatus were made of inert material, including PEEK, titanium, and Inconel. Inlet solutions were pumped at a flow rate of ~0.20 ml/min using an HPLC pump (Chromatech®). The pressure was controlled at the end of the line by a back-pressure regulator (BPR, Biotech).

The first reactor (SubC), representing subcritical conditions, was heated to 260°C and filled with fine-grained

Table 2: Basaltic glass composition (BAS)[a].

Element		
SiO_2	wt.%	48.12
Al_2O_3	wt.%	14.62
FeO	wt.%	9.82
Fe_2O_3	wt.%	1.11
MgO	wt.%	9.08
CaO	wt.%	11.82
Na_2O	wt.%	1.97
K_2O	wt.%	0.29
Cl[b]	ppm	220
CO_2[b]	ppm	100
B[b]	ppm	1.0

[a]Basaltic glass from Stapafell [62]. [b]Taken as for average basalts in Iceland, after Kaasalainen and Stefánsson [64].

Table 3: Chemical composition of the solutions from the SubC and SupC reactors. Concentrations are in ppm.

Run #	t (°C)	pH	/	°C	SiO_2	B	Na	K	Ca	Mg	Fe	Al	Cl	CO_2	SO_4	H_2S
Subcritical																
SubC-1-S1	260	8.08	/	21	535	3.46	165	21.1	0.70	0.023	0.029	6.88	45.4	82.3	98.0	44.0
SubC-1-S2	260	8.02	/	21	526	3.36	160	30.8	1.00	0.010	0.060	6.21	43.2	87.1	180	38.5
SubC-1-S3	260	8.21	/	21	548	3.44	165	22.5	0.69	0.003	0.023	6.69	43.6	83.2	138	57.9
SubC-1-S4	260	8.50	/	21	493	3.46	168	23.0	1.72	0.004	0.154	5.13	44.7	99.0	142	40.9
SubC-1-S5	260	8.70	/	21	440	3.41	173	22.0	2.71	0.003	0.028	4.86	44.0	94.2	124	40.6
SubC-1-S6	260	9.03	/	21	383	3.38	177	21.9	3.04	0.002	0.019	5.61	43.2	73.9	164	40.6
SubC-1-S7	260	9.18	/	21	356	3.35	186	21.3	2.90	0.000	0.032	6.50	44.0	78.3	173	36.1
SubC-1-S8	260	9.37	/	21	336	3.38	196	20.7	2.45	0.005	0.020	6.48	46.1	76.6	137	49.1
SubC-1-S9	260	9.79	/	21	327	3.36	200	19.5	2.43	0.000	0.017	6.61	44.7	70.9	158	36.1
SubC-1-S10	260	9.63	/	21	332	3.38	205	19.3	2.22	0.002	0.046	6.48	45.4	63.8	188	36.1
SubC-1-S11	260	9.64	/	21	325	3.36	207	18.6	2.14	0.007	0.036	6.15	45.4	65.1	164	37.8
SubC-1-S12	260	9.60	/	21	329	3.36	212	55.5	2.21	0.005	0.058	5.96	50.0	66.0	202	26.9
SubC-1-S13	260	8.09	/	21	634	3.48	167	21.5	1.47	0.054	0.079	8.04	44.7	55.5	154	30.7
SubC-1-S14	260	8.00	/	21	674	3.46	161	21.9	1.58	0.012	0.042	5.26	44.0	90.7	152	27.3
SubC-1-S15	260	8.40	/	21	559	3.46	171	22.4	1.44	0.005	0.012	6.23	44.3	67.3	207	17.4
SubC-1 inlet[a]	260	8.82	/	21	453	3.41	181	24.1	1.91	0.009	0.044	6.21	44.8	76.9	159	37.3
Krafla w17[b]	275[d]	9.30	/	21	699	1.49	144	24.0	0.35	0.012	0.025	1.94	24.6	49.1	79.6	53.5
Krafla w37[c]	265[e]	7.95	/	20	488	3.46	156	22.8	7.61	0.012	0.018	0.84	46.1	106	90.8	40.9
Supercritical																
SupC-1-S17	420	5.06	/	21	5.3	3.19	0.2	0.07	0.06	0.002	0.050	0.022	0.35	8.32	0.45	13.9
SupC-1-S18	420	4.96	/	21	3.6	4.16	0.1	0.06	0.09	0.005	0.069	0.062		19.8	0.49	17.2
SupC-1-S19	420	4.75	/	21	2.3	3.30	0.1	0.02	0.02	0.002	0.042	0.027	0.46	24.5	0.32	8.18
SupC-1-S20	420	4.90	/	21	2.1	3.35	0.1	0.02	0.02	0.002	0.026	0.018	0.37	15.7	0.27	10.5
SupC-1-S21	420	4.50	/	21	1.5	2.58	0.2	0.04	0.02	0.003	0.024	0.044	0.48	268	0.40	12.0
SupC-1-S22	420	5.00	/	21	1.4	3.47	0.2	0.05	0.05	0.003	0.029	0.029	0.46	25.1	0.38	7.56
SupC-1-S23	420	4.40	/	21	1.4	3.42	0.1	<0.1	0.03	0.004	0.039	0.081		225	0.35	28.0
SupC-1-S24	420	4.60	/	21	1.3	2.92	0.1	0.04	0.02	0.003	0.037	0.064	0.36	105	0.33	13.9
SupC-2-SSE1	400	3.99	/	22	4.6	1.30	0.5	<0.1	0.12	0.029	0.208	0.173	1.89	46.5	0.26	13.8
SupC-2-SSE2	400	4.17	/	22	4.3	1.43	1.6	0.25	0.15	0.041	0.181	0.060	2.13	35.4	0.78	10.7
SupC-2-SSE3	400	3.97	/	22	3.1	1.47	1.1	0.26	0.08	0.019	0.099	0.075	1.90	38.0	0.67	40.0
SupC-2-SS34	400	3.68	/	22	2.9	1.32	1.5	0.19	0.06	0.021	0.083	0.059	2.85	59.6	0.54	29.9
SupC-2-SSE5	400	3.24	/	21	2.8	1.37	0.4	<0.1	0.11	0.019	0.058	0.041	2.05	55.3	0.36	24.9
SupC-2-SSE6	400	3.65	/	21	1.2	1.38	1.0	<0.1	0.17	0.028	0.102	0.071	1.41	53.7	1.74	25.1
SupC-2-SSE7	400	3.41	/	21	1.4	1.44	0.8	<0.1	0.04	0.023	0.080	0.056	1.75	135	1.50	31.2

[a]The average inlet composition of subcritical experiments SubC-1-n that served as inlet solution for supercritical experiment SupC-1-n. [b]Krafla w17 was used as an inlet for subcritical experiments SubC-1-n. Note: the inlet solution represents the liquid phase only discharge from the well w17. [c]The Krafla w37 was used as inlet for the supercritical experiments SupC-2-n. Note: the inlet solution represents the liquid phase only discharge from the well w37. [d]Based on Gudmundsson and Arnórsson [41]. [e]Based on Ntihabose [63].

basaltic glass (grain size fraction < 45 μm) from Stapafell, Iceland (Table 2). The second reactor (SupC), representing supercritical conditions, was heated to 400-420°C. This reactor contained a stainless steel (316) threaded rod to capture deposits precipitating from the fluids. Three different experiments were carried out to test the effects of temperature and solution composition on fluid composition and alteration mineralogy. The initial solution in all cases was of natural geothermal water from Krafla, Iceland (Table 3). In experiment 1, interaction between geothermal liquid water and basaltic rocks at subcritical temperatures (260°C) was conducted. In experiments 2 and 3, the geothermal water either from the outlet subcritical reactor or directly from the inlet solution was pumped into a flow-through reactor with a supercritical temperature of 400-420°C. In all cases, the fluids were cooled down by an in-line cooling jacket, followed by depressurization by a BPR and collection of fluid samples. At the end of each experiment, the solid deposits from the reactor were collected, dried at 50°C, and mounted on a sample holder. Loose precipitates from the rod collected from the supercritical reactor were directly mounted on a sample holder to study the

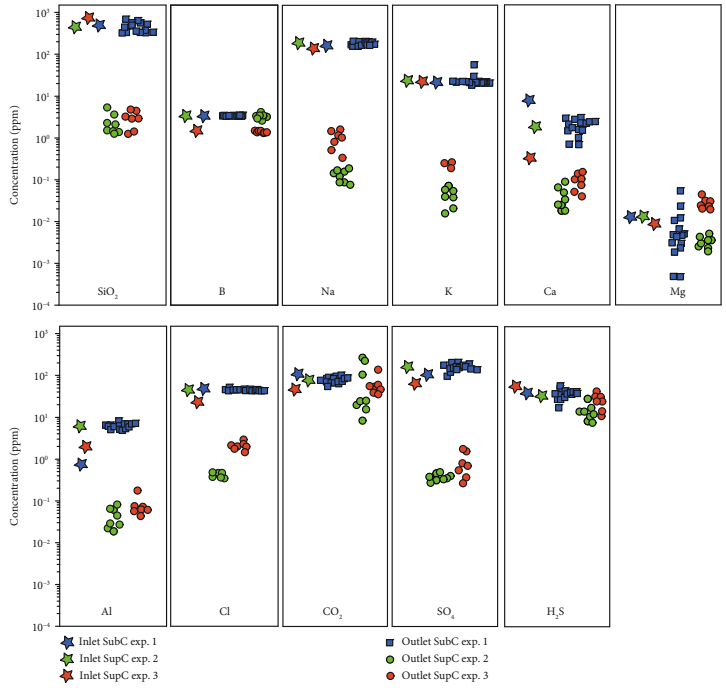

Figure 3: Elemental concentrations of inlet and outlet solutions of the experiments. Abbreviations: SubC and SupC refer to subcritical and supercritical conditions, respectively.

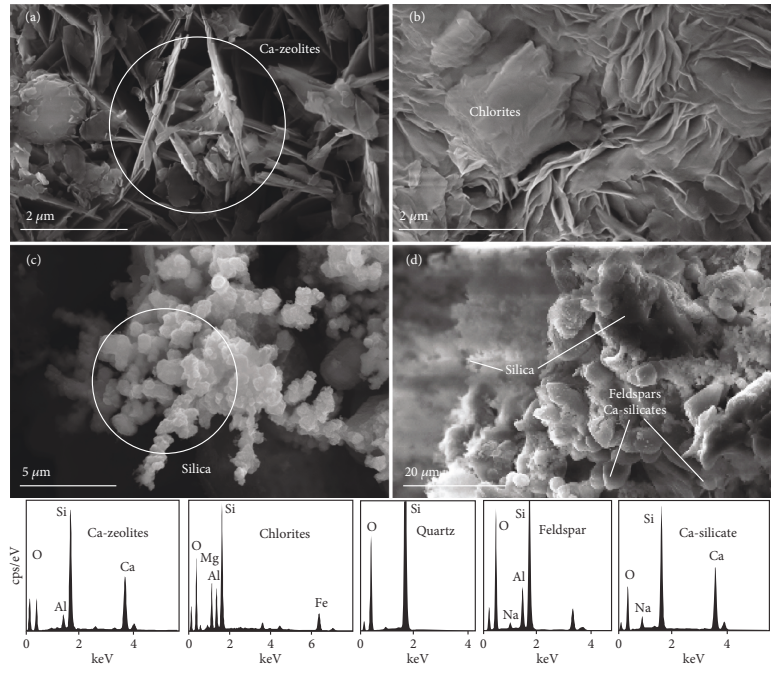

Figure 4: Selected SEM microphotographs and EDS spectras of minerals precipitated at both subcritical (a, b) and supercritical temperatures (c, d).

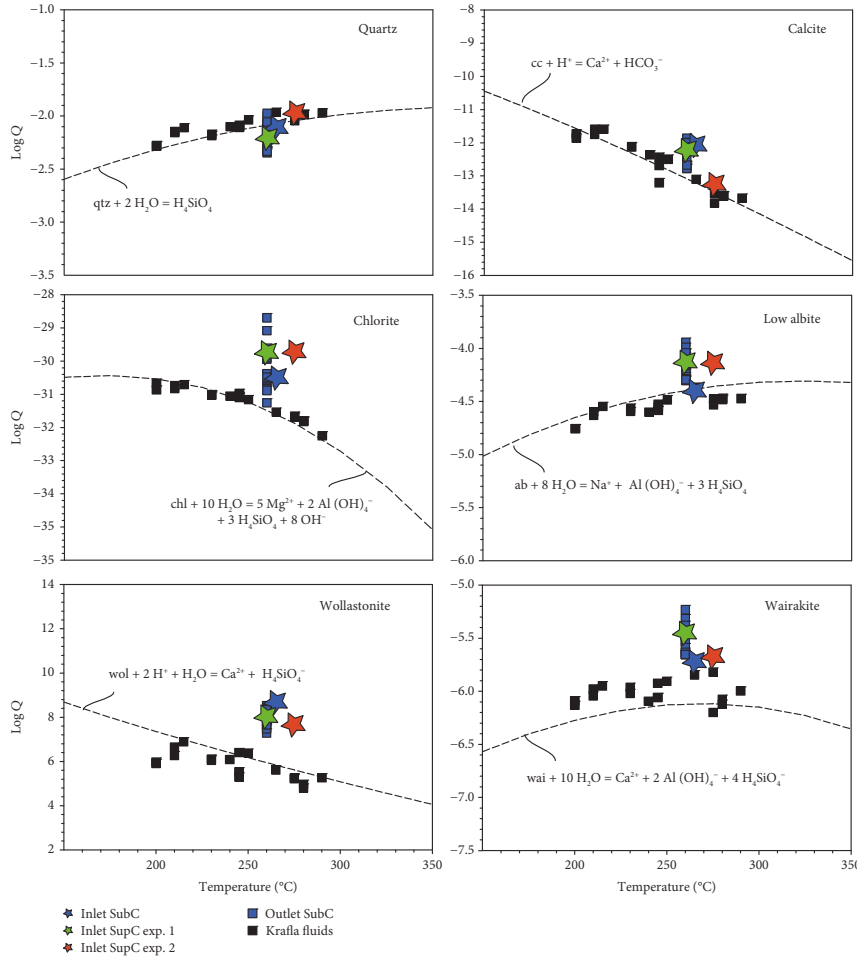

Figure 5: Mineral saturation state of selected minerals at subcritical conditions. The reaction quotients were calculated using the Phreeqc program [61] and the llnl.dat database. Also shown are mineral solubilities and the mineral reaction quotients for reservoir fluids at Krafla at the measured reservoir temperatures, both obtained from Gudmundsson and Arnórsson [41].

morphology of the deposits. The rod itself was imbedded into epoxy and cut parallel and perpendicular to the flow direction in the reactor and then polished.

2.2. Chemical Analyses. For the fluid samples, the pH was analyzed using a pH electrode and meter calibrated against commercial buffer solutions. Measurements of CO_2 and H_2S concentrations were carried out using a modified alkalinity and Hg-precipitation titration using dithizone as an indicator, respectively [33, 34]. For CO_2 determination, the samples from the supercritical reactor were collected into a base (0.01 M NaOH) to prevent degassing prior to analyses. For major elemental analyses (Si, B, Na, K, Ca, Mg, Al, Fe, Cl, and SO_4), the samples were filtered through a 0.2 μm filter (cellulose acetate), acidified to 1% with HNO_3 (Merck, Suprapur®), followed by analysis using ICP-OES (Spectro Ciros Vision). The analytical precision of major element

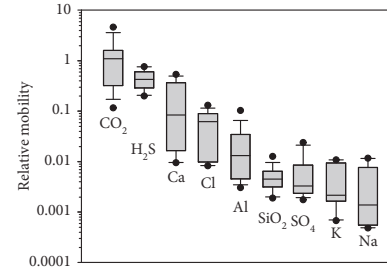

Figure 6: Relative mobility of major elements upon boiling of subcritical geothermal fluids by conductive heating to form supercritical fluids. Elements showing relative mobility close to 1 may be regarded as mobile, whereas elements with relative mobility of <0.1 are immobile.

Table 4: Mineral-fluid reactions that describe how aqueous neutral species and ion activity ratios are presumably controlled at subcritical and supercritical conditions.

Buffer reactions	Controlled neutral species and ion activity ratios
Subcritical buffer reactions	
$qtz + 2H_2O = H_4SiO_4$	H_4SiO_4
$py + pyrr + 2pre + H_2O = 2epi + 3H_2S$	H_2S
$4pyrr + 2pre + 2H_2O = 2epi + 2py + 3H_2$	H_2
$2czo + 2\,cc + 3qtz + 2H_2O = 3pre + 2CO_2$	CO_2
$1.5pre + 2H^+ = 1.5qtz + 1.5czo + 2H_2O + Ca^{2+}$	$Ca^{2+}/(H^+)^2$
$4.5qtz + czo + 2Na^+ = 0.5pre + 2alb + Ca^{2+}$	$Ca^{2+}/(Na^+)^2$
$alb + K^+ = mic + Na^+$	Na^+/K^+
$0.67epi + 0.67pyrr + 2H^+ = 0.33py + 0.67pre + 1.5H_2O + Fe^{2+}$	$Fe^{2+}/(H^+)^2$
$czo + 2H_2O + OH^- = pre + Al(OH)_4^-$	$Al(OH)_4^-/OH^-$
$chl + 3wai + 5Ca^{2+} = 4pre + 3qtz + 6H_2O + 5\,Mg^{2+}$	Mg^{2+}/Ca^{2+}
Supercritical reactions	
$qtz = SiO_2(g)$	$SiO_2(g)$
$NaCl(s) + nH_2O = NaCl \cdot nH_2O(g)$	Na (NaCl)
$KCl(s) + nH_2O = NaCl \cdot nH_2O(g)$	K (KCl)
$CaCl_2(s) + nH_2O = CaCl_2 \cdot nH_2O(g)$	Ca ($CaCl_2$)
$MgCl_2(s) + nH_2O = CaCl_2 \cdot nH_2O(g)$	Mg ($MgCl_2$)
	Cl (sum of $MCl_x(g)$ species)

analyses was based on repeated analysis of the GYG13 standard and was found to be <3% at the 95% confidence level for all elements except Fe, where it was ~14%. The analytical precision for pH was ±0.05.

The secondary mineral phases and the morphology of the solid products from the two reactors were determined using a HITACHI TM-3000 scanning electron microscope (SEM) with an accelerating voltage of 15 kV.

3. Results

3.1. Chemical Composition of the Outlet Solutions. The chemical compositions of the outlet solutions from the experiments are given in Table 3 and shown in Figure 3. The outlet solutions from the subcritical reactor (experiment 1) were mildly alkaline (pH 8.00- 9.79 at 21°C) with concentrations of SiO_2 (325-674 ppm), B (3.35-3.48 ppm), Na (160-212 ppm), K (18.6-55.5 ppm), Cl (43.2-50.0 ppm), CO_2 (55.5-99.0 ppm), SO_4 (98-207 ppm), and H_2S (17.4-57.9 ppm) similar to concentrations in the inlet solution (Table 3). Concentrations of Ca (0.69-3.04 ppm) were significantly lower than corresponding concentrations in the inlet solution (7.61 ppm) whereas Al concentrations (4.86-8.04 ppm) were significantly higher in the outlet solutions than in the inlet solution (0.84 ppm). The outlet solutions from the supercritical reactors were mildly acidic (pH 3.24 to 5.06 at 21°C). In experiment 2, concentrations of SiO_2 (1.3-5.3 ppm), Na (0.1-0.2 ppm), K (<0.07 ppm), Ca (0.02-0.09 ppm), Al (0.018-0.081 ppm), Cl (0.35-0.48 ppm), and SO_4 (0.27-0.49 ppm) were considerably lower than the corresponding concentrations of the inlet solution from the subcritical reactor. Concentrations of B (2.58-4.16 ppm), CO_2 (8.32-225 ppm), and H_2S (7.56-28.0 ppm) of the outlet solution did not differ much from the inlet solution (Figure 3). In experiment 3, similar trends were observed. Concentrations of SiO_2 (1.2-4.6 ppm), Na (0.4-1.6 ppm), K (<0.3 ppm), Ca (0.06-0.17 ppm), Al (0.041-0.17 ppm), Cl (1.41-2.85 ppm), and SO_4 (0.26-1.74 ppm) were substantially lower than the corresponding concentrations in the inlet solution (Figure 3). Again, concentrations of B (1.30-1.47 ppm), CO_2 (35.4-135 ppm), and H_2S (10.7-40.0 ppm) of the outlet solutions did not differ significantly from the inlet solution. Concentrations of Fe and Mg in all fluid samples were close to the detection limit and/or affected by contamination and were not considered further in this study.

3.2. Mineralogy and Chemical Composition of the Solid Products. Secondary minerals associated with alteration of the basaltic glass at subcritical temperatures (260°C) occurred mainly as thin layers on the surface of the primary glass. The main secondary minerals identified were chlorites, Na-Ca zeolite (wairakite), Ca-silicate (wollastonite), and calcite (Figure 4(a) and (b)). For supercritical temperatures, abundant white deposits on the steel rod were observed, mainly composed of quartz (Figure 4(c)). Microcline and wollastonite were found in minor amounts. Thick deposits (1-2 mm) occurred on the part of the rod located closest to the inlet of the reactor. Here, silicate layers were most massive closest

to the rod, becoming highly porous with increasing distance from the rod. Towards the outlet of the reactor, quartz precipitates occurred as amorphous silica (spheres with <1 μm in diameter) interconnected with fine silica branches up to 10 μm long (Figure 4(d)).

4. Discussion

4.1. Geochemistry of Subcritical Geothermal Fluids. Studies of alteration mineralogy and fluid composition in geothermal systems show that equilibrium is closely approached between the geothermal fluids and secondary minerals formed in the systems, except for mobile elements such as Cl [35–39]. At Krafla, the most common secondary minerals identified include calcite, quartz, epidote, various clays, chlorite, feldspars, and pyrite. Anhydrite, prehnite, actinolite, wollastonite, garnet, pyrrhotite, and various zeolites, including wairakite, have also been observed [40]. Previous studies on mineral-fluid interaction at Krafla have demonstrated that the major fluid components were in equilibrium with these minerals, which in turn control the fluid composition at depth (Figure 5) [41].

Our experimental results indicate a similar process of mineral-fluid interaction at subcritical temperatures, with formation of secondary minerals upon interaction of geothermal water with the primary basaltic rock and glass. The calculated saturation indices with respect to commonly observed secondary minerals revealed near-equilibrium between the fluids and quartz, whereas supersaturation occurs with respect to calcite, chlorite, feldspars, wollastonite, and zeolites (Figure 5). Supersaturation may have resulted from high initial concentrations in the inlet experimental solutions relative to the equilibrium composition at 260°C and experimental durations of hours, compared to residence times of fluids in natural geothermal systems like at Krafla that are in the order of months to years [42, 43]. We conclude that the chemical composition of geothermal fluids at subcritical temperatures is controlled by near-equilibrium with secondary minerals. This agrees with previous findings [35–39, 41].

4.2. Supercritical Fluid Formation, Fluid-Rock Interaction, and Control of Elemental Transport. The solubility of mineral-forming elements and salts including Si, Ca, K, Na, and Cl is orders of magnitude lower in supercritical fluids compared to subcritical fluids and has been observed to decrease with decreasing fluid density [44–46]. Indeed, a recent modeling study of the formation of supercritical fluid by conductive boiling of subcritical fluids revealed that the process is expected to result in mineral deposition dominated by silica, aluminum silicates, and salts around the heat source [31]. In contrast, volatile elements like B, CO_2, and H_2S are expected to partition into the vapor phase upon boiling, resulting in insignificant concentration changes in the total fluid.

Elemental behavior upon conductive heating of subcritical liquid water to form supercritical fluid may be demonstrated from the elemental relative mobilities (RM), given by the elemental concentration (m_i) ratio between

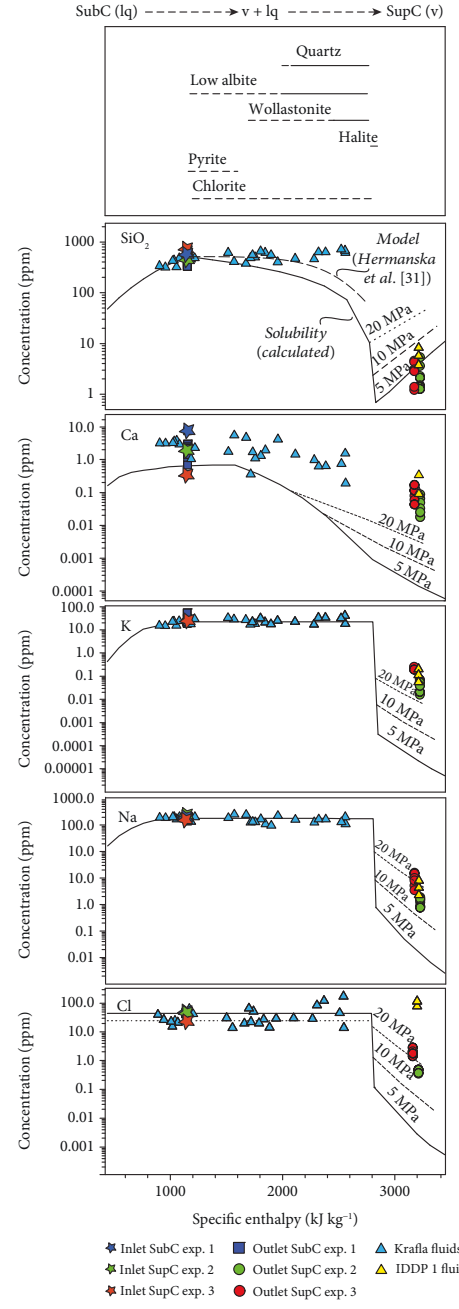

Figure 7: The concentration of subcritical and supercritical geothermal fluids observed in the experiments and at Krafla, Iceland [31, 41]. Also shown are predicted equilibrium concentrations assuming mineral-fluid equilibria at subcritical conditions [41, 47] as well as quartz and salt equilibrium solubility concentrations in supercritical water [44–46].

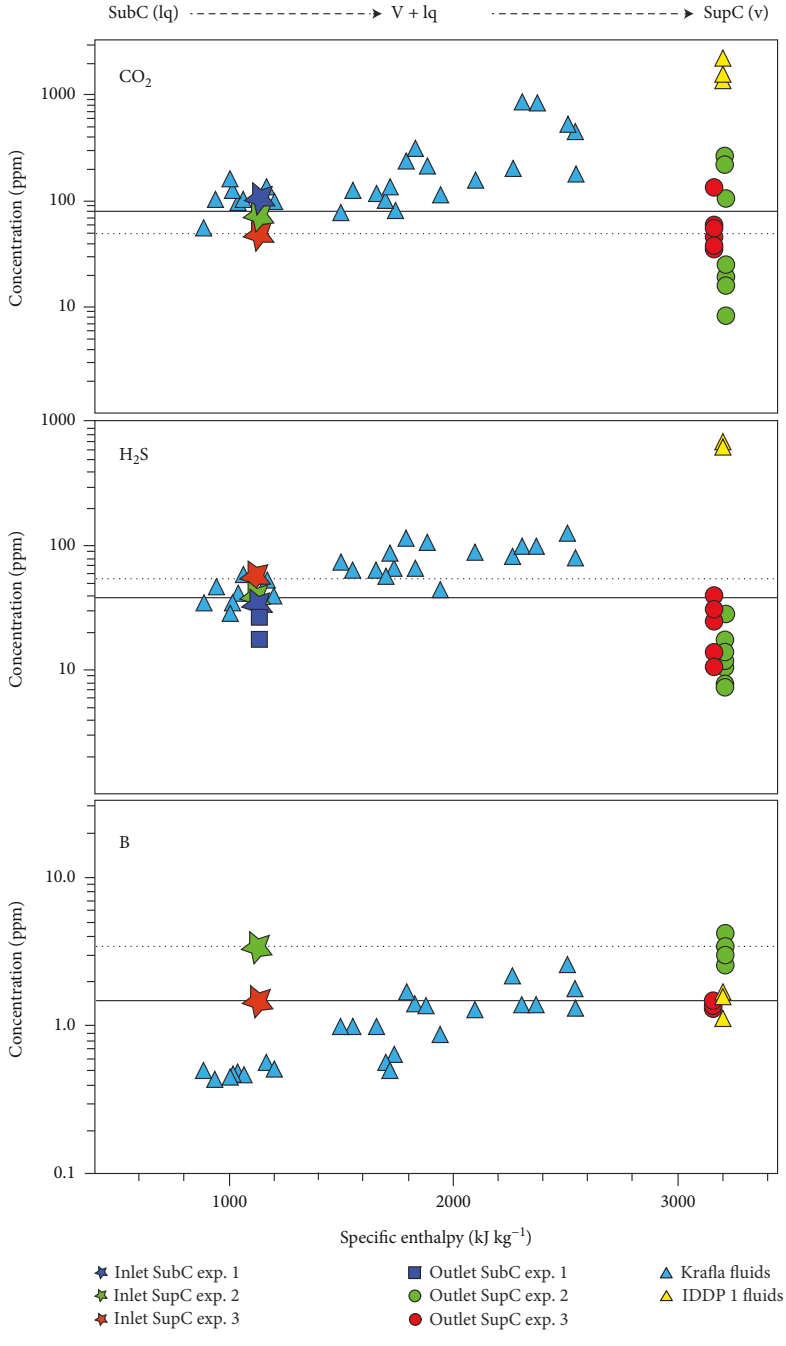

Figure 8: Concentrations of B, CO_2, and H_2S in the subcritical to supercritical fluids. Experimental results, concentrations in subcritical geothermal reservoir fluids at Krafla and the IDDP-1 fluid discharge composition [31, 41], and concentration trends predicted by previous geochemical modeling calculations [31].

Table 5: Comparison of measured and modeled geothermal fluids at Krafla. Concentrations are in ppm.

	Subcritical fluid		Supercritical fluid			
	Experiment[a]	Krafla[b]	Experiment w37[a]	Experiment w17[a]	IDDP-1[c]	Model[c]
t (°C)	260	295	420	400	440	
SiO_2	453 ± 121	659	2.4 ± 1.4	2.9 ± 1.3	6.0	3.2
B	3.41 ± 0.05	1.23	3.30 ± 0.46	1.39 ± 0.06	1.41	1.39
Na	181 ± 18	178	0.13 ± 0.04	0.99 ± 0.46	0.51	168
K	21.1 ± 9.1	40.9	0.04 ± 0.02	0.23 ± 0.04	0.12	31.8
Ca	1.91 ± 0.76	1.18	0.04 ± 0.03	0.10 ± 0.05	0.16	0.0002
Mg	0.009 ± 0.013	0.001	0.003 ± 0.001	0.026 ± 0.008	0.024	0.000001
Fe	0.044 ± 0.036	0.036	0.04 ± 0.01	0.12 ± 0.06	5.25	0.004
Al	6.20 ± 0.79	1.27	0.04 ± 0.02	0.08 ± 0.04	0.054	0.001
Cl	44.8 ± 1.6	112	0.41 ± 0.06	1.99 ± 0.44	105	109
CO_2	76.9 ± 12.5	858	87 ± 104	60.5 ± 34.2	1637	1628
SO_4	157 ± 29	127	0.37 ± 0.07	0.84 ± 0.57	32.7	4.13
H_2S	37.3 ± 9.6	266	13.9 ± 6.5	25.1 ± 10.2	630	395

[a]An average from the experimental runs (Table 3). [b]From Kaasalainen and Stefánsson [64]. [c]From Heřmanská et al. [31].

the inlet and outlet solution relative to a mobile element like B:

$$\mathrm{RM} = \frac{(m_i/m_B)_{\mathrm{outlet}}}{(m_i/m_B)_{\mathrm{inlet}}}. \quad (1)$$

The results demonstrate that volatile elements separate from the major rock-forming elements upon boiling of subcritical fluids to supercritical temperatures (Figure 6). Boron, CO_2, and H_2S partition into the vapor phase, whereas nonvolatile elements like Si, Ca, Na, K, Al, Cl, and SO_4 are precipitated into the observed secondary minerals, mainly silica, aluminum silicates, and chlorides. Chloride may also precipitate into salts like halite and sylvite (Figure 4). In this way, <1-10% of these elements are quantitatively removed from the initial concentration of the subcritical fluids.

The elemental concentrations can be further compared with the mineral-fluid equilibrium conditions considered to control their concentrations. At subcritical conditions, these reactions and equilibrium conditions are well established and include single mineral reactions as well as mineral-pair reactions [41] (Table 4). In order to calculate the individual elemental concentrations from these mineral-fluid equilibria buffers, further knowledge of the reservoir pH is needed. Here, pH conditions for Krafla fluids were adopted from Stefánsson and Arnórsson [47]. Experimental results are compared with calculated equilibrium compositions in Figure 7. Both experimental results and calculated equilibrium compositions showed good agreement between the two demonstrating a mineral-fluid equilibria control on the subcritical fluid compositions.

At supercritical conditions, it is less certain what processes control the fluid composition. Mineral solubilities are poorly known except for quartz and some common salts [44–46], therefore the experimental results are compared with the calculated solubility of quartz (SiO_2) and simple salts (NaCl, KCl, and $CaCl_2$), shown in Figure 7. Excellent agreement was observed for silica, suggesting that equilibrium between quartz and the supercritical fluid controls Si concentration in the fluid. In the case of other mineral-forming elements, concentrations obtained in the experiments were similar to or somehow higher to the calculated equilibrium concentrations of the salts. The elemental concentrations of these salts in the supercritical fluids may be influenced by a combination of different mineral solubilities including salts, oxides, and aluminum silicates. In contrast, the concentration of volatile elements like B, C, and S (Figure 8) remained unchanged in the fluid from subcritical to supercritical conditions, which is in agreement with previous geochemical modeling calculations [31].

4.3. Comparison of Experimental and Modeling Results with IDDP-1 Fluids. Experimental conductive boiling of a subcritical geothermal fluid to form supercritical fluid decreased mineral-forming element concentrations, whereas concentrations of volatile components remained mostly unchanged. Similar trends were observed in the elemental concentrations measured in the IDDP-1 supercritical fluid discharge when compared to subcritical fluids at Krafla (Table 5). However, direct comparison of experimental and IDDP-1 fluids shows that most concentrations of mineral-forming elements (Si, Na, K, and Ca) fall into a similar range, whereas Cl and volatile (CO_2, H_2S) concentrations differed significantly (Table 5). Concentrations of Cl at laboratory conditions were considerably lower than concentrations observed in the IDDP-1 discharge. Low concentrations of Cl in experimental fluids were caused by precipitation of minor amounts of salts (e.g., halite) in the very late stage of the boiling process. High concentrations of Cl and other volatile elements such as C and S in the IDDP-1 fluids could be attributed to minor magmatic degassing [48–50]. The experimental results thus support previous findings that supercritical IDDP-1

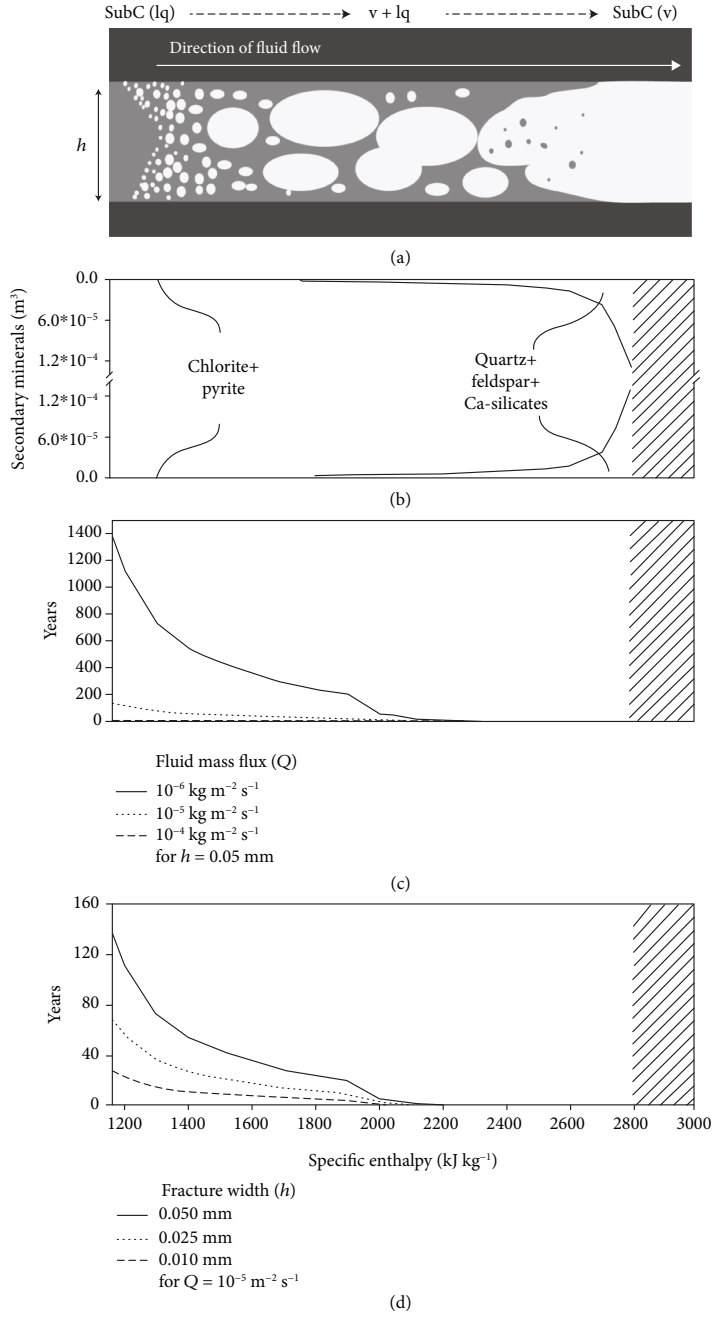

Figure 9: Mechanism of conductive boiling of subcritical fluids in cracks near the brittle-ductile transition (BDT). (a) Conductive boiling of a subcritical fluid to supercritical conditions along a single crack. (b) Volumes of secondary minerals (from Heřmanská et al. [31]) formed upon conductive boiling as a function of specific enthalpy along a crack. (c) Time for closure of a crack with a width of 0.05 mm as a function of specific enthalpy and fluid mass flux. Values for the range of fluid mass flux are taken from Norton and Knight [54]. (d) Time for closure of a crack with variable width based on permeability values of Norton and Knapp [53], Lamur et al. [51], and Watanabe et al., [52] using an average fluid mass flux of 10^{-5} kg m^{-2} s^{-1} [54]. Closure of the crack accelerates as soon as quartz starts to precipitate.

fluids likely form by conductive heating of subcritical geothermal reservoir fluids of meteoric water origin with minor input of magmatic gases [31, 48, 50]. Our experiments, in combination with geochemical modeling [31], revealed that varying the initial concentrations of volatile elements (C, S, and B) in the reservoir geothermal fluid does not affect the chemical composition of the supercritical fluid nor the alteration mineralogy, due to early partitioning of volatile elements into the vapor (Figure 8).

4.4. Mechanism of Boiling in Cracks and Implications for Exploitation of Supercritical Resources. Our experiments suggest that quartz and other silicates such as feldspar and wollastonite are the dominant secondary mineral phases that precipitate upon conductive boiling of subcritical fluids to form supercritical fluids. Boiling of 1 kg of subcritical fluids from Krafla has been modeled to produce ~50 cm^3 of silica [31], and using such results, the time required for complete closure of cracks by secondary mineral formation can be calculated (Figure 9). The permeability in volcanic geothermal systems like Krafla has been shown to range typically from 10^{-14} to 10^{-16} m^2, which can be equated to a single crack with a width of up to 0.05 mm cutting each cubic meter in the system [51–53]. Based on an average fluid mass flux of 10^{-5} $kg\,m^{-2}\,s^{-1}$ [54], conductive boiling of a subcritical fluid to supercritical conditions could lead to the complete closure of a 0.01 to 0.05 mm wide crack over a time period as short as a few hours or as long as ~140 years (Figure 9). These calculated time scales are in line with previous findings on permeability reduction in geothermal systems [25, 30, 32, 55–58]. However, the calculations should be considered as a simplification of real conditions. Mineral deposition was assumed to be immediate and independent of fluid flow, and possible reduced fluid flow upon decreased permeability associated with the mineral deposition was not considered. Formation of supercritical fluids may thus contribute to silica deposits, for example, as observed at the IDDP-1 well orifices [16]. However, such scaling will not occur during the supercritical fluid condensation as supercritical fluids exhibit low concentrations in mineral-forming elements (Figure 7).

5. Conclusions

The chemical and mineralogical changes associated with supercritical fluid formation by conductive heating and boiling of subcritical geothermal fluids were studied experimentally. Our results showed that the chemical composition of geothermal fluids at subcritical temperatures is controlled by near-equilibrium between the geothermal fluids and secondary minerals, except for mobile elements like Cl, which is in line with previous studies [35–39]. Upon conductive heating and boiling of such fluids to form supercritical fluids having a temperature >400°C, rock-forming elements like Si, Na, K, Ca, Mg, and Cl are quantitatively deposited into silicate, aluminum silicate, and salt deposits. In contrast, volatile element concentrations like CO_2, H_2S, and B remained unchanged. The observed concentrations of the nonvolatile elements are similar to those predicted from the solubility of quartz (SiO_2) and salts (NaCl, KCl, and $CaCl_2$) suggesting that reactions between these solids and the fluid influence and even control the elemental concentrations in the supercritical fluid. Similar concentration trends were observed for the IDDP-1 supercritical and subcritical geothermal fluids at Krafla, Iceland, and have been predicted from geochemical modeling [31]. The experimental results further support findings that the supercritical IDDP-1 fluids likely form by conductive heating of subcritical geothermal fluids of meteoric origin, with minor input of magmatic gases [31, 48, 50]. Such fluids may be suitable for power production.

Data Availability

The experimental data used to support the findings of this study are included within the article. The data from the Krafla geothermal field are from previously reported studies and datasets, which have been cited.

Disclosure

Preliminary results of selected parts of this study were previously presented during the Goldschmidt conference in Boston in 2018 [57].

Conflicts of Interest

The authors declare that there are no conflicts of interest regarding the publication of this paper.

Acknowledgments

We would like to thank Ríkey Kjartansdóttir, Andri Ísak Thórhallsson, and Helgi Arnar Alfreðsson for their valuable help. This work was funded by the Swiss National Science Foundation (CRSII2_1418431/1, Sinergia COTHERM), Georg (11-04-003), and The Energy Research Fund of Landsvirkjun in 2018 and 2019.

References

[1] D. O. Hayba and S. E. Ingebritsen, "Multiphase groundwater flow near cooling plutons," *Journal of Geophysical Research: Solid Earth*, vol. 102, no. B6, pp. 12235–12252, 1997.

[2] S. K. Sanyal and J. W. Morrow, "Success and the learning curve effect in geothermal well drilling," in *Proceedings Thirty-Seventh Workshop on Geothermal Reservoir Engineering*, Stanford, California, 2012.

[3] A. Richter, *Global geothermal capacity reaches 14,369 MW – top 10 geothermal countries, Oct 2018*, Think GeoEnergy - Geothermal Energy News, 2018.

[4] G. Ó. Friðleifsson, W. A. Elders, and A. Albertsson, "The concept of the Iceland Deep Drilling Project," *Geothermics*, vol. 49, pp. 2–8, 2014.

[5] L. Haar, J. S. Gallagher, and G. S. Kell, *NBS/NRC steam tables thermodynamic and transport properties and computer programs for vapor and liquid states of water in SI units*, Hemisphere Publishing, Washington, DC, USA, 1984.

[6] A. Liebscher and C. A. Heinrich, "Fluid–fluid interactions in the Earth's lithosphere," *Reviews in Mineralogy and Geochemistry*, vol. 65, no. 1, pp. 1–13, 2007.

[7] S. Scott, T. Driesner, and P. Weis, "Geologic controls on supercritical geothermal resources above magmatic intrusions," *Nature Communications*, vol. 6, no. 1, article 7837, 2015.

[8] S. Scott, T. Driesner, and P. Weis, "The thermal structure and temporal evolution of high-enthalpy geothermal systems," *Geothermics*, vol. 62, pp. 33–47, 2016.

[9] B. Mack Kennedy and A. H. Truesdell, "The northwest Geysers high-temperature reservoir: evidence for active magmatic degassing and implications for the origin of the Geysers geothermal field," *Geothermics*, vol. 25, no. 3, pp. 365–387, 1996.

[10] J. B. Lowenstern, D. Bergfeld, W. C. Evans, and A. G. Hunt, "Origins of geothermal gases at Yellowstone," *Journal of Volcanology and Geothermal Research*, vol. 302, pp. 87–101, 2015.

[11] A. Stefánsson, "Gas chemistry of Icelandic thermal fluids," *Journal of Volcanology and Geothermal Research*, vol. 346, pp. 81–94, 2017.

[12] T. Reinsch, P. Dobson, H. Asanuma, E. Huenges, F. Poletto, and B. Sanjuan, "Utilizing supercritical geothermal systems: a review of past ventures and ongoing research activities," *Geothermal Energy*, vol. 5, no. 1, p. 16, 2017.

[13] W. A. Elders, G. Ó. Friðleifsson, and A. Albertsson, "Drilling into magma and the implications of the Iceland Deep Drilling Project (IDDP) for high-temperature geothermal systems worldwide," *Geothermics*, vol. 49, pp. 111–118, 2014.

[14] G. Axelsson, T. Egilson, and S. S. Gylfadóttir, "Modelling of temperature conditions near the bottom of well IDDP-1 in Krafla, northeast Iceland," *Geothermics*, vol. 49, pp. 49–57, 2014.

[15] T. Hauksson and S. H. Markusson, "IDDP-1 flow test 2010-2012," *Landsvirkjun report, LV-2013-050*, National Power Company of Iceland, Reykjavik, 2013.

[16] T. Hauksson, S. Markusson, K. Einarsson et al., "Pilot testing of handling the fluids from the IDDP-1 exploratory geothermal well, Krafla, N.E. Iceland," *Geothermics*, vol. 49, pp. 76–82, 2014.

[17] G. Ó. Friðleifsson, W. A. Elders, R. A. Zierenberg et al., "The Iceland Deep Drilling Project 4.5 km deep well, IDDP-2, in the seawater-recharged Reykjanes geothermal field in SW Iceland has successfully reached its supercritical target," *Scientific Drilling*, vol. 23, pp. 1–12, 2017.

[18] E. Bali, L. E. Aradi, Á. Szabó, Cs. Szabó, G. Ó. Friðleifsson, and R. Zierenberg, "Fluid composition in the deepest part of the IDDP-2 deep borehole in Iceland based on fluid inclusions," in *Acta Mineralogica-Petrographica Abstract series, ECROFI XXV abstract book*, p. 16, Department of Mineralogy, Geochemistry and Petrology, University of Szeged, 2019.

[19] R. Brooks Hanson, "The hydrodynamics of contact metamorphism," *GSA Bulletin*, vol. 107, no. 5, pp. 595–611, 1995.

[20] R. B. Hanson, "Hydrodynamics of magmatic and meteoric fluids in the vicinity of granitic intrusions," in *Special Paper 315: The Third Hutton Symposium on the Origin of Granites and Related Rocks*, pp. 251–259, Geological Society of America, 1996.

[21] P. Weis, T. Driesner, and C. A. Heinrich, "Porphyry-copper ore shells form at stable pressure-temperature fronts within dynamic fluid plumes," *Science*, vol. 338, no. 6114, pp. 1613–1616, 2012.

[22] J. Hasenclever, S. Theissen-Krah, L. H. Rüpke et al., "Hybrid shallow on-axis and deep off-axis hydrothermal circulation at fast-spreading ridges," *Nature*, vol. 508, no. 7497, pp. 508–512, 2014.

[23] P. Weis, "The dynamic interplay between saline fluid flow and rock permeability in magmatic-hydrothermal systems," *Geofluids*, vol. 15, no. 1–2, pp. 350–371, 2015.

[24] T. P. Fischer and G. Chiodini, "Chapter 45 - Volcanic, magmatic and hydrothermal gases," in *The Encyclopedia of Volcanoes(Second edition)*, H. Sigurdsson, Ed., pp. 779–797, Academic Press, Amsterdam, 2015.

[25] R. O. Fournier, "Hydrothermal processes related to movement of fluid from plastic into brittle rock in the magmatic-epithermal environment," *Economic Geology*, vol. 94, no. 8, pp. 1193–1211, 1999.

[26] R. O. Foumier, "The transition from hydrostatic to greater than hydrostatic fluid pressure in presently active continental hydrothermal systems in crystalline rock," *Geophysical Research Letters*, vol. 18, no. 5, pp. 955–958, 1991.

[27] A. Okamoto, H. Saishu, N. Hirano, and N. Tsuchiya, "Mineralogical and textural variation of silica minerals in hydrothermal flow-through experiments: implications for quartz vein formation," *Geochimica et Cosmochimica Acta*, vol. 74, no. 13, pp. 3692–3706, 2010.

[28] A. Okamoto, T. Kikuchi, and N. Tsuchiya, "Mineral distribution within polymineralic veins in the Sanbagawa belt, Japan: implications for mass transfer during vein formation," *Contributions to Mineralogy and Petrology*, vol. 156, no. 3, pp. 323–336, 2008.

[29] H. Saishu, A. Okamoto, and N. Tsuchiya, "The effect of Al and Na on the precipitation rate of silica minerals: hydrothermal flow-through experiments at 430 °C and 31 MPa," *Procedia Earth and Planetary Science*, vol. 7, pp. 762–765, 2013.

[30] H. Saishu, A. Okamoto, and N. Tsuchiya, "The significance of silica precipitation on the formation of the permeable–impermeable boundary within Earth's crust," *Terra Nova*, vol. 26, no. 4, pp. 253–259, 2014.

[31] M. Heřmanská, A. Stefánsson, and S. Scott, "Supercritical fluids around magmatic intrusions: IDDP-1 at Krafla, Iceland," *Geothermics*, vol. 78, pp. 101–110, 2019.

[32] S. W. Scott and T. Driesner, "Permeability changes resulting from quartz precipitation and dissolution around upper crustal intrusions," *Geofluids*, vol. 2018, Article ID 6957306, 19 pages, 2018.

[33] S. Arnórsson, J. Ö. Bjarnason, N. Giroud, I. Gunnarsson, and A. Stefánsson, "Sampling and analysis of geothermal fluids," *Geofluids*, vol. 6, no. 3, pp. 203–216, 2006.

[34] A. Stefánsson, I. Gunnarsson, and N. Giroud, "New methods for the direct determination of dissolved inorganic, organic and total carbon in natural waters by Reagent-Free™ Ion Chromatography and inductively coupled plasma atomic emission spectrometry," *Analytica Chimica Acta*, vol. 582, no. 1, pp. 69–74, 2007.

[35] W. F. Giggenbach, "Geothermal mineral equilibria," *Geochimica et Cosmochimica Acta*, vol. 45, no. 3, pp. 393–410, 1981.

[36] W. F. Giggenbach, "Geothermal solute equilibria. Derivation of Na-K-Mg-Ca geoindicators," *Geochimica et Cosmochimica Acta*, vol. 52, no. 12, pp. 2749–2765, 1988.

[37] Z.-H. Pang and M. Reed, "Theoretical chemical thermometry on geothermal waters: problems and methods," *Geochimica et Cosmochimica Acta*, vol. 62, no. 6, pp. 1083–1091, 1998.

[38] A. Stefánsson and S. Arnórsson, "Feldspar saturation state in natural waters," *Geochimica et Cosmochimica Acta*, vol. 64, no. 15, pp. 2567–2584, 2000.

[39] S. Arnórsson, E. Gunnlaugsson, and H. Svavarsson, "The chemistry of geothermal waters in Iceland. II. Mineral equilibria and independent variables controlling water compositions," *Geochimica et Cosmochimica Acta*, vol. 47, no. 3, pp. 547–566, 1983.

[40] Á. Sveinbjörnsdóttir, "Composition of geothermal minerals from saline and dilute fluids — Krafla and Reykjanes, Iceland," *Lithos*, vol. 27, no. 4, pp. 301–315, 1991.

[41] B. T. Gudmundsson and S. Arnórsson, "Secondary mineral–-fluid equilibria in the Krafla and Námafjall geothermal systems, Iceland," *Applied Geochemistry*, vol. 20, no. 9, pp. 1607–1625, 2005.

[42] D. Kadko, K. Gronvold, and D. Butterfield, "Application of radium isotopes to determine crustal residence times of hydrothermal fluids from two sites on the Reykjanes peninsula, Iceland," *Geochimica et Cosmochimica Acta*, vol. 71, no. 24, pp. 6019–6029, 2007.

[43] A. Stefánsson, Á. E. Sveinbjörnsdóttir, J. Heinemeier, S. Arnórsson, R. Kjartansdóttir, and H. Kristmannsdóttir, "Mantle CO_2 degassing through the Icelandic crust: evidence from carbon isotopes in groundwater," *Geochimica et Cosmochimica Acta*, vol. 191, pp. 300–319, 2016.

[44] R. O. Fournier and R. W. Potter II, "An equation correlating the solubility of quartz in water from 25° to 900°C at pressures up to 10,000 bars," *Geochimica et Cosmochimica Acta*, vol. 46, no. 10, pp. 1969–1973, 1982.

[45] I. Leusbrock, S. J. Metz, G. Rexwinkel, and G. F. Versteeg, "The solubility of magnesium chloride and calcium chloride in near-critical and supercritical water," *The Journal of Supercritical Fluids*, vol. 53, no. 1-3, pp. 17–24, 2010.

[46] I. Leusbrock, S. J. Metz, G. Rexwinkel, and G. F. Versteeg, "Solubility of 1:1 alkali nitrates and chlorides in near-critical and supercritical water," *Journal of Chemical & Engineering Data*, vol. 54, no. 12, pp. 3215–3223, 2009.

[47] A. Stefánsson and S. Arnórsson, "Gas pressures and redox reactions in geothermal fluids in Iceland," *Chemical Geology*, vol. 190, no. 1–4, pp. 251–271, 2002.

[48] A. Stefánsson, D. R. Hilton, Á. E. Sveinbjörnsdóttir et al., "Isotope systematics of Icelandic thermal fluids," *Journal of Volcanology and Geothermal Research*, vol. 337, pp. 146–164, 2017.

[49] H. Ármannsson, J. Benjamínsson, and A. W. A. Jeffrey, "Gas changes in the Krafla geothermal system, Iceland," *Chemical Geology*, vol. 76, no. 3-4, pp. 175–196, 1989.

[50] A. Stefánsson and J. D. Barnes, "Chlorine isotope geochemistry of Icelandic thermal fluids: implications for geothermal system behavior at divergent plate boundaries," *Earth and Planetary Science Letters*, vol. 449, pp. 69–78, 2016.

[51] A. Lamur, J. E. Kendrick, G. H. Eggertsson, R. J. Wall, J. D. Ashworth, and Y. Lavallée, "The permeability of fractured rocks in pressurised volcanic and geothermal systems," *Scientific Reports*, vol. 7, no. 1, article 6173, 2017.

[52] N. Watanabe, T. Numakura, K. Sakaguchi et al., "Potentially exploitable supercritical geothermal resources in the ductile crust," *Nature Geoscience*, vol. 10, no. 2, pp. 140–144, 2017.

[53] D. Norton and R. Knapp, "Transport phenomena in hydrothermal systems: the nature of porosity," *American Journal of Science*, vol. 277, no. 8, pp. 913–936, 1977.

[54] D. Norton and J. E. Knight, "Transport phenomena in hydrothermal systems; cooling plutons," *American Journal of Science*, vol. 277, no. 8, pp. 937–981, 1977.

[55] R. O. Fournier, "The behavior of silica in hydrothermal solutions," in *Geology and Geochemistry of Epithermal Systems*, Society of Economic Geologists, 1985.

[56] J. T. Wells and M. S. Ghiorso, "Coupled fluid flow and reaction in mid-ocean ridge hydrothermal systems: the behavior of silica," *Geochimica et Cosmochimica Acta*, vol. 55, no. 9, pp. 2467–2481, 1991.

[57] R. P. Lowell, P. Van Cappellen, and L. N. Germanovich, "Silica Precipitation in Fractures and the Evolution of Permeability in Hydrothermal Upflow Zones," *Science*, vol. 260, no. 5105, pp. 192–194, 1993.

[58] S. P. White and E. K. Mroczek, "Permeability Changes During the Evolution of a Geothermal Field Due to the Dissolution and Precipitation of Quartz," *Transport in Porous Media*, vol. 33, no. 1, pp. 81–101, 1998.

[59] M. Heřmanská and A. Stefánsson, "Supercritical fluids in geothermal systems – an experimental study," *Goldschmidt Abstracts*, vol. 1004, 2018.

[60] S. Arnórsson, A. Stefánsson, and J. Ö. Bjarnason, "Fluid-fluid interactions in geothermal systems," *Reviews in Mineralogy and Geochemistry*, vol. 65, no. 1, pp. 259–312, 2007.

[61] D. Parkhurst and T. Appelo, "Description of input and examples for PHREEQC version 3—a computer program for speciation, batch-reaction, one-dimensional transport, and inverse geochemical calculations," US Geological Survey, 2013.

[62] E. H. Oelkers and S. R. Gislason, "The mechanism, rates and consequences of basaltic glass dissolution: I. An experimental study of the dissolution rates of basaltic glass as a function of aqueous Al, Si and oxalic acid concentration at 25°C and pH = 3 and 11," *Geochimica et Cosmochimica Acta*, vol. 65, no. 21, pp. 3671–3681, 2001.

[63] L. Ntihabose, *Well test analysis and temperature and pressure monitoring of Krafla and Nesjavellir high-temperature geothermal fields, Iceland*, UNU-Geothermal Training Programme, 2014.

[64] H. Kaasalainen and A. Stefánsson, "The chemistry of trace elements in surface geothermal waters and steam, Iceland," *Chemical Geology*, vol. 330-331, pp. 60–85, 2012.

Appendix C: Research article III

Heřmanská, M., Kleine, B.I., Stefánsson, A. Chemical constraints on supercritical fluids in geothermal systems

(accepted for publication in *Journal of Volcanology and Geothermal Research* in February 2020)

Reprinted with the permission of Elsevier Science Ltd.

GEOCHEMICAL CONSTRAINTS ON SUPERCRITICAL FLUIDS IN GEOTHERMAL SYSTEMS

Matylda Heřmanská*, Barbara I. Kleine, Andri Stefánsson

Institute of Earth Sciences, University of Iceland, Sturlugata 7, 101 Reykjavík, Iceland

*corresponding author. e-mail address mattylda@hi.is

Keywords: geothermal; supercritical fluids; fluid composition; alteration mineralogy

Highlights:

- Supercritical fluids form in various geotectonic settings by conductive heating of subcritical fluids of diverse origin
- Supercritical fluids display low concentrations of mineral-forming elements
- Supercritical fluids have comparable volatile element concentrations with the source geothermal fluids
- Supercritical fluid formation results in the secondary mineral deposition in the vicinity of magmatic bodies
- Alteration sequence is dominated by quartz, salts, wollastonite and aluminum silicates

Abstract

Supercritical fluids with temperatures of ~400-500°C have been reported from several active geothermal fields worldwide. Although the utilization of such fluids may multiply power production from new and already exploited geothermal systems, the fluid origin and chemical controls on their composition remain unclear. We performed flow-through high-temperature

(400-420°C) experiments at 34-69 bar to study the chemical and mineralogical changes associated with supercritical fluid formation upon boiling of subcritical geothermal fluids of varying chemical composition. Based on geochemical modeling and laboratory results, we propose that an important mechanism of supercritical fluid formation is conductive heating and boiling of subcritical geothermal groundwater by a magmatic intrusion. Such supercritical fluids will display low concentrations of mineral-forming elements (Si, Na, K, Ca, Mg, Al) with their concentrations being controlled by the solubility of salts, oxides, and aluminum silicates in high-temperature (>400°C) and low-density (ρ <0.3 g cm^{-3}) fluids. In contrast, supercritical fluids will show elevated concentrations of volatile elements (C, S, B) of crustal and/or mantle origin, with their concentrations often being similar to those of subcritical geothermal fluids. Associated mineral deposition, dominated by quartz, aluminum silicates, and salts, may form in the vicinity of the intrusion. Comparison of the modeling and laboratory results with observed chemical composition of natural supercritical fluid discharges indicates that conductive heating and boiling of subcritical geothermal groundwater may indeed be the formation mechanism of such fluids observed for example at Krafla (Iceland), Menengai (Kenya), Los Humeros (Mexico), and Larderello (Italy) with an addition of volcanic gases in many cases. Metal and salt-rich supercritical fluids, for example, at Kakkonda (Japan), may also exist in geothermal systems. However, such supercritical fluids are considered to have been trapped upon crystallization of the magmatic intrusion.

1. Introduction

Volcanic geothermal systems are commonly associated with a magmatic heat source at ~2-6 km depth (e.g., Hayba and Ingebritsen, 1997; Stimac et al., 2015). Utilization of the systems for energy production typically involves drilling of 2-3 km deep boreholes into the geothermal

reservoir and discharging liquid and vapor at the surface with subcritical temperatures to produce ~3–5 MW electric power per well (Sanyal and Morrow, 2012). Conductive heat transfer from the magmatic body to the circulating geothermal water above commonly occurs below the depth of the production wells, within the roots of the geothermal systems (Fig. 1). Recent studies have suggested that the geothermal fluids at these depths may have temperatures exceeding the critical temperature of pure water or T_c >374°C (Hayba and Ingebritsen, 1997; Scott et al., 2015, 2016, 2017). Indeed, such fluid temperatures have been observed in several active geothermal systems worldwide including those at The Geysers, Salton Sea, and Hawaii, USA (e.g., Garcia et al. 2016; Kaspereit et al. 2016; Teplow et al. 2009); Kakkonda, Japan (Kato et al. 1998); Larderello, Italy (e.g., Bertini et al. 1980; Ruggieri and Gianelli, 1995); Krafla, Nesjavellir, and Reykjanes, Iceland (e.g., Steingrímsson et al. 1990; Friðleifsson et al. 2010; Marks et al. 2010; Mortensen et al. 2010; Friðleifsson and Elders 2017); Los Humeros, Mexico (e.g., Espinosa-Paredes and Garcia-Gutierrez 2003); and Menengai, Kenya (Sekento 2012; Kipyego et al. 2013; Mbia 2015) (Fig. 1). However, the occurrence of such supercritical fluids[1] and, in particular, their chemical composition is not well understood. They have been predicted to form upon conductive heat transfer to the surrounding subcritical geothermal waters that boil and produce high-temperature and low-density fluids, accompanied by precipitation of non-volatile elements (Heřmanská et al., 2019a, 2019b). Supercritical fluids may also originate from magmatic degassing, characterized by elevated CO_2, SO_2, HCl, and

[1]Supercritical geothermal fluids have been commonly defined based on critical temperature (T_c = 373.976 °C) and pressure (P_c = 220.1 bar) of pure water (H_2O). However, such a definition can lead to an artificial and unphysical boundary in the phase diagram of water across which there is a continuous region of single-phase fluid. Moreover, for binary salt-water fluids the term supercritical is meaningless as - unlike in a pure fluid such as water - temperature changes may lead to fluid phase separation rather than the homogenization implied by the term supercritical. Here and following Liebscher and Heinrich (2007), supercritical fluid is defined here as fluid with temperatures above the critical temperature of fluid, irrespective of density (in the case of pure water) or phase state (in the case of binary and higher salt-water systems).

HF concentrations (Fischer and Chiodini, 2015), or form upon fluid entrapment during magma crystallization (e.g., Kasai et al., 1998a, 1998b).

Geothermal fluids usually originate from meteoric water, seawater, or a mixture thereof. Components of connate, magmatic, and metamorphic fluids may also be present (White 1974). The reservoir temperatures generally range from ~200 to 350°C. The main salt is commonly NaCl, and the NaCl concentration typically ranges from a few ppm to thousands of ppm and varies depending on the geological setting. The NaCl content is lowest in fluids associated with rift volcanism and basaltic rocks and higher in geothermal systems at subduction zones (Arnórsson et al., 2007). The concentrations of most major elements in the fluids are considered to be controlled by close approaches to local equilibrium with secondary minerals (e.g., Giggenbach, 1980; Arnórsson et al., 1983; Hedenquist, 1990) including reactive gases like CO_2, H_2S, and H_2, which may be mostly of magmatic origin (e.g., Giggenbach, 1992; Stefánsson, 2017). Secondary processes, including boiling, vapor condensation, and mixing with non-thermal water, may further modify the geothermal reservoir water upon fluid ascent to the surface. The geochemical composition of supercritical fluids occurring in the roots of active geothermal systems is largely unknown as well as the processes controlling their composition.

In this study, we performed experiments to investigate the supercritical fluid geochemistry associated with conductive heating of subcritical reservoir fluids by a magmatic body in the rift and subduction-related geothermal systems. To explore the chemical reactions occurring upon supercritical fluid formation, we performed reaction-path modeling. The current approach is the simplicity of the complex nature of most natural systems; however, it may be used to gain additional insight into the key parameters influencing the supercritical fluid composition and related alteration. Both experiment and modeling results were subsequently compared to previously reported data on natural supercritical fluid composition.

2. Methods

2.1. Experimental set-up

Supercritical fluid geochemistry was studied using flow-through experiments. The experiments were conducted by heating geothermal solutions to 400-420°C at a set minimum pressure of 34-69 bar to reach supercritical conditions. Consequently, the fluid phases changed from liquid to vapor to supercritical fluid with specific enthalpy increase to h >3000 kJ kg^{-1} (Fig. 2). These temperature, pressure, and enthalpy (*P*-*T*-*h*) conditions correspond to heat and mass transfer regimes upon conductive heating and boiling of subcritical geothermal fluids to form supercritical fluids predicted previously to occur within the roots of volcanic geothermal systems (Hayba and Ingebritsen, 1997; Scott et al., 2015, 2016, 2017).

Four experiments were carried out to test the effects of the subcritical geothermal fluid source on the formed supercritical fluid composition. The conditions of experiment #1 (low NaCl) were related to the formation of supercritical fluids formed by the heating of low-chloride, low-volatile, and mostly unreacted water of meteoric origin. Such conditions are typical for young geothermal systems at rift settings. Experiment #2 (low NaCl+reacted) was similar in nature but represented a reacted geothermal fluid that is in fluid-mineral equilibrium with the basaltic host rock. The conditions of experiments #3 (NaCl+HCl) and #4 (NaCl+CO_2) were related to the formation of supercritical fluids from Cl-rich fluids typical for geothermal systems associated with subduction zones with elevated volatile gas input, either HCl or CO_2.

A summary of the experimental conditions and the experimental solution composition is given in Table 1. In all cases, the inlet solutions were taken from natural geothermal waters and subsequently spiked to provide the representative chemical composition. The experiments were carried out using a high-temperature, flow-through reactor (Fig. 3). All wetted parts of the

flow-through experimental apparatus were made of inert material, including PEEK, titanium, and Inconel. Inlet solutions were pumped into a flow-through reactor (Inconel) at a flow rate of <0.50 g min^{-1} using an HPLC pump (Chromotech®). The pressure was controlled at the end of the line of each reactor outlet using a back-pressure regulator (BPR, Biotech). The reactor contained a stainless steel (316) threaded rod to capture deposits precipitating from the fluids. Samples of the outlet solutions of the reactor were collected at the low-pressure end of the back-pressure regulator, and samples of the inlet solutions were collected directly from the inlet solution bottle.

2.2. Sampling and analysis

For fluid chemical analysis, vapor samples were cooled and condensed in-line using a cooling jacket followed by collection into a polypropylene syringe at the low-pressure end of the back-pressure regulator. Samples for determining major elements (SiO_2, B, Na, K, Ca, Mg, Al, Fe, Cl, and SO_4) were filtered (0.2 μm cellulose acetate) into PP bottles, acidified (1% HNO_3, Merck Suprapur®), and analyzed by ICP-OES (Spectro Ciros Vision). Samples for pH were analyzed immediately after collection using a pH electrode calibrated against commercial buffer solutions. The samples for CO_2 determination were collected into degassed 0.01 M NaOH to prevent degassing before analyses. Dissolved inorganic carbon (CO_2) and H_2S were analyzed using a modified alkalinity titration (Stefánsson et al., 2007) and Hg precipitation titration with dithizone as an indicator (Arnórsson et al., 2006), respectively. The analytical precision of major element analyses was based on repeated analysis of a standard solution, and it was found to be < 3% for all elements except for Fe where it was ~15% at a 95% confidence level. The analytical precision for pH was ±0.05.

At the end of each experiment, the reactor was opened, and precipitates on the rod from inside of the reactor were collected. The sampling rod was imbedded in epoxy, cut

perpendicular to the flow direction in the reactor, and polished. The lose solid samples from the rod were mounted on a sample holder to study the morphology of the deposits. The secondary mineral phases and the morphology of the solid products from the two reactors were subsequently determined using a HITACHI TM-3000 scanning electron microscope (SEM) with an accelerating voltage of 15 keV.

2.3 Geochemical model

Based on the heat and mass transfer regimes upon boiling by conductive heat addition of subcritical geothermal waters to form supercritical fluids, schematic pressure, temperature, and enthalpy (*P*-*T*-*h*) paths were assessed and used as input conditions for the geochemical modeling (Fig. 2). The associated fluid chemical composition and secondary mineral formation were simulated assuming conservation of mass (closed-system behavior). The elements and compounds included in the calculations were SiO_2, B, Na, K, Ca, Mg, Al, Fe, Cl, SO_4, H_2S, and CO_2, along with appropriate aqueous and vapor species and selected minerals. The secondary minerals considered were those typically associated with high-temperature geothermal systems and included quartz, chlorite, epidote, wollastonite, albite, microcline, wairakite, calcite, actinolite, pyrite, and salts (e.g., halite, sylvite). The calculations were carried out using PHREEQC (Parkhurst and Appelo, 2013) and WATCH (Bjarnason, 2010) programs and the llnl.dat database was updated for mineral solubility constants (Holland and Powell, 1998; Holland and Powell, 2011; Stefánsson et al., 2011) and H_2S and CO_2 gas solubility constants (Fernández-Prini et al., 2003). Moreover, the solubility of common salts and oxides in supercritical fluids were calculated using literature data (Fournier and Potter, 1982; Leusbrock et al., 2009, 2010a, 2010b). The starting solution composition used in the geochemical calculations was the same as the inlet solutions used in the experiments (Table 1).

3. Results

3.1. Fluid chemical composition

The chemical compositions of the fluid samples collected from the outlet side of the experiments are reported in Table 2 and shown in Figure 4. The concentrations of Mg and Fe were affected by low detection limits or possible contamination by the sampling rod placed inside the reactor and, therefore, were not considered further in this study.

In experiment #1 (low NaCl), the outlet condensed solution had a mildly acidic pH value of 3.71-5.00 (at room temperature) and low concentrations of most elements relative to the inlet solution with SiO_2 of 0.40-2.68 ppm, Na of 0.25-5.89 ppm, Ca of 0.025-0.089 ppm, K of ~0.4 ppm, and Cl of 1.00-5.94 ppm. Concentrations of CO_2 of 23.4-201 ppm and B of 0.185-0.388 ppm in the outlet solution were similar to the inlet solution concentrations.

In experiment 2 (low NaCl+reacted), the outlet solution was similar in composition compared to the experiment #1 with pH of 3.24-4.17 (at room temperature) and concentrations of SiO_2 of 1.22-4.57 ppm, Na of 0.353-1.60 ppm, K of <0.10-0.256 ppm, Ca of 0.043-0.171 ppm, and Cl of 1.41-2.85 ppm. Concentrations of volatile elements in the outlet solutions were similar compared to the inlet solution with B of 1.30-1.47 ppm, CO_2 of 35.4-135 ppm, and H_2S of 10.7-40.0 ppm.

In experiment #3 (NaCl+HCl), the condensed outlet solution had a pH value of 0.80-1.69 (at room temperature)- much lower than other experimental solutions. As for the previous experiments, the concentrations of many mineral-forming elements in the outlet solutions were low compared to the inlet solution composition with SiO_2 of 1.70-2.68 ppm, Na of 0.30-15.7 ppm, K of 0.126-0.660 ppm, and Ca of 0.200-0.971 ppm. Concentrations of volatile elements like B, CO_2, and H_2S in the outlet solutions were similar to the inlet solution with concentrations of 1.27-1.62 ppm, 5.84-61.3 ppm, and 2.66-13.2 ppm, respectively. In contrast

to experiments #1 and #2, the concentration of Cl in the outlet solution was initially much lower (87.9-347 ppm) but increased at the end of the experiment to 706-1356 ppm and reached the concentration in the inlet solution.

In experiment #4 ($NaCl+CO_2$), the outlet condensed supercritical fluid had a mildly acidic pH value of 4.55-5.06 (at room temperature), low concentrations of SiO_2 of 0.582-0.748 ppm, Na of 0.186-33.3 ppm, K of 0.055-0.128 ppm, Ca of 0.009-0.035 ppm, and Cl of 0.446-0.7 ppm. As for the previous experiments, concentrations of B, CO_2, and H_2S were similar in the outlet solutions compared to the inlet solution with concentrations of 2.62-3.35 ppm, 89.5-419 ppm, and 19.5-40.1 ppm, respectively.

In summary, the concentrations of most mineral-forming elements like SiO_2, Na, K, Ca, and Al were observed to be low in the outlet supercritical fluids compared to the inlet subcritical fluids. The concentrations of volatile elements like B, CO_2, and H_2S in the outlet supercritical fluids were observed to be comparable to those concentrations of the respective inlet subcritical fluids. Chlorine displayed low concentrations in the supercritical fluids except when the inlet solutions contained elevated HCl concentrations.

3.2. Mineralogy and chemical composition of the solids

SEM microphotographs of the mineral deposits formed in experiments #1, # 2, and #4 are shown in Figure 5. In experiment #1 (low NaCl), the mineral deposits consisted mainly of unidentified layers of (Ca, Na, K)-Al-silicates and quartz with occasional appearances of K-feldspars and wollastonite. Close to the inlet of the reactor, the deposits on the rod were dense but became porous with increasing distance. In experiment #2 (low NaCl+reacted), the mineral deposits on the rod were similar as for experiment #1 with (Ca, Na, K)-Al-silicates and quartz dominating, the latter being replaced by amorphous silica at the outlet of the reactor. Occasional K-feldspar and wollastonite were also found in the deposits. In experiment #4

(NaCl+CO_2), solid products were distributed similarly to experiments #1 and #2, with most of the mineral deposits on the rod occurring in dense layers of 1-1.5 mm in thickness at the inlet of the reactor and becoming less abundant and porous at the outlet. The mineral deposits mainly consisted of interconnected halite cubes with amorphous silica, quartz, K-feldspar, and Ca-rich silicates presumably wollastonite. For experiment #3 (NaCl+HCl), a limited mineral deposition was observed except occasional silica.

In summary, similar mineral deposits occurred in all NaCl- experiments with cation (Na-Ca-K)-rich silicates, quartz being the dominant alteration products accompanied by halite in the case of elevated NaCl fluid concentrations. Fluids containing high concentrations of acids (HCl) resulted in insignificant mineral deposition upon the boiling of subcritical geothermal fluids to form supercritical fluids.

3.3. Geochemical modeling

The results of the geochemical modeling associated with isobaric boiling of subcritical geothermal waters by conductive heating to form supercritical fluids are shown in Figure 6. The relevant modeling results are presented for all four experimental scenarios, i.e., low NaCl fluid (experiment #1), low NaCl and reacted fluid (experiment #2), NaCl fluids with an elevated HCl input (experiment #3) and NaCl fluids with a high CO_2 input (experiment #4). In all cases, a distinct geochemical trend was observed. The concentrations of mineral-forming elements including Si, Na, K, Ca, Mg, Al, and Cl were reduced for all NaCl fluids upon boiling by the deposition of secondary mineral phases dominated by silica (quartz and amorphous silica), aluminum silicates (clays, chlorite, and K-feldspars), and salts (sylvite and halite). In contrast, for fluids containing elevated HCl with Cl concentrations greatly exceeding those of Na and K, a limited mineral deposition was predicted except for silica (quartz and amorphous silica) and simple Na-silicates. The total concentration of volatile components such as B, CO_2,

and H_2S remained constant due to the partitioning of volatile components into the vapor phase and undersaturation of carbonate and sulfide minerals in the liquid phase. It follows that the chemical composition of supercritical fluids formed upon conductive heating of a subcritical geothermal fluid has a similar volatile composition as the source fluid but low concentrations of reactive and mineral-forming elements. The input of acid magma gases like HCl may, however, drastically change the elemental geochemistry enhancing elemental mobility and reducing mineral deposition.

4. Discussion

4.1. Comparison between experimental and modeled supercritical fluid composition

Previous studies have demonstrated that major elemental concentrations of geothermal fluids with temperatures between ~50 and 350°C are controlled by an equilibrium between the geothermal fluids and secondary minerals except for mobile elements like Cl (e.g., Giggenbach, 1981, 1988; Arnórsson et al., 1983; Pang and Reed, 1998; Stefánsson and Arnórsson, 2000). The typical secondary minerals in the geothermal systems include, for instance, calcite, quartz, epidote, various clays, zeolites, chlorite, feldspars, and pyrite (e.g., Browne, 1978). Thus, the geothermal fluid composition is primarily controlled by temperature-dependent mineral solubility.

Upon supercritical fluid formation by boiling of subcritical fluids, the elemental mobility was experimentally observed and predicted by geochemical modeling to be significantly reduced for mineral-forming elements like SiO_2, Na, K, Ca, Mg and Al, but unchanged for volatile elements such as B, CO_2, and H_2S (Figs. 4 and 7). This suggests that mineral-fluid reactions also control the concentration of many major elements in supercritical fluids, as concluded previously for geothermal fluids at subcritical conditions. However, such

predictions are limited to our knowledge of mineral solubilities in low-density (ρ <0.3 g cm^{-3}) and high-temperature (>400°C) fluids as available data are restricted to solubility of quartz, common salts such as NaCl, KCl, and $CaCl_2$ and some volcanic gases at these conditions (e.g., Fournier and Potter, 1982; Symonds et al., 1992; Leusbrock et al., 2009, 2010a, 2010b,). In Figure 7, the experimental results are compared with the calculated solubility of quartz (SiO_2) and salts (NaCl, KCl, $CaCl_2$) in such low-density supercritical fluid. The experimental results compare well with the predicted mineral solubility in most cases, suggesting that concentrations of elements like SiO_2, Na, K, Ca, and Cl in supercritical geothermal fluids may indeed be controlled by mineral solubility of, for example, silicates, aluminum silicates, oxides, and salts. The mineral solubilities at these supercritical temperatures and low pressure have been observed to be mainly controlled by water density and the hydration of the gaseous species (e.g., Leusbrock et al., 2009, 2010a, 2010b; Hurtig and Williams-Jones, 2014a, 2014b). It follows that the chemical composition of supercritical geothermal fluids may be constrained knowing the important mineral solubilities in low-density and high-temperature hydrothermal fluids, provided such data are available for minerals of interest.

Our experiments were carried out with geothermal fluids that were previously in mineral-fluid equilibrium but were not in contact with any rock during the experiments. A recent experimental study demonstrates that supercritical fluid composition is not affected to a great extent by surrounding rocks (Passarella et al., 2017). Instead, elemental concentrations in supercritical fluids are considered to be controlled by mineral solubilities that are controlled mainly by fluid density and gas species hydration.

4.2. Supercritical geothermal fluids in active geothermal systems

Supercritical temperatures have been reported from geothermal systems at rift zones, for example, at Krafla (Iceland; Steingrímsson et al., 1990; Friðleifsson et al., 2010; Mortensen et

al., 2010) and Menengai (Kenya; (Sekento 2012; Kipyego et al. 2013; Mbia 2015) (Table 3). At Krafla the IDDP-1 well discharge had temperatures of ~440°C and displayed low concentrations of SiO_2, Na, K, Ca, Mg, and Al, and similar concentrations of volatile elements like B, CO_2 and H_2S as the subcritical geothermal reservoir fluids in the system (Ármannsson et al., 2014; Heřmanská et al., 2019b). Moreover, the chemical composition of the supercritical IDDP-1 fluid was similar to the composition predicted here by the geochemical modeling and laboratory experiment. At Menengai, a deep high-temperature supercritical reservoir has been identified with maximum temperatures of ~390°C and with a ~210°C liquid dominant reservoir above and at shallow depth (Montegrossi et al., 2015; O'Sullivan et al., 2015). Many of the well fluid discharges at Menengai are dominated by the shallow liquid reservoir fluids and may, therefore, not be characteristic of the deep supercritical reservoir. Instead, for the supercritical or vapor dominated fluid discharges, data are only available on the major gas composition (Malimo, 2013). These data show elevated CO_2 and H_2S concentrations compared to the Krafla supercritical fluids suggesting a possibly higher magmatic gas input. However, these elevated concentrations in the supercritical fluids are similar to those measured in the shallow subcritical liquid dominated fluids at Menengai. These findings suggest that the supercritical fluids at both Krafla and Menengai were formed by conductive heating from a magmatic body and boiling of the subcritical reservoir fluids with possible input of magmatic gases such as CO_2, H_2S, and Cl. At Krafla, these findings are further supported by the similarity of the isotopic composition of the IDDP-1 and subcritical reservoir fluids with δD of –85.8 to -84.9‰, $\delta^{18}O$ of -10.5 to -9.8‰, suggesting meteoric water as a source of the supercritical fluids (Ármannsson et al., 2014; Pope et al., 2015). In contrast, values of $\delta^{34}S$-H_2S of +0.5 to +1.1‰, $\delta^{13}C$-CO_2 being -5.3 to -1.4‰ and $\delta^{37}Cl$ 0.0 to +0.4‰ correspond to values of a magmatic source, however, a magmatic contribution is considered to be low (Stefánsson and Barnes, 2016; Arnórsson and Barnes 1983; Sano et al., 1985; Barry et al., 2014;

Ármannsson et al., 1989; Stefánsson et al., 2015,2017; Marini et al., 2011). Unfortunately, no isotope data are available for the supercritical fluids at Menengai to further constrain the origin of fluid and volatile elements.

Supercritical temperatures have also been reported for geothermal systems at subduction settings, for example, at The Geysers (USA), Los Humeros (Mexico), Larderello (Italy), and Kakkonda (Japan) (Table 3) (Reinsch et al., 2017). At The Geysers field, supercritical temperatures have been encountered in several boreholes, with maximum temperatures of ~400°C (e.g., Elders, 2015). Based on the δD and $\delta^{18}O$ isotope ratios, the water originates from a local meteoric source in addition to connate and volcanic water. The supercritical fluids display low concentrations of mineral-forming elements but higher concentrations of volatile elements like CO_2 and H_2S (Table 3). These elevated volatile concentrations have been considered to originate from connate and metamorphic fluids, high-temperature breakdown of metasediments, and boiling of condensed reservoir liquid (Truesdell et al., 1989; Lowenstern and Janik, 2005). At Los Humeros, several boreholes have also encountered supercritical fluids at depth, with maximum temperatures of ~400°C. However, most of the boreholes have been abandoned because of the highly-corrosive nature of the fluids (Diez et al., 2015). Based on water isotopes (δD and $\delta^{18}O$), the source fluids are a mixture of local meteoric and andesitic water. As for The Geysers field, the supercritical fluid discharges at Los Humeros have low mineral-forming element concentrations where the concentrations of gases like CO_2 and H_2S are high. The concentrations of B in the fluids are also very high or up to ~1000 ppm (Bernard et al., 2011). The isotope values of the volatile elements suggest a magmatic source with $\delta^{11}B$ of -0.8‰ and $\delta^{13}C$-CO_2 of -3.5‰ (Bernard, 2008). The geothermal reservoir at Larderello is vapor dominated with supercritical temperatures of up to ~430°C (Minissale, 1991; Ruggieri and Gianelli, 1995). The water is believed to be of meteoric origin with possible input of magmatic water (e.g., D'Amore and Bolgnesi, 1994; Panichi et al., 1995; Scandiffio et al.,

1995). Carbon dioxide is the dominant gas in the fluid of crustal and/or mantle origin based on the $\delta^{13}C\text{-}CO_2$ value of -6.3 to -2.8‰ (Gherardi et al., 2005). Boron concentrations are high and are considered to originate from evaporitic and carbonitic sediments based on their $\delta^{11}B$ ratio with values of +3.4 to +16.1‰ (Pennisi et al., 2001). Based on these findings, it is evident that supercritical fluids for geothermal systems in subduction settings may, in many cases, originate from conductive heating of the geothermal groundwater by the magmatic heat source, often with input from connate and magmatic water. The concentrations of mineral-forming elements in these fluids are low (on the lower ppm and ppb scale) as observed for supercritical fluids associated with rift systems and predicted here by geochemical modeling and experimentally. Differences in elemental concentrations between the localities might also be ought to differences in fluid pressures of the individual geothermal system. Mineral-forming element solubilities such as for Si, Na, and Cl may be a function of pressure, and elemental concentrations in supercritical fluids may become higher with increasing fluid density (Fig. 7; Fournier and Potter, 1982; Leusbrock et al., 2009, 2010a, 2010b). Thus, the elemental concentrations of supercritical fluids may not only be dependent on the fluid composition of the subcritical fluid but also may depend on the pressure conditions and depth of supercritical fluid formation in the geothermal system.

On the other hand, concentrations of volatile elements like CO_2, H_2S, and B are variable between systems and often high, originating from the crust upon fluid-rock interaction and magmatic gases. Variable and elevated Cl concentrations have also been observed and associated with supercritical geothermal fluids, for example, at Krafla and The Geysers. At Krafla, high Cl concentrations can be explained by the contribution of a magmatic source where fluid ascent and depressurization to the surface may lead to the partitioning of the volatile HCl in the vapor phase into the liquid phase, possibly resulting in very high Cl concentrations (e.g., Heřmanská et al., 2019b). Elevated Cl concentrations in supercritical

fluids from The Geysers geothermal field are considered to be of magmatic origin and/or the result of boiling of NaCl-rich connate or metamorphic water (Truesdell et al., 1989, Moore and Gunderson 1995, Moore et al., 2001). Supercritical fluids have also been observed at the Kakkonda geothermal systems. The geothermal system consists of two parts - a shallow liquid dominated reservoir with temperatures of 230-260°C and a deep zone in the vicinity of granite intrusions with less permeable rocks and temperatures of up to ~500°C. The supercritical fluids at the highest temperatures are hypersaline and metal-rich with ~55% NaCl. However, these supercritical fluids are considered to have been trapped in the Kakkonda granite during crystallization with a small addition of meteoric water that permeated into the conductive heat zone around the granite intrusion (Kasai et al., 1998a, 1998b, 2000).

In conclusion, despite different chemical compositions of supercritical fluid discharges in geothermal settings like Krafla, Menengai, The Geysers, Los Humeros, and Larderello, all of them most likely originate from conductive heating of the surrounding subcritical geothermal groundwater with elevated volatile concentrations derived from the addition of connate, magmatic or metamorphic gases.

5. Conclusions

We have carried out flow-through experiments and geochemical modeling to describe the chemical and mineralogical changes associated with supercritical fluid formation upon conductive heating of subcritical geothermal fluids with varying chemical composition. Based on our experimental modeling results, we conclude the following:

- Supercritical fluids formed by conductive heating and boiling of ~200-300°C subcritical geothermal water are predicted to have low concentrations of mineral-forming elements (Si, Na, K, Ca, Mg, Al) with their concentrations controlled by the solubility of salts, oxides, and aluminum silicates in high-temperature (>400°C) and low-density (ρ <0.3 g cm^{-3})

water. The concentration of the volatile elements (C, S, B) will be higher than in the case of mineral-forming elements and similar to the concentration of volatile elements in subcritical geothermal fluids.

- Upon supercritical fluid formation by conductive heating and boiling of subcritical ~200-300°C geothermal water, the secondary mineral deposition will occur. These deposits are dominated by quartz, salts (e.g., halite), wollastonite, and aluminum silicates such as feldspars.

A comparison of the results with the observed chemical composition of natural supercritical fluid discharges indicates that conductive heating and boiling of subcritical geothermal groundwaters may indeed be the mechanism responsible for the formation of naturally observed supercritical fluids. Metal and salt-rich supercritical fluids observed in some of the geothermal systems (e.g., Kakkonda, Reykjanes) are considered to be of magmatic origin, formed by exsolution of fluids upon crystallization magmatic intrusion and/or may derive from the separation of vapor and steam.

Acknowledgments

This research was funded by the Swiss National Science Foundation [CRSII2_141843/1, Sinergia COTHERM] and Landsvirkjun Energy Research Fund. We would like to thank Ríkey Kjartansdóttir, Ísak Þórhallsson, and Gylfi Sigurðsson for their help during this work.

References

Allegrini, G., Benvenuti, G.C., 1970. Characteristics and geothermal power plant protection (collateral processes of abrasion, erosion, and scaling). Geothermics 2, 865-881.

Ármannsson, H., Benjamínsson, J., Jeffrey, A.W.A., 1989. Gas changes in the Krafla geothermal system, Iceland. Chem. Geol. 76, 175–196.

Ármannsson, H., Fridriksson, T., Gudfinnsson, G.H., Ólafsson, M., Óskarsson, F., Thorbjörnsson, D., 2014. IDDP—The chemistry of the IDDP-01 well fluids in relation to the geochemistry of the Krafla geothermal system. Geothermics 49, 66–75.

Arnórsson, S., Barnes, I., 1983. The nature of carbon dioxide waters in Snaefellsnes, Western Iceland. Geothermics 12, 171-176.

Arnórsson, S., Bjarnason, J.Ö., Giroud, N., Gunnarsson, I., Stefánsson, A., 2006. Sampling and analysis of geothermal fluids. Geofluids 6, 203-216.

Arnórsson, S., Gunnlaugsson, E., Svavarsson, H., 1983. The chemistry of geothermal waters in Iceland. II. Mineral equilibria and independent variables controlling water compositions. Geochim. Cosmochim. Acta 47, 547–566.

Arnórsson, S., Stefánsson, A., Bjarnason, J.Ö., 2007. Fluid-Fluid Interactions in Geothermal Systems. Rev. Mineral. Geochem. 65, 259–312.

Barry, P.H., Hilton, D.R., Füri, E., Halldórsson, S.A., Grönvold, K., 2014. Carbon isotope and abundance systematics of Icelandic geothermal gases, fluids and subglacial basalts with implications for mantle plume-related CO_2 fluxes. Geochim. Cosmochim. Acta 134, 74–99.

Bernard, R., 2008. Isotopos de H, O, He, C and N en fluidos hidrotermales del Cinturon Volcanico Mexicano. M.S. Thesis, Posgrado de Ciencias de la Tierra, UNAM, 157 p.

Bernard, R., Taran, Y., Pennisi, M., Tello, E., Ramirez, A., 2011. Chloride and Boron behavior in fluids of Los Humeros geothermal field (Mexico): A model based on the existence of deep acid brine. Appl. Geochem. 26, 2064–2073.

Bertini, G., Giovannoni, A., Stefani, G.C., Gianelli, G., Puxeddu, M., Squarci, P., 1980. Deep Exploration in Larderello Field: Sasso 22 Drilling Venture. In: Strub, A.S., Ungemach, P. (Eds), Advances in European Geothermal Research. Springer Netherlands, 303–311.

Bjarnason, J.Ö., 2010. The Chemical Speciation Program WATCH, Version 2.4. Iceland GeoSurvey, Reykjavík, Iceland

Browne, P.R.L., 1978. Hydrothermal alteration in active geothermal fields. Ann. Rev. Earth Planet. Sci. 6, 229–250.

Cruz, I., Tovar, R., 2008. Evaluación Preliminar de la Cantidad de Inhibidor de Corrosión para la Neutralización del Fluido del H-43. CFE Files, DINYAC-012-2008.

D'Amore, F., Bolgnesi, L., 1994. Isotopic evidence for a magmatic contribution to fluids of the geothermal systems of Larderello, Italy, and the Geysers, California. Geothermics 23, 21-32.

Diez, H., Flores, M., Ramírez, M., Tovar, R., Rosales, C., Solano, F., Sandoval, F., 2015. Neutralization of Acid Fluids from Well H-43 (Superheated Steam), Los Humeros Geothermal Field, Mexico. Proc. World Geotherm. Cong. 2015, Melbourne, Australia, 19-25 April 2015, 1-6.

Elders, W.A., 2015. The potential for on- and off-shore high-enthalpy geothermal systems in the USA. Proc. 40th Workshop Geotherm. Res. Eng. 2015, Stanford University, Stanford, CA, 26-28 January 2015.

Espinosa-Paredes, G., Garcia-Gutierrez, A., 2003. Estimation of static formation temperatures in geothermal wells. Energy Conversion and Management 44, 1343–1355.

Fernández-Prini, R., Alvarez, J.L., Harvey, A.H., 2003. Henry's constants and vapor-liquid distribution constants for gaseous solutes in H_2O and D_2O at high temperatures. J. Phys. Chem. Ref. Data. 32, 903–916.

Fischer, T.P., Chiodini, G., 2015. Volcanic, Magmatic and Hydrothermal Gases. In: H. Sigurdsson (Ed.), The Encyclopedia of Volcanoes. Academic Press, Amsterdam, Second Edition, 779–797.

Fournier, R.O., Potter, R.W., 1982. An equation correlating the solubility of quartz in water from 25° to 900°C at pressures up to 10,000 bars. Geochim. Cosmochim. Acta 46, 1969–1973.

Friðleifsson, G.Ó., Elders, W.A., 2017. Successful Drilling for Supercritical Geothermal Resources at Reykjanes in SW Iceland. GRC Trans. 41, 1095–1106.

Friðleifsson, G.Ó., Pálsson, B., Stefánsson, B., Albertsson, A., Gunnlaugsson, E., Ketilsson, J., Lamarche, R., Andersen, P.E., 2010. Iceland Deep Drilling Project. The first IDDP Drill Hole Drilled and Completed in 2009. Proc. World Geotherm. Cong. 2010, Bali, Indonesia, 25–29 April 2010.

Garcia, J., Hartline, C., Walters, M., Wright, M., Rutqvist, J., Dobson, P.F., Jeanne, P., 2016. The Northwest Geysers EGS Demonstration Project, California: Part 1: Characterization and reservoir response to injection. Geothermics 63, 97–119.

Gherardi, F., Panichi, C., Gonfiantini, R., Magro, G., Scandiffio, G., 2005. Isotope systematics of C-bearing gas compounds in the geothermal fluids of Larderello, Italy. Geothermics 34, 442–470.

Giggenbach, W.F., 1980. Geothermal gas geochemistry. Geochim. Cosmochim. Acta 44, 2021–2032.

Giggenbach, W.F., 1981. Geothermal mineral equilibria. Geochim. Cosmochim. Acta 45, 393–410.

Giggenbach, W.F., 1988. Geothermal solute equilibria. Derivation of Na–K–Mg–Ca geoindicators. Geochim. Cosmochim. Acta 52, 2749–2765.

Giggenbach, W.F., 1992. Isotopic shift in waters from geothermal and volcanic systems along convergent plate boundaries and their origin. Earth Planet. Sci. Lett. 113, 495–510.

Haizlip, J., Truesdell, A.H., 1988. Hydrogen chloride in superheated steam and chloride in deep brine at The Geysers geothermal field, California. Proc. 13th Workshop Geotherm. Res. Eng. 1988, Stanford University, Stanford, CA, 19-21 January 1988.

Hayba, D.O., Ingebritsen, S.E., 1997. Multiphase groundwater flow near cooling plutons. J. Geophys. Res. Solid Earth 102, 12235–12252.

Hedenquist, J.W., 1990. The thermal and geochemical structure of the Broadlands-Ohaaki geothermal system, New Zealand. Geothermics 19, 151–185.

Heřmanská, M., Kleine, B.I., Stefánsson, A., 2019a. Supercritical Fluid Geochemistry in Geothermal Systems. Geofluids 2019, Article ID 6023534.

Heřmanská, M., A Stefánsson, A., Scott, S., 2019b. Supercritical fluids around magmatic intrusions: IDDP-1 at Krafla, Iceland. Geothermics 78, 101-110.

Holland, T.J.B., Powell, R., 1998. An internally consistent thermodynamic data set for phases of petrological interest. J. Metamorph. Geol. 16, 309–343.

Holland, T.J.B., Powell, R., 2011. An improved and extended internally consistent thermodynamic dataset for phases of petrological interest, involving a new equation of state for solids. J. Metamorph. Geol. 29, 333–383.

Hurtig, N.C., Williams-Jones, A.E., 2014a. An experimental study of the transport of gold through hydration of AuCl in aqueous vapour and vapour-like fluids. Geochim. Cosmochim. Acta 127, 305-325.

Hurtig, N.C., Williams-Jones, A.E., 2014b. An experimental study of the solubility of MoO_3 in aqueous vapour and low to intermediate-density supercritical fluids. Geochim. Cosmochim. Acta 136, 169-193.

Kasai, K., Sakagawa, Y., Komatsu, R., Sasaki, M., Akaku, K., Uchida, T., 1998a. The origin of hypersaline liquid in the quaternary Kakkonda granite, sampled from well WD-1a, Kakkonda geothermal system, Japan. Geothermics 27, 631–645.

Kasai, K., Sakagawa, Y., Miyazaki, S., Akaku, K., Uchida, T., 1998b. Supersaline and metal-rich brine obtained from Quaternary Kakkonda granite by Nedo WD-1a in the Kakkonda geothermal field, Japan. Min. Deposit. 33, 298-301.

Kasai, K., Hishi, Y., Fukuda, D., Kato, O., Doi, N., Akaku, K., Ominato, T., Tosha, T., 2000. The fluid geochemistry and reservoir model for the Kakkonda geothermal system, obtained by Nedo's deep-seated geothermal reservoir survey, Japan. Proc. World Geotherm. Cong. 2000, Kyushu-Tohoku, Japan, 28 May – 10 June 2000.

Kaspereit, D., Mann, M., Sanyal, S., Rickard, B., Osborn, W., Hulen, J., 2016. Updated Conceptual Model and Reserve Estimate for the Salton Sea Geothermal Field, Imperial Valley, California. GRC Trans. 2016, 40, 57–66.

Kato, O., Doi, N., Sakagawa, Y., Uchida, T., 1998. Fracture systematics in and around well WD-1, kakkonda geothermal field, Japan. Geothermics 27, 609–629.

Kipyego, E., O'Sullivan, J., O'Sullivan, M., 2013. An Initial Resource Assessment of the Menengai Caldera Geothermal System Using an Air-Water TOUGH2 Model. Proc., 35th New Zealand Geothermal Workshop, Rotorua, New Zealand.

Leusbrock, I., Metz, S.J., Rexwinkel, G., Versteeg, G.F., 2009. Solubility of 1:1 Alkali Nitrates and Chlorides in Near-Critical and Supercritical Water. J. Chem. Eng. Data. 54, 3215–3223.

Leusbrock, I., Metz, S.J., Rexwinkel, G., Versteeg, G.F., 2010a. The solubility of magnesium chloride and calcium chloride in near-critical and supercritical water. J. Supercrit. Fluids 53, 17–24.

Leusbrock, I., Metz, S.J., Rexwinkel, G., Versteeg, G.F., 2010b. The solubilities of phosphate and sulfate salts in supercritical water. J. Supercrit. Fluids 54, 1–8.

Liebscher, A., Heinrich, C.A., 2007. Fluid–Fluid Interactions in the Earth's Lithosphere. Rev. Mineral. Geochem. 65, 1–13.

Lowenstern, J.B., Janik, C.J., 2005. The origins of reservoir liquids and vapors from The Geysers geothermal field, California (USA). In: Simmons, S.F., Graham, I. (Eds), Volcanic, Geothermal, and Ore-Forming Fluids: Rulers and Witnesses of Processes within the Earth. Special Publ. Soc. Econ. Geol. 10.

Malimo, S.J., 2013. Fluid Chemistry of Menengai Geothermal Wells, Kenya. GRC Trans. 37, 425-429.

Marini, L., Moretti, R., Accornero, M.,2011. Sulfur Isotopes in Magmatic-Hydrothermal Systems, Melts, and Magmas. Rev. Mineral. Geochem. 73 (1), 423–492.

Marks, N., Schiffman, P., Zierenberg, R.A., Franzson, H., Friðleifsson, G.Ó., 2010. Hydrothermal alteration in the Reykjanes geothermal system: Insights from Iceland deep drilling program well RN-17. J. Volcanol. Geotherm. Res. 189, 172–190.

Mbia, P., Mortensen, A., Oskarsson, N., Hardarson, B., 2015. Sub-surface geology, petrology and hydrothermal alteration of the Menengai geothermal field, Kenya: case study of wells MW-02, MW-04, MW-06, and MW-07. Proc. World Geotherm. Cong. 2015, Melbourne, Australia, 19-25 April 2015, 1-15.

Minissale, A., 1991. The Larderello geothermal field: A review. Earth Sci. Rev. 31, 133-151.

Montegrossi, G., Pasqua, C., Battistelli, A., Mwawongo, G., Ofwona, C., 2015. 3D natural state model of the Menengai geothermal system, Kenya. Proc. World Geotherm. Cong. 2015, Melbourne, Australia, 19-25 April 2015, 1-15.

Moore, J.N., Gunderson, R.P., 1995. Fluid inclusion and isotopic systematics of an evolving magmatic-hydrothermal system. Geochim. Cosmo. Acta 59, 3887-3908.

Moore, J.N., Norman, D.I., Mack Kennedy, B., 2001. Fluid inclusion gas compositions from an active magmatic–hydrothermal system: a case study of The Geysers geothermal field, USA. Chemical Geology, 173, 3-30.

Mortensen, A.K., Grönvold, K., Gudmundsson, Á., Steingrímsson, B., Egilson, Þ., 2010. Quenched Silicic Glass from Well KJ-39 in Krafla, North-Eastern Iceland. Proc. World Geotherm. Cong. 2010, Bali, Indonesia, 25–29 April 2010.

Nicholson, K., 1993. Geothermal Fluids. Berlin, Heidelberg: Springer-Verlag.

O'Sullivan, J., Kipyego, E., Croucher, A., Ofwona, C., O'Sullivan, M., 2015. A supercritical model of the Menengai geothermal system. Proc. World Geotherm. Cong. 2015, Melbourne, Australia, 19-25 April 2015.

Pang, Z.-H., Reed, M. H., 1998. Theoretical chemical thermometry on geothermal waters: Problems and methods. Geochim. Cosmochim. Acta 62, 1083–1091.

Panichi, C., Scandiffio, G., Baccarin, F., 1995. Variation of geochemical parameters induced by reinjection in the Lardarello area. Proc. World Geotherm. Congr. 1995, Florence, Italy, 18-31 May 1995, 1845-1849.

Parkhurst, D., Appelo, T., 2013. Description of input and examples for PHREEQC version 3—a computer program for speciation, batch-reaction, one-dimensional transport, and inverse geochemical calculations., US Geological Survey, 2013.

Passarella, M., Mountain, B.W., Seward T.M., 2017. Experimental Simulations of Basalt-fluid Interaction at Supercritical Hydrothermal Condition (400°C – 500bar). Procedia Earth Planet. Sci. 17, 770-773.

Pennisi, M., Magro, G., Adorni-Braccesi, A., 2001. Boron and helium isotopes in geothermal fluids from Larderello (Italy). WRI 2001, 899-902.

Pope, E.C., Bird, D.K., Arnórsson, S., Giroud, N., 2015. Hydrology of the Krafla geothermal system, northeast Iceland. Geofluids 16, 175-197.

Reinsch, T., Dobson, P., Asanuma, H., Huenges, E., Poletto, F., Sanjuan, B., 2017. Utilizing supercritical geothermal systems: A review of past ventures and ongoing research activities. Geotherm. Energy 5, 16.

Ruggieri, G., Gianelli, G., 1995. Fluid inclusion data from the Carboli 11 well, Larderello geothermal field, Italy. Proc. World Geotherm. Cong. 1995, Florence, Italy, 18-31 May 1995, 1087-91.

Sano, Y., Urabe, A., Wakita, H., Chiba, H., Sakai, H., 1985. Chemical and isotopic compositions of gases in geothermal fluids in Iceland. Geochem. J. 19, 135–148.

Sanyal, S.K., Morrow, J.W., 2012. Success and the learning curve effect in geothermal well drilling. Proc. 37th Workshop Geotherm. Res. Eng. 2012, Stanford University, Stanford, CA, 30 January- 1 February 2012, 1-8.

Scandiffio, G., Panichi, C., Valenti, M., 1995. Geochemical evolution of fluids in the Larderello geothermal field. Proc. World Geotherm. Cong. 1995, Florence, Italy, 18-31 May 1995, 1839–1843.

Scott, S., Driesner, T., Weis, P., 2015. Geologic controls on supercritical geothermal resources above magmatic intrusions. Nature Comm. 61.

Scott, S., Driesner, T., Weis, P., 2016. The thermal structure and temporal evolution of high-enthalpy geothermal systems. Geothermics 62, 33–47.

Scott, S., Driesner, T., Weis, P., 2017. Boiling and condensation of saline geothermal fluids above magmatic intrusions. Geophys. Res. Let. 44, 1696-1705.

Sekento, L.R., 2012. Geochemical and isotopic study of the Menengai geothermal field, Kenya. Geothermal Training Programme Reports 2012, 31.

Stefánsson, A., 2017. Gas chemistry of Icelandic thermal fluids. J. Volcanol. Geotherm. Res. 346, 81-94.

Stefánsson, A., Arnórsson, S., 2000. Feldspar saturation state in natural waters. Geochim. Cosmochim. Acta 64, 2567-2584.

Stefánsson, A., Arnórsson, S., Gunnarsson, I., Kaasalainen, H., Gunnalugsson, E., 2011. The geochemistry and sequestration of H_2S into the geothermal system at Hellisheidi, Iceland. J. Volcanol. Geotherm. Res. 202, 179-188.

Stefánsson, A., Barnes, J.D., 2016. Chlorine isotope geochemistry of Icelandic thermal fluids: Implications for geothermal system behavior at divergent plate boundaries. Earth. Planet. Sci. Let. 449, 69-78.

Stefánsson, A., Gunnarsson, I., Giroud, N., 2007. New method for the direct determination of dissolved inorganic, organic and total carbon in natural water by Reagent-Free ion chromatography and inductively coupled plasma atomic emission spectrometry. Anal. Chim. Acta 582, 69-74.

Stefánsson, A., Hilton, D.R., Sveinbjörnsdóttir, Á.E., Torssander, P., Heinemeier, J., Barnes, J.D., Ono, S., Halldórsson, S.A., Fiebig, J., Arnórsson, S., 2017. Isotope systematics of Icelandic thermal fluids. J. Volcanol. Geotherm. Res. 337, 146-164.

Stefánsson, A., Keller, N.S., Gunnarsson-Robin, J., Ono, S., 2015. Multiple sulfur isotope systematics of Icelandic geothermal fluids and the source and reactions of sulfur in volcanic geothermal systems at divergent plate boundaries. Geochim. Cosmochim. Acta 165, 307-323.

Steingrímsson, B., Guðmundsson, Á., Franzson, H., Gunnlaugsson, E., 1990. Evidence of a supercritical fluid at depth in the Nesjavellir field. Proc. 15th Workshop Geotherm. Reserv. Eng. 81–88.

Stimac, J., Goff, F., Goff, C.J., 2015. Intrusion-related geothermal systems. In: H. Sigurdsson (Ed.), The Encyclopedia of Volcanoes. Academic Press, Amsterdam, Second Edition, 799–822.

Symonds, R.B., Reed, M.H., Rose, W.I., 1992. Origin, speciation, and fluxes of trace-element gases at Augustine volcano, Alaska: Insights into magma degassing and fumarolic processes. Geochim. Cosmochim. Acta 56 (2), 633-657.

Teplow, W.J., Marsh, B.D., Hulen, J., Spielman, P., Kaleikini, M., Fitch, D.C., Rickard, W., 2009. Dacite melt at the Puna geothermal venture wellfield, Big Island of Hawaii. GRC Trans. 33, 989–94.

Truesdell, A.H., 1991. Origin of acid fluids in geothermal reservoirs. GRC Trans. 15, 289-296.

Truesdell, A.H., Haizlip, J.R., Ármannsson, H., D'Amore, F., 1989. Origin and transport of chloride in superheated geothermal steam. Geothermics 18, 295-304.

Truesdell, A.H., Nehring, N.L., 1978. Gases and water isotopes in a geochemical section across the Larderello, Italy, geothermal field. Pure Appl. Geophys. 117, 276-289.

White, D.E., 1974. Diverse Origins of Hydrothermal Ore Fluids. Econ. Geol. 69, 954–973.

Figure and table captions

Figure 1: Main characteristics of a volcanic geothermal system. (A) Conceptual model of a volcanic geothermal system showing fluid flow paths (black arrows) and the zone of heat convection where supercritical conditions may appear (red area) between the heat source (magmatic intrusion) and the circulating geothermal fluid. Depressurization boiling occurs near the surface (after Arnórsson et al., 2007; Scott et al., 2016). Conventional production wells do not commonly reach the supercritical zone. (B) The boiling curve of water. Dashed lines indicate temperature-depth profiles above magmatic intrusions at selected times (after Hayba and Ingebritsen, 1997). The red shaded area shows fluids having temperature exceeding the critical temperature of water (T_c >374°C). Wells with reported temperatures above the critical temperature of the water are also shown (see Reinsch et al., 2017).

Figure 2: The subcritical to supercritical conditions of the experiments are shown (A) in connection to the boiling curve water and (B) in the phase diagram of water. The pressure, enthalpy, and temperature relations are also displayed.

Figure 3: Schematic experimental set-up used for the experiments carried out in this study.

Figure 4: Measured elemental concentration of the outlet solutions of the four experiments. The average compositions of the respective inlet solutions are included for comparison.

Figure 5: Selected SEM microphotographs of the solid products precipitated for experiment #1 (low NaCl), experiment #2 (low NaCl+reacted) and experiment #4 (NaCl+CO_2). Also shown are representative EDS analysis of the major phases identified in experiments #1, #2, and #4. No precipitates were found in experiment #3 (NaCl+HCl).

Figure 6: Moles of secondary minerals and the elemental loss calculated for the conditions of the experiments using the PHREEQC software (Parkhurst and Appelo, 2013).

Figure 7: A) Comparison of modeling and experimental results for elemental concentrations at subcritical and supercritical conditions. Predicted solubilities of silica, sodium, and chlorine in supercritical fluids were calculated based on quartz and salt solubility in low-density (ρ <0.3 g cm^{-3}) and high-temperature (T>374°C) water using data reported by Fournier and Potter (1982) and Leusbrock et al. (2009, 2010a, 2010b). B) Naturally observed data of reservoir fluid compositions from wells that reported supercritical conditions in rift and subduction zones (Malimo, 2013; Montegrossi et al. 2015; Truesdell 1991; Truesdell et al., 1989; Diez et al., 2015; Allegrini and Benvenuti, 1970; Nicholson, 1993; Haizlip and Truesdell, 1988; Kasai et al., 1998a; Cruz and Tovar 2008; Heřmanská et al., 2019b).

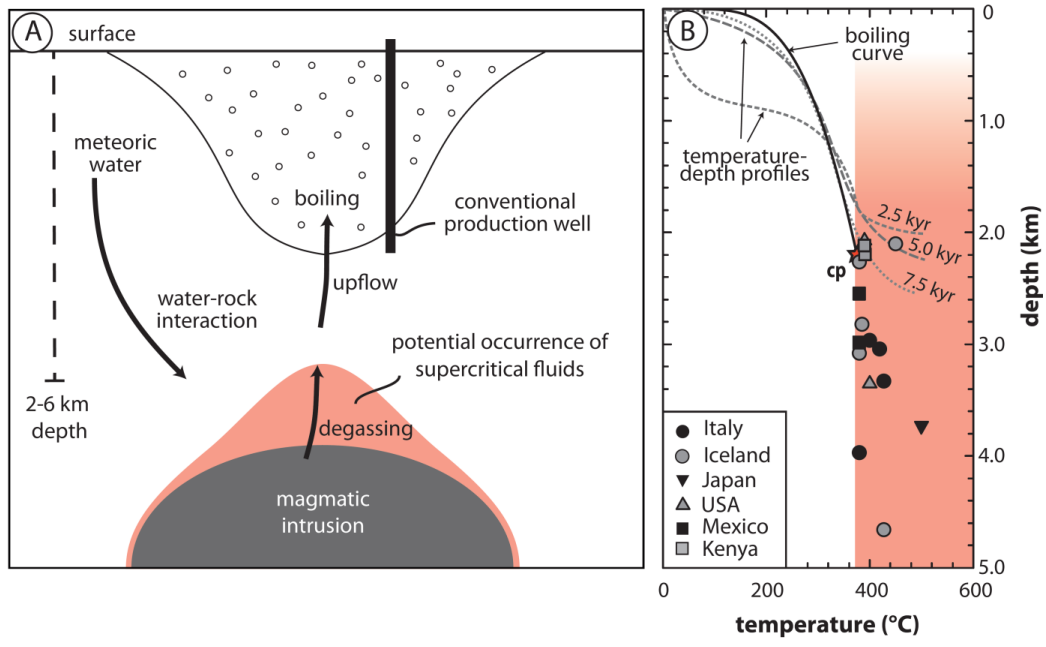
A
surface
meteoric water
boiling
conventional production well
upflow
water-rock interaction
potential occurrence of supercritical fluids
2-6 km depth
degassing
magmatic intrusion
B
boiling curve
temperature-depth profiles
2.5 kyr
5.0 kyr
7.5 kyr
cp
Italy
Iceland
Japan
USA
Mexico
Kenya
0
200
400
600
temperature (°C)
0
1.0
2.0
3.0
4.0
5.0
depth (km)

Figure 1

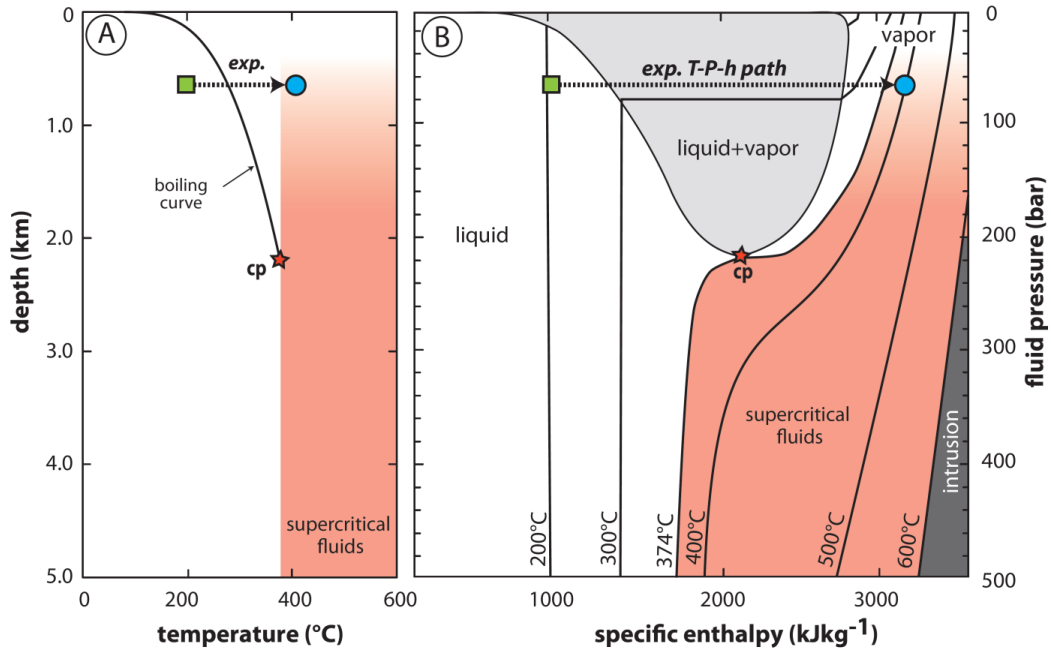
A
B
exp.
boiling
curve
cp
supercritical
fluids
depth (km)
temperature (°C)
0
1.0
2.0
3.0
4.0
5.0
0
200
400
600
exp. T-P-h path
vapor
liquid+vapor
liquid
cp
supercritical
fluids
intrusion
200°C
300°C
374°C
400°C
500°C
600°C
1000
2000
3000
specific enthalpy (kJkg-1)
fluid pressure (bar)
0
100
200
300
400
500

Figure 2

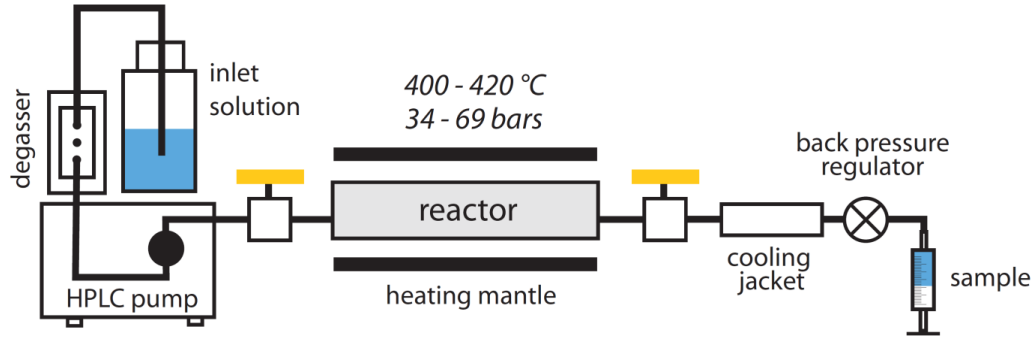
degasser
inlet
solution
400 - 420 °C
34 - 69 bars
back pressure
regulator
reactor
cooling
jacket
sample
HPLC pump
heating mantle

Figure 3

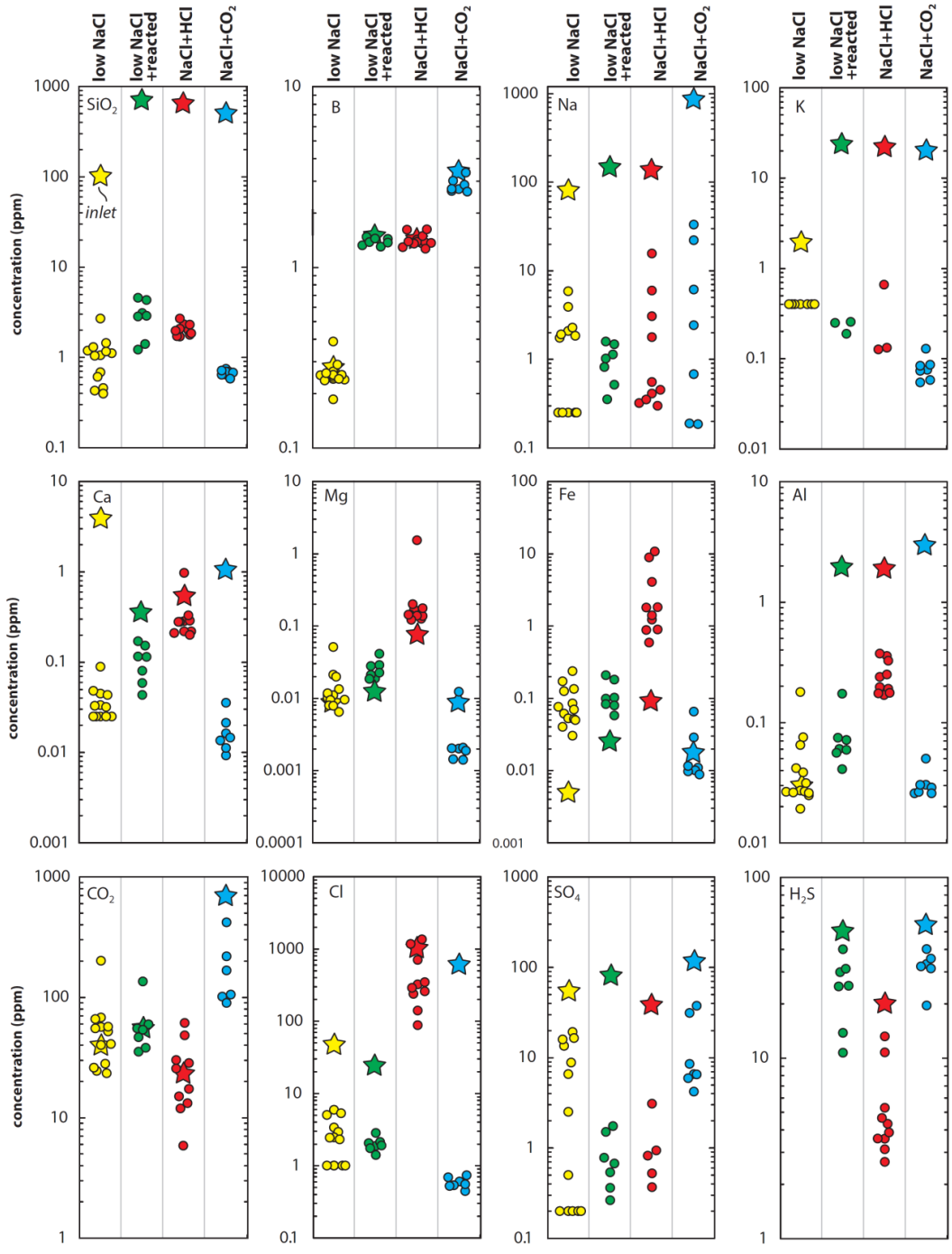
low NaCl
low NaCl +reacted
NaCl+HCl
NaCl+CO2
SiO2
inlet
B
Na
K
Ca
Mg
Fe
Al
CO2
Cl
SO4
H2S
concentration (ppm)

Figure 4

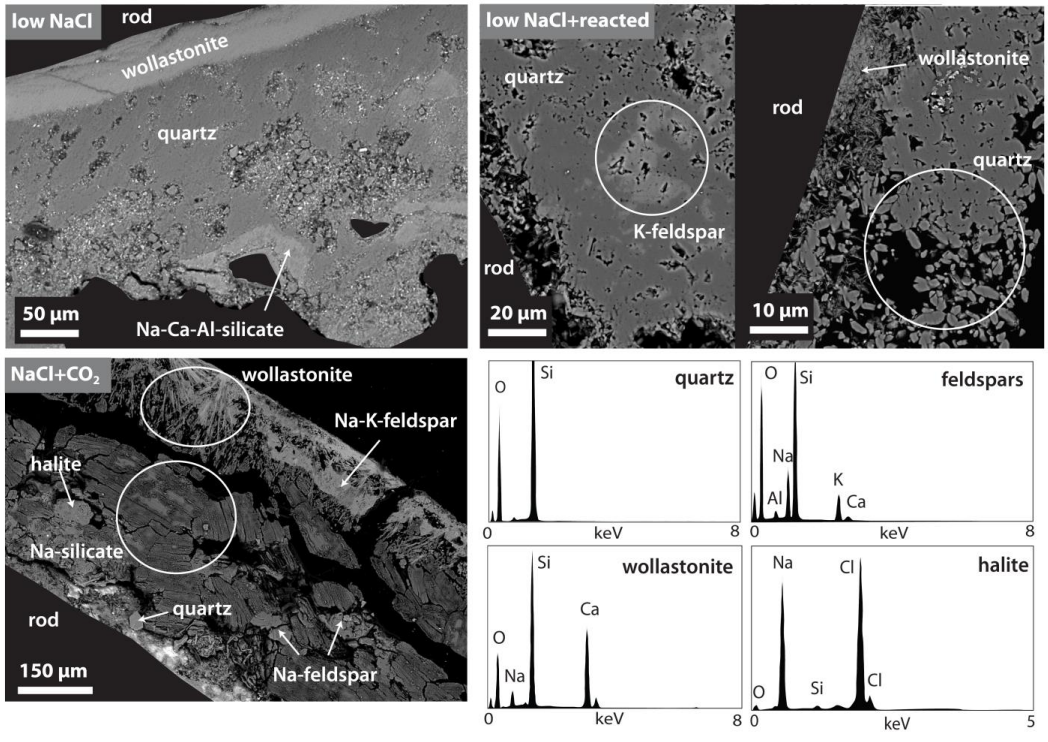
low NaCl
rod
wollastonite
quartz
50 µm
Na-Ca-Al-silicate
low NaCl+reacted
quartz
K-feldspar
rod
20 µm
rod
wollastonite
quartz
10 µm
NaCl+CO2
wollastonite
Na-K-feldspar
halite
Na-silicate
rod
quartz
150 µm
Na-feldspar
O
Si
quartz
0
keV
8
O
Si
feldspars
Na
Al
K
Ca
0
keV
8
Si
wollastonite
Ca
O
Na
0
keV
8
Na
Cl
halite
O
Si
Cl
0
keV
5

Figure 5

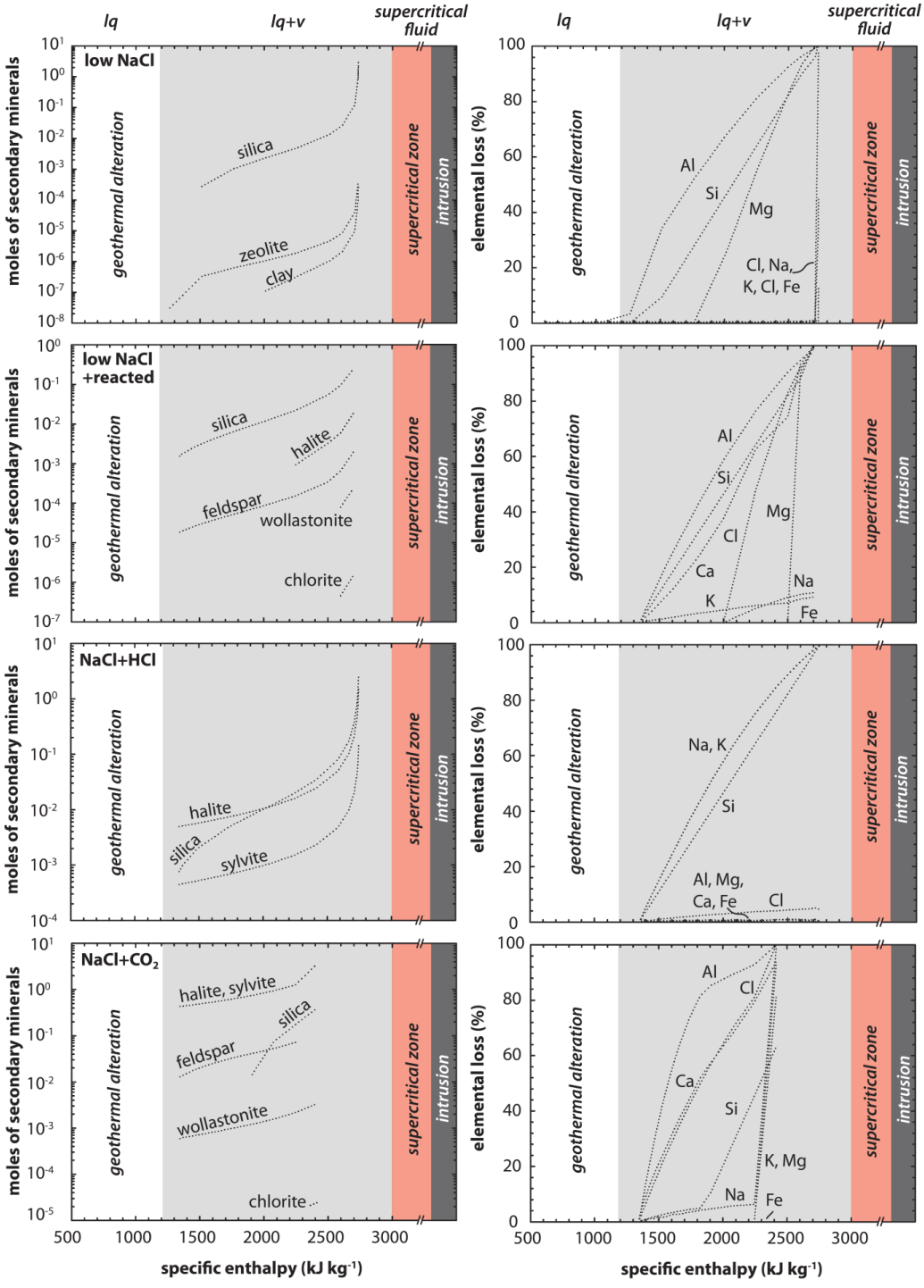
lq
lq+v
supercritical fluid
low NaCl
low NaCl +reacted
NaCl+HCl
NaCl+CO2
moles of secondary minerals
elemental loss (%)
geothermal alteration
supercritical zone
intrusion
silica
zeolite
clay
halite
feldspar
wollastonite
chlorite
sylvite
halite, sylvite
Al
Si
Mg
Cl, Na, K, Cl, Fe
Ca
Na
K
Fe
Na, K
Al, Mg, Ca, Fe
Cl
K, Mg
specific enthalpy (kJ kg-1)

Figure 6

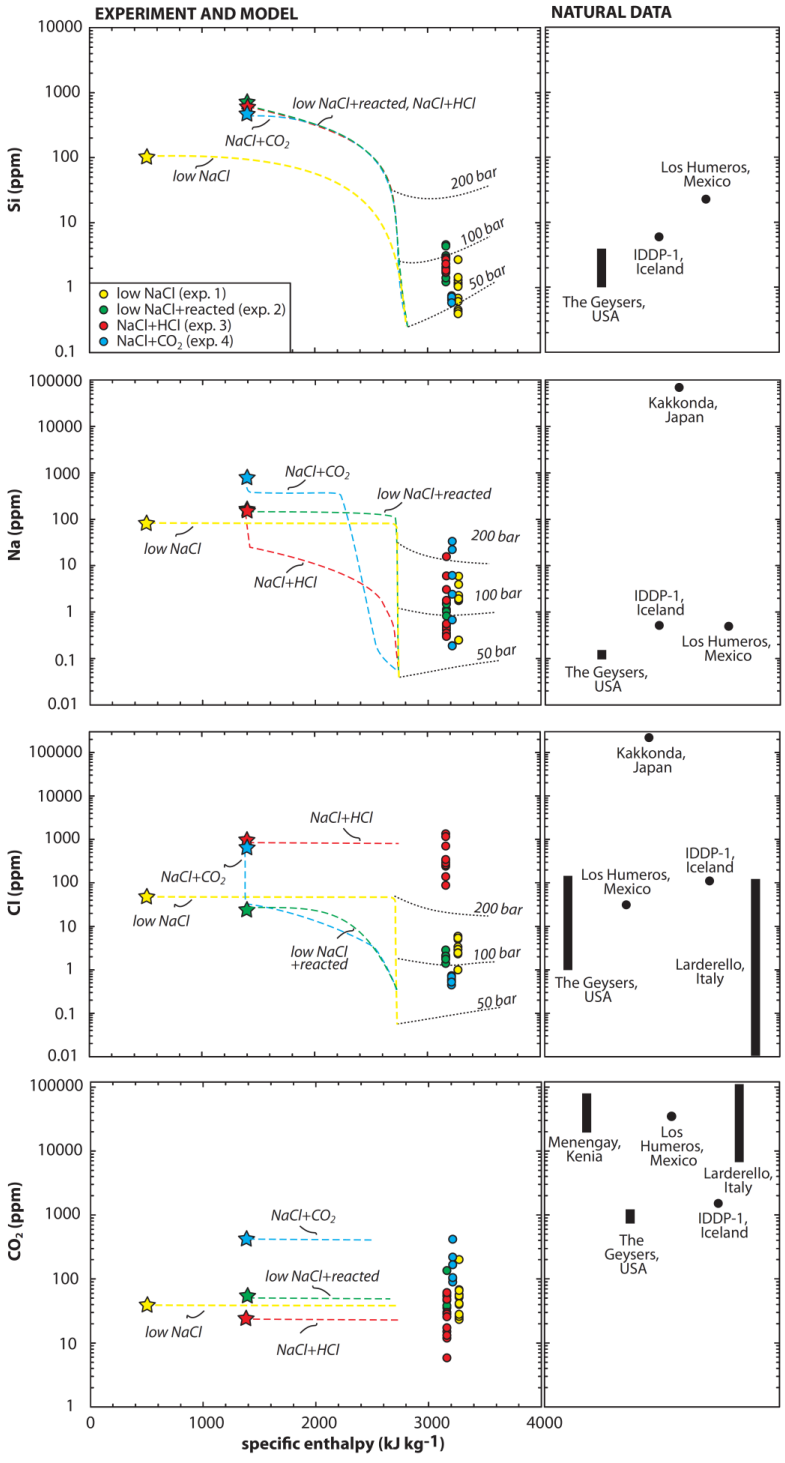
EXPERIMENT AND MODEL
NATURAL DATA
Si (ppm)
low NaCl+reacted, NaCl+HCl
NaCl+CO2
low NaCl
200 bar
100 bar
50 bar
low NaCl (exp. 1)
low NaCl+reacted (exp. 2)
NaCl+HCl (exp. 3)
NaCl+CO2 (exp. 4)
Los Humeros, Mexico
IDDP-1, Iceland
The Geysers, USA
Na (ppm)
NaCl+CO2
low NaCl+reacted
low NaCl
NaCl+HCl
200 bar
100 bar
50 bar
Kakkonda, Japan
IDDP-1, Iceland
Los Humeros, Mexico
The Geysers, USA
Cl (ppm)
NaCl+HCl
NaCl+CO2
low NaCl
low NaCl +reacted
200 bar
100 bar
50 bar
Kakkonda, Japan
Los Humeros, Mexico
IDDP-1, Iceland
Larderello, Italy
The Geysers, USA
CO2 (ppm)
NaCl+CO2
low NaCl+reacted
low NaCl
NaCl+HCl
Menengay, Kenia
Los Humeros, Mexico
Larderello, Italy
IDDP-1, Iceland
The Geysers, USA
specific enthalpy (kJ kg-1)

Figure 7

Table 1
Experimental conditions and chemical composition of the inlet solutions used in the experiments and for the geochemical model calculations. Concentrations are in ppm.

		Exp. #1 low NaCl	Exp. #2 low NaCl + reacted	Exp. #3 NaCl + HCl	Exp. #4 NaCl + CO_2
Experimental conditions					
T	°C	420	400	420	420
P	bar	34	69	69	69
h	kJ kg^{-1}	3269	3159	3159	3211
Inlet solution chemical composition					
pH/ °C		8.90/19	9.29/22	1.55/22	8.89/21
SiO_2		102	699	645	494
B		0.275	1.49	1.42	3.34
Na		81.8	144	138	858
K		1.86	24.0	22.5	20.4
Ca		3.89	0.346	0.537	1.04
Mg		0.009	0.012	0.076	0.009
Fe		0.005	0.025	0.090	0.017
Al		0.029	1.94	1.86	2.96
CO_2		39.1	53.5	23.3	685
Cl		47	24.6	1055	604
SO_4		53.8	79.6	36.6	116
H_2S		nd	49.1	19.8	54.3

Table 2
Chemical composition of the outlet solutions.

#	T °C	P bar	Q ml min^{-1}	pH/ °C	SiO_2 ppm	B ppm	Na ppm	K ppm	Ca ppm	Mg ppm	Fe ppm	Al ppm	CO_2 ppm	Cl ppm	SO_4 ppm	H_2S ppm
low NaCl																
#1	420	34	0.50	4.90/19	1.05	0.241	2.08	< 0.40	0.045	0.021	0.237	0.076	201	3.37	19.3	
#2	420	34	0.51	4.77/19	1.11	0.247	2.28	< 0.40	0.048	0.020	0.172	0.065	56.6	2.92	13.5	
#3	420	34	0.52	5.00/19	1.19	0.265	1.75	< 0.40	0.043	0.013	0.126	0.042	24.5	2.46	8.85	
#4	420	34	0.51	4.77/19	1.17	0.238	1.85	< 0.40	0.033	0.011	0.085	0.027	23.4	2.32	6.57	
#5	420	34	0.50	4.80/19	2.68	0.254	5.89	< 0.40	0.033	0.010	0.061	0.031	52.1	5.94	16.5	
#6	420	34	0.49	4.78/19	1.30	0.253	1.92	< 0.40	0.032	0.011	0.076	0.027	40.0	2.44	15.9	
#7	420	34	0.56	4.60/19	1.04	0.254	3.93	0.40	0.025	0.010	0.070	0.025	41.0	5.06	2.51	
#8	420	34	0.51	4.44/19	0.686	0.236	0.250	0.40	0.025	0.012	0.053	0.038	26.0	1.00	0.20	
#9	420	34	0.52	4.60/19	0.609	0.388	0.250	0.40	0.025	0.009	0.052	0.027	57.0	1.00	0.20	
#10	420	34	0.52	4.60/19	0.457	0.289	0.250	0.40	0.025	0.008	0.050	0.026	55.0	1.00	0.20	
#11	420	34	0.51	4.65/19	0.427	0.259	0.250	0.40	0.025	0.007	0.030	0.019	28.0	1.00	0.20	
#12	420	34	0.51	4.53/19	0.395	0.185	0.250	0.40	0.025	0.008	0.040	0.026	68.0	1.00	0.20	
#13	420	34	0.50	3.71/19	1.44	0.241	0.250	0.40	0.089	0.051	0.135	0.179	66.0	5.34	0.50	
low NaCl + reacted																
#1	400	69	0.15	3.99/22	4.57	1.30	0.518	< 0.100	0.115	0.029	0.208	0.173	46.5	1.89	0.264	13.8
#2	400	69	0.10	4.17/22	4.32	1.43	1.60	0.249	0.152	0.041	0.181	0.060	35.4	2.13	0.776	10.7
#3	400	69	0.18	3.97/22	3.08	1.47	1.14	0.256	0.080	0.019	0.099	0.075	38.0	1.90	0.671	40.0
#4	400	69	0.19	3.68/22	2.89	1.32	1.48	0.189	0.059	0.021	0.083	0.059	59.6	2.85	0.538	29.9
#5	400	69	0.19	3.24/21	2.83	1.37	0.353	< 0.100	0.114	0.019	0.058	0.041	55.3	2.05	0.361	24.9
#6	400	69	0.19	3.65/21	1.22	1.38	1.02	< 0.100	0.171	0.028	0.102	0.071	53.7	1.41	1.74	25.1
#7	400	69	0.15	3.41/21	1.40	1.44	0.819	< 0.100	0.043	0.023	0.080	0.056	135	1.75	1.50	31.2
NaCl + HCl																
#1	400	69	0.18	1.69/20	2.31	1.38	15.7	0.660	0.971	1.54	0.894	0.356	30.1	140	3.10	13.2
#2	400	69	0.19	1.22/19	1.70	1.35	5.99	0.132	0.284	0.126	0.591	0.197	11.9	87.9	0.368	5.31
#3	400	69	0.20	1.38/20	1.99	1.37	0.320	< 0.100	0.280	0.171	1.83	0.239	15.0	322	< 0.200	3.57
#4	400	69	0.21	1.33/19	1.78	1.29	0.411	< 0.100	0.219	0.144	1.79	0.190	5.84	239	< 0.200	2.66
#5	400	69	0.19	1.03/19	1.72	1.49	0.454	< 0.100	0.209	0.138	0.877	0.169	48.3	259	< 0.200	4.32
#6	400	69	0.20	1.22/20	2.07	1.36	1.78	< 0.100	0.220	0.139	1.22	0.176	17.3	289	< 0.200	3.87
#7	400	69	0.20	0.98/20	1.98	1.39	0.352	< 0.100	0.200	0.122	1.40	0.175	61.3	347	< 0.200	4.65
#8	400	69	0.22	1.03/20	1.85	1.27	3.07	< 0.100	0.288	0.143	4.07	0.250	13.2	706	0.521	3.58
#9	400	69	0.18	1.28/20	2.68	1.61	0.299	< 0.100	0.329	0.201	8.89	0.374	28.3	1356	0.938	10.8
#10	400	69	0.10	0.80/20	2.31	1.62	0.557	0.126	0.280	0.176	10.7	0.326	25.6	1167	0.822	3.12
NaCl + CO_2																
#1	420	69	0.110	5.06/21	0.642	3.35	0.189	0.058	0.016	0.002	0.066	0.030	101	0.446	6.58	19.5
#2	420	69	0.135	4.86/21	0.748	3.02	0.186	0.055	0.021	0.002	0.011	0.029	90	0.605	8.53	33.2
#3	420	69	0.142	4.78/21	0.695	2.71	2.43	0.128	0.015	0.002	0.010	0.026	105	0.736	4.20	40.1
#4	420	69	0.145	4.70/21	0.678	2.86	0.678	0.075	0.009	0.001	0.010	0.026	219	0.538	5.91	32.2
#5	420	69	0.143	4.55/21	0.641	2.65	33.3	0.073	0.014	0.002	0.012	0.030	167	0.555	6.54	31.4
#6	420	69	0.145	4.55/21	0.716	2.72	22.2	0.084	0.035	0.012	0.029	0.050	419	0.691	37.5	35.6
#7	420	69	0.150		0.582	2.62	6.15	0.085	0.011	0.001	0.009	0.026		0.523	31.3	

Table 3
Comparison of predicted supercritical fluid composition from geochemical modeling and laboratory experiments and observed natural supercritical fluid composition.

		low-NaCl fluids				NaCl-fluids					
		Experiments[a]	Modeling[a]	Krafla[b]	Menengai[c]	Experiments[a]	Modeling[a]	Kakkonda[d]	The Geysers[e]	Los Humeros[f]	Larderello[g]
				Iceland	Kenya			Japan	USA	Mexico	Italy
T	°C			440	~290			~500°C	~400°C	~400°C	~430°C
SiO_2	ppm	1.0-2.9	33-148	6.0	-	0.7-2.0	2.3-8.7		<1-4.1	22.0	-
B	ppm	0.3-1.4	0.24-1.5	1.41	-	1.4-2.9	1.4-3.3	~1700		958	~20-90
Na	ppm	1.0-1.6	45-130	0.51	-	2.9-9.3	0.05-3.7	~72,000	<0.1-0.15	0.58	-
K	ppm	0.2-0.4	1.6-21	0.12	-	0.08-0.3	0.01-1.8	~47,000	<0.5	0.36	-
Ca	ppm	0.04-0.1	0.00001-3.40	0.16	-	0.02-0.3	0.004-0.5	~21,000	<0.1-1.3	0.55	-
Mg	ppm	0.02-0.03	<0.00001	0.024	-	0.003-0.3	0.005-0.08	~40	0.005-0.05	0.04	-
Fe	ppm	0.1	0.004-0.025	5.25	-	0.02-3.2	0.02-0.09	~51,000	1	8.21	-
Al	ppm	0.05-0.08	0.00002-0.016	0.054	-	0.03-0.3	1.9-2.2				-
Cl	ppm	2.0-2.7	0.5-0.7	105	-	0.6-490	295-830	~270,000	<1-120	31	<0.01-120
CO_2	ppm	57-61	38-49	1637	27,000-80,000	26-185	23-420		~780-11,200	~32,000	~7000-115,000
SO_4	ppm	0.8-6.5	0.0001-79	32.7	-	1.2-14	37-163	~250	<0.01-10	45	
H_2S	ppm	10-40	54	630	1000-2700	5.5-32	20-54		~100-650	~3700	~90-1500

[a] This study

[b] IDDP-1 fluid composition based on Heřmanská et al. (2019a) for IDDP-1

[c] Based on Malimo (2013) and Montegrossi (2015)

[d] Based on data reported by Kasai et al. (1998a). The data have been corrected for mixing with drilling fluid as proposed by Kasai et al. (1998a) taken the mixing ratio of the deep fluid to the non-thermal drilling water to be 69/31.

[e] Based on Truesdell et al (1989) for vapor only well discharges except for CO_2 and H_2S that is based on the upper and lower quarter of gas data reported by Lowenstern and Janik (2005)

[f] Total discharge for H-43 as reported by Cruz and Tovar (2008) and Diez et al. (2015)

[g] Based on data reported by Ruggieri and Gianelli (1995), Truesdell and Nerhing (1978) and Truesdell et al. (1989)